

MASTER THESIS

Morphodynamic modelling of migrating mid-channel bars in rivers using dynamic vegetation

A case study on the Ayeyarwady River

D.G.R. Booij (s1543792)

University of Twente
Faculty of Engineering Technology: Civil Engineering
Water Engineering and Management

EXAMINATION COMMITTEE
Dr. ir. B.W. Borsje (University of Twente)
Dr. ir. A. Bomers (University of Twente)
Dr. F. Huthoff (HKV Lijn in Water)



08/05/2020

UNIVERSITY OF TWENTE.

Preface

Before you lies the thesis report ‘Morphodynamic modelling of migrating mid-channel bars in rivers using dynamic vegetation - A case study on the Ayeyarwady River’. It has been written to fulfil the graduation requirements of the master programme Civil Engineering and Management at the University of Twente. The research was carried out at HKV Lijn in water in Lelystad. I am glad that I had the chance to conduct this research at HKV. I was engaged in researching and writing this thesis report from December 2019 to May 2020.

Firstly, I would like to extend my deepest gratitude to my supervisors at HKV: Andries Paarlberg and Freek Huthoff. Their enthusiasm, the feedback they provided and the discussions we had from time to time have been very helpful and gave me additional inspiration during my research. I would like to thank all the other colleagues of HKV as well. They provided an open working environment and they were always eager to answer my questions. Additionally, I should not forget to mention the nice atmosphere during the lunch breaks. Thank you all!

I am also very grateful to my supervisors at the University of Twente, Anouk Bomers and Bas Borsje, for their excellent guidance and support during this research. They provided useful feedback, came up with inspiring ideas and assisted me to academically write this thesis report.

I wish to thank Jasper Dijkstra, Bert Jagers and Erik de Goede from Deltares as well. They provided the necessary tools to model dynamic vegetation (Basic Model Interface for Delft3D-FM) and they provided support to interpret and understand the sometimes unexpected modelling results.

Finally, I would like to thank my family, friends and fellow students for their support during my study and this research. Special thanks go to my girlfriend. Floor, thank you for your love and support.

I hope that you enjoy reading this thesis report.

Danny Booij

Hengelo, May 2020

Summary

Braided rivers are highly dynamic river systems which are characterized by multiple, unstable channels and mid-channel bars. The morphological development of these systems is a result of the complex interactions between the discharge regime, sediment transport and alluvial vegetation. Numerical modelling of braided rivers is increasingly used by river managers to get insight in the behaviour of bars and river patterns and to evaluate the response of these system to interventions, such as the construction of groynes and dams. Present morphodynamic models can produce many of the large-scale morphodynamics of braided rivers. However, these models often neglect the spatial and temporal development of vegetation on bars and floodplains. Neglecting vegetation dynamics can potentially result into unrealistic model predictions because vegetation does affect the morphological development of river in nature significantly. At present, sophisticated dynamic vegetation methodologies exist which include small-scale ecological processes and progressing vegetation characteristics (e.g. growth and mortality). However, these are not easy-to-use for engineering purposes, in particular when the large-scale morphodynamic development of mid-channel bars is mainly of interest. Therefore, our objective is to model and explore the effect of incorporating vegetation dynamics on the large-scale morphodynamics of vegetated migrating mid-channel bars in dynamic rivers.

The highly dynamic and monsoonal Ayeyarwady river in Myanmar was used as a case study. This river shows intense migration of large vegetated mid-channel bars up to several hundred meters per year. Alluvial vegetation mortality normally occurs at the upstream side of these bars during the high-flow season and it returns to the downstream side of these bars during the low-flow season. First, we studied the effect of two static vegetation representations in space and time on the morphological development of mid-channel bars in a morphodynamic model (Delft3D-Flexible Mesh). Thereafter, we developed a procedure based on two conditions to include dynamic vegetation removal and return in space and time on mid-channel bars in the morphodynamic model. The conditions are specifically developed to mimic the development of natural vegetation patterns on mid-channel bars in the Ayeyarwady River and they read: vegetation is removed from areas if the flow velocity exceeds a certain *critical flow velocity* in the high-flow season and vegetation returns to areas which are dry during the low-flow season. The *vegetation update interval* determines how often we check whether vegetation should be removed. The procedure was coupled to the morphodynamic model using a Basic Model Interface which has a direct control over model time steps and variables during a simulation. The adequacy of the procedure was studied using a schematized model of the case study. Finally, we tested the procedure in a more realistic model setup of the Ayeyarwady river.

Our results show that a conventional roughness formulation such as *Manning's* n can not be used to represent vegetation resistance in numerical morphodynamic models. A *Manning's* roughness formulation led to overly high bed shear stresses and major erosion at locations where alluvial vegetation was specified. The use of the vegetation roughness predictor by Baptist gave more realistic results. Vegetation significantly reduced the flow velocity and associated bed shear stress. Consequently, this reduction led to less sediment transport and erosion. However, the Baptist roughness predictor did not enable the migration of the mid-channel bar, because the location of the modelled vegetation on the bar was static in space and time.

The use of the proposed *dynamic vegetation procedure* increased the ability of the morphodynamic model to simulate large-scale morphodynamics of a vegetated migrating mid-channel bar over short time scales. Instead of being static over space and time, the vegetated mid-channel bar was exposed to upstream erosion and downstream deposition of sediments resulting in the formation of bar-tailed limbs and the migration of the bar as a whole. We found that the *critical flow velocity* and the *vegetation update interval* are strongly interconnected and that a slight change in one of these input parameters can result in a significantly different, potentially unrealistic, development of the vegetation and river morphology. Hence, it is important to devote much attention to the selection process of a suitable input parameters combination (*critical flow velocity* and *vegetation update interval*) for the *dynamic vegetation procedure*. Patterns were identified which can be used to guide this selection process for engineering purposes. It is recommended to use low *critical flow velocities* together with long duration of the *vegetation update interval* and to use high *critical flow velocities* together with short durations of the *vegetation update interval* to obtain natural morphodynamics and vegetation dynamics. Also, it is recommended to use calibration data, such as satellite imagery and in-situ measurements, to further steer this selection process.

We also found that the procedure can only improve model results when the flow velocity is the main driver of vegetation removal in a modelled river system. This always needs to be verified using the discharge regime, vegetation characteristics and topography of the bed. If not, another condition with a different driver (process) for vegetation removal, for example a critical erosion depth or bed shear stress, can potentially be used to end up with more realistic results. Furthermore, the use of the procedure over long time scales gives new challenges, because we are not modelling the precise behaviour of vegetation, but we are only mimicking the development of natural vegetation patterns. We recommend to look into this for further research. Yet, this study is a step forward in modelling the large-scale morphological behaviour of vegetated migrating mid-channel bars in dynamic rivers over short time scales. For engineering purposes, the proposed procedure can be used to obtain more realistic predictions of the effects of river training works on the morphological development of migrating mid-channel bars.

Contents

Preface	iii
Summary	v
1 Introduction	1
1.1 Context	1
1.2 Problem definition	2
1.3 Objective and research questions	2
1.4 Thesis outline	3
2 Literature review	5
2.1 Braided river dynamics	5
2.1.1 Morphodynamics	5
2.1.2 Mid-channel bars	6
2.2 Hydraulic resistance	8
2.2.1 Physical background	8
2.2.2 Modelling hydraulic resistance	9
2.3 Alluvial vegetation	9
2.3.1 Vegetation dynamics	9
2.3.2 Modelling vegetation	10
3 Methodology	13
3.1 Case: the Ayeyarwady River	14
3.1.1 Ayeyarwady River basin	14
3.1.2 Study area: Nyaungdon	15
3.2 Hydrodynamic & morphodynamic model	17
3.2.1 Hydrodynamics	17
3.2.2 Morphodynamics	18
3.3 Schematized model	19
3.3.1 Model setup	19
3.3.2 Manning scenario	21
3.3.3 Static vegetation scenario	22
3.3.4 Dynamic vegetation scenario	22
3.4 Ayeyarwady River model	25
3.4.1 Model setup	25
3.4.2 Scenarios	26

4	Results	27
4.1	Schematized model	27
4.1.1	Reference scenario	28
4.1.2	Manning scenario	28
4.1.3	Static vegetation scenario	30
4.1.4	Sensitivity analysis	31
4.1.5	Dynamic vegetation scenario	34
4.2	Ayeyarwady River model	41
5	Discussion	45
5.1	Scope	45
5.2	Morphodynamic modelling	46
5.2.1	Bank erosion	46
5.2.2	Sediment transport formula	47
5.2.3	Morphological acceleration factor	47
5.3	Vegetation modelling	47
5.4	Dynamic vegetation procedure	48
5.4.1	Critical flow velocity	48
5.4.2	Interconnectedness of input parameters	49
5.4.3	Applicability to other rivers	49
5.4.4	Long-term applicability	50
6	Conclusions and recommendations	51
6.1	Conclusions	51
6.2	Recommendations	53
6.2.1	Future research	53
6.2.2	Practical usage	54
	Bibliography	57
	Appendix A Baptist roughness predictor	64
	Appendix B Model set-up: Ayeyarwady River model	67
	Appendix C Results: Schematized model	71
	Appendix D Results: Ayeyarwady River model	78

Chapter 1

Introduction

This introductory chapter serves to outline the motivation for this research. The first section presents the context of this thesis report. Thereafter, the problem definition and research gap are presented in section 1.2. Section 1.3 elaborates on the research objective and the research questions. Finally, the structure of this report is given.

1.1 Context

River systems and their physical changes have always been the basis of the development and progress of communities living close to it. Furthermore, these systems serve as drivers of urban evolution and they are often cause of floods and droughts (Hydro-Informatics Centre, 2017). Therefore, trying to control and manage the evolution of rivers has always been the focus of human activity, e.g. for flood safety, water supply and transportation. As a result, many rivers in the Western world are highly affected by humans actions (Duivendijk et al., 2002). These altered rivers preserve a simplified and attractive form but have lost their natural functions. Their hydrologic and geomorphic processes no longer maintain the regime necessary for a balanced system. A perfect example of such a river is the river Rhine. This river has been transformed from a natural meandering river into a man-made river by flow regulation, channelization and construction of dams and groynes (Duivendijk et al., 2002).

In contrast, the morphology of pristine alluvial rivers is predominantly a consequence of complex interactions among several physical processes, such as flow and sediment transport (Church and Ferguson, 2015). For river managers, evaluating the response of these dynamic rivers to interventions is essential. For example, this is important for evaluating measures to avoid undermining of bridge pillars caused by the migration of mid-channel bars in braided rivers (Steijn et al., 2019). Mid-channel bars are dynamic land forms which can rapidly migrate through rivers due to very active channel processes as sedimentation and erosion (Ashmore, 2013). Modelling of these migrating mid-channel bars in braided river systems is typically used by scientists and river managers to acquire a better understanding of the interactions between the flow, sediment transport and river morphology to predict the development of a river over time (Williams et al., 2016a).

Present morphodynamic models are able to sufficiently produce many of the large-scale morphological characteristics and dynamics of braided rivers (Schuurman et al., 2013; Williams et al., 2016a). For example, the shape and size of individual bars compared well to those in natural rivers. However, the models contain many simplifications such as neglecting the spatial and temporal development of vegetation on bars and floodplains. Adequate modelling of vegetation is important because the presence of vegetation significantly affects the morphological development of (mid-channel) bars. Vegetation slows down the migration of bars because it stabilizes the erodible sediment and it reduces the bed shear stresses leading to erosion (Kleinhans, 2010). Two approaches are often used to represent the effects of vegetation in numerical models: changing the hydraulic roughness of the river bed, bars or floodplains (e.g. Manning’s n) or using a vegetation model to incorporate the effects of vegetation upon momentum and turbulence equations (e.g. Baptist or Uittenbogaard). However, the location of vegetation is typically static over space and time in a simulation neglecting the dynamic character of vegetation on migrating mid-channel bars. This can potentially result in unrealistic model results as vegetation directly affects sediment transport and the morphological development of bed forms (Baptist, 2005).

1.2 Problem definition

Several studies have been executed which tried to include the dynamics of vegetation in hydrodynamic and morphodynamic models (Bertoldi et al., 2014; Oorschot et al., 2016; Jourdain et al., 2018). The proposed methodologies often include small-scale dynamic ecological processes and progressing vegetation characteristics. Consequently, they need several very specific input parameters such as a logarithmic growth factor and a life-stage dependent desiccation threshold. Therefore, these approaches cannot be called easy-to-use for engineering purposes when the large-scale morphodynamic development of rivers is mainly of interest. Furthermore, these approaches desire frequent vegetation updating leading to significantly higher computation times. Nicholas et al. (2013) used a more simple and robust approach for vegetation development in an anabranching mega-river. They used simple rules to remove and return vegetation on bars and floodplains of an idealized river over periods of several hundred years. For example, they removed vegetation when an area was exposed to a certain amount of erosion. Such a procedure only includes the determination of a few so-called ‘calibration-parameters’ which is ideal for engineering purposes. Up till now, we do not know the effect of such a procedure on the ability of a numerical morphodynamic model to simulate the large-scale morphodynamics of individual vegetated migrating mid-channel bars in rivers over short time-scales (years).

1.3 Objective and research questions

The objective of this research is:

to model and explore the effect of incorporating vegetation dynamics on the large-scale morphodynamics of vegetated migrating mid-channel bars in dynamic rivers.

Several research questions have to be answered to meet this objective. First, a proper understanding of the present competence of morphodynamic models to simulate migrating mid-channel bars is required. Furthermore, it is important to determine the effect of static vegetation in space and time on the morphodynamics of migrating mid-channel bars. Hence, the first research question is:

1. To what extent are present numerical morphodynamic models capable of simulating the development of vegetated migrating mid-channel bars in dynamic rivers using different static (in space and time) approaches to include vegetation?

Afterwards, the second research questions elaborates on the inclusion of dynamic vegetation in numerical morphodynamic river models:

2. How can we include the removal and return of vegetation in space and time on migrating mid-channel bars in numerical morphodynamic models in a simplistic and dynamic way?

Finally, it is important to evaluate whether the proposed procedure can easily be implemented in a case study and whether it results into more realistic morphodynamic model results. Thus, the last research question is:

3. To what extent can the proposed modelling procedure for dynamic vegetation be used to improve morphodynamic model results of a vegetated migrating mid-channel bar in a real-life case study?

These research questions are answered using the Ayeyarwady River from Myanmar as a case study. A highly schematized model representation is used for the first and second research question, whereas a more realistic extended model representation is used for the third research question.

1.4 Thesis outline

Chapter 2 presents a literature review on the most important morphodynamic processes in braided river systems. Furthermore, it explains the processes affecting the hydraulic resistance experienced by rivers and it elaborates on how vegetation affects hydro- and morphodynamics in rivers. Thereafter, chapter 3 describes the methodology. It gives a description of the used numerical model (Delft3D-FM) to simulate river dynamics and it describes the various models setups and conducted simulations. Chapter 4 presents the results from both the schematized model as well as the Ayeyarwady River model. The report concludes with a discussion (chapter 5) and conclusions and recommendations (chapter 6).

Chapter 2

Literature review

This chapter provides the relevant background knowledge required for this thesis report. It consists of three sections. The first section presents the state-of-the art knowledge on the dynamics of braided rivers. Section 2.2 elaborates on the hydraulic resistance in the context of rivers modelling and the last section (2.3) presents the relevant state-of-the art knowledge on vegetation dynamics in rivers and the influence of vegetation on river hydro- and morphodynamics.

2.1 Braided river dynamics

Alluvial rivers respond to changes in regional physical processes, hydrology and sediment load by adjusting their geometry (e.g. slope or cross-sectional shape) and river planform (Nanson and Knighton, 1996). Changes in these processes may occur naturally or may be a result of human activities such as the construction of bank protection (Chang, 2008). The feedbacks between bars, channels, floodplain and vegetation also have a major effect on the planform of rivers (Kleinhans, 2010). This is caused by the self-organisational characteristic of rivers. Rivers always tend to develop towards a new equilibrium state if the environment distorts the dynamic equilibrium of a river (Kleinhans, 2010). A new equilibrium state is reached through changes in important river processes all affecting the sediment transport. The main drivers of the transport, erosion and deposition of sediment are the magnitude and direction of the primary flow, spiral (secondary) flow and turbulent flow (Coleman and Smart, 2011).

2.1.1 Morphodynamics

Braided rivers are characterized by multiple, unstable channels and mid-channel bars formed by intense bed-load transport, and a set of very active channel processes (Ashmore, 2013). See figure 2.1 for a schematization of a braided river planform.

The dynamics within braiding rivers include the interaction between mid-channel bars, branches, islands, and floodplains (Ashworth et al., 2000). A major role is played by channel bar bifurcations that distribute discharge and sediment through the network (Schuurman et al., 2016). This distribution can change rapidly over time due to changes in the flow regime during high flow conditions. Furthermore, this distribution determines the formation, migration and reshaping of bars, and

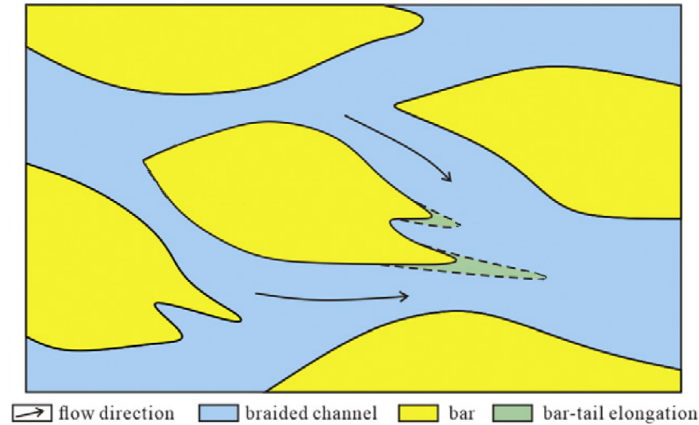


Figure 2.1 – Schematization of a braided river. Figure adapted from Fig. 1 in Zhang et al. (2020).

it determines the initiation and closure of branches (Ashmore, 2013). A branch can close if the discharge and sediment distribution in a bifurcation become highly asymmetrical. Bifurcations can emerge due to cross-bar flows or chute cut-offs which initiate the development of a new branch (Schuurman, 2015). A bifurcation consists of two branches: a dominating branch and recessive branch. A dominant branch is the branch with the smallest angle to the approaching flow. This branch is likely to be exposed to the least amount of sedimentation.

In a braided network, bars migrate in downstream direction by upstream erosion and deposition at their lee. The position of bars in rivers can shift up to kilometres within a year. Schuurman et al. (2016) mentioned that bar migration and reshaping changes the local flow pattern in two ways. It affects the nearby upstream bifurcation through the backwater effect and it changes the downstream bifurcations by affecting the approaching flow direction. This starts a cascade of effects that links all bars and branches together (Schuurman et al., 2016). These active channel processes, associated with intense bed-load transport, lead to morphological development and regularity in the structure of the network of channels (Ashmore, 2013).

2.1.2 Mid-channel bars

Mid-channel bars commonly occur in braided rivers. Figure 2.2 shows two real-life examples of mid-channel bars in braided river. They are unstable bed forms and generally show longitudinal migration (Mukherjee, 2011). Mid-channel bars emerge, submerge and re-emerge continuously due to process of erosion and sedimentation. Accumulated sediments can lead to minor perturbations on the river bed. Such a perturbation starts the formation of a mid-channel bar. Among others, these perturbations can develop due to inflow asymmetry at a confluence or the formation of chute cut-offs and channel avulsions (Schuurman et al., 2013). The perturbations obstruct the river and, consequently, the river divides into two channels with the perturbation in between. This causes a deflection of the flow against the adjacent river banks by secondary flow, causing bank erosion and a widening of the channel (Ashworth, 1996). The secondary flow also causes sediment transport laterally from



Figure 2.2 – Bare and vegetated mid-channel bars including bar-tailed limbs and bar-top hollows in the Ayeyarwady River (Left) and the Yenisei River (Right). Source: *GoogleEarth*.

the main channel, causing deepening of the channel, onto the bar consequently leading to further bar development. This increasingly redirects the flow around the bar and sediment is eroded at the upstream side of the bar and deposited at the downstream side of the bar causing bar migration in downstream direction (Ashworth, 1996).

Downstream deposition of sediments causes the formation of bar-tailed limbs, as shown in figures 2.1-2.3. The evolution of these limbs depends on the dominance of the bifurcation branches. Elongation occurs parallel to the flow and sediment transport in the dominant branch, whereas the bar-tail limb in the recessive branch remains short. Elongation in the downstream direction occurs until it reaches a confluence scour hole or a downstream located bar, causing closure of the channel between the two bars. The bar-tail limb widens if flow occurs from the recessive branch towards the dominant branch, e.g. because of downstream closure of the recessive branch (Schuurman, 2015). The flow around the bar can also initiate the formation of bed forms somewhere downstream since it transports the eroded sediments in downstream direction (Mukherjee, 2011).

A hole commonly develops between the two bar-tailed limbs. Best et al. (2006) recognizes this morphological element as a *bar-top hollow*, see figure 2.3. The wrapping of the limbs around the bar-tail leads to the isolation of a region that can only be reached by sediments occasionally (Best et al., 2006). Sediments can only reach this region by overbank flow and large turbulent eddies, during high discharge (high water levels) and when bed forms migrate in upstream direction.

The presence of vegetation can slow down the processes of erosion and sedimentation because it stabilizes the erodible sediment and reduced the shear stress on the bed (Kleinhans, 2010). Thus, the development and long-term stability of mid-channel bars does not only depends on the upstream water and sediment supply, but it also relies on the vegetation development on the bar surface (Li et al., 2014). Furthermore, vegetation affects the horizontal and vertical shape of mid-channel bars. In general, vegetation first develops on the tails of bars if those areas have been stable for a while, and only sparse vegetation or no vegetation develops initially on the heads of bars. Vegetated areas remain relatively static over time, whereas the sandy sections of the bar migrate further downstream. This ensures that vegetation is eventually

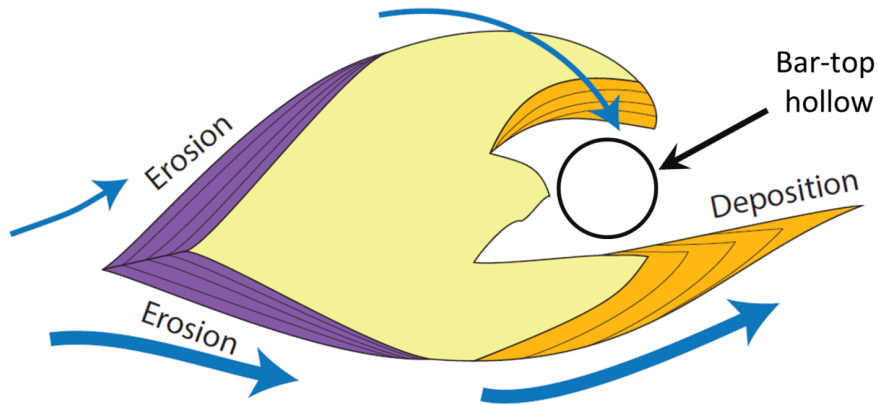


Figure 2.3 – Migration of bars and formation of bar-tail limbs. Blue arrows indicate the direction and magnitude of the flow. Black circle is showing a *bar-top hollow*. Figure adapted from Fig. 3.14 in Schuurman (2015).

located on the upstream bar edge (Ashworth, 1996). Vegetation mortality occurs on the bar surface when the upstream bar edge fails (bank erosion) or when the individual stems are removed through high bed shear stresses, flow velocities, burial or scour (Li et al., 2014; Oorschot et al., 2016).

2.2 Hydraulic resistance

Firstly, this section elaborates on the physical background of hydraulic resistance in rivers. Afterwards, this section shortly touches upon the modelling of hydraulic resistance in numerical morphodynamic models.

2.2.1 Physical background

In most natural rivers, the bed and bank roughness are the primary source of hydraulic resistance (Ferguson, 2010). Hydraulic resistance results from forces that act on and within the flow to resist motion. This resistance causes a shear stress on the bed and banks leading to energy dissipation and a reduction of the flow velocity in rivers. This leads to changes in water levels and corresponding safety during flood events and changes in the shape and propagation speed of flood waves. Consequently, it influences the rate and composition of the sediment transport and morphological behaviour of rivers. In general, an increase in flow resistance causes deeper and slower flow (Powell, 2014). Resistance to flow is due to blocking by irregularities at all scales from individual grains and pebbles to structures on floodplains (Ferguson, 2010).

The main process affecting the hydraulic resistance is commonly referenced to as boundary resistance (Powell, 2014). This is the mechanical friction (drag force) exerted on the flow by the individual grains and bed forms in the river. The drag force, also called bed shear stress, causes energy dissipation of the kinetic and potential energy in the river. Next to the boundary resistance, other factors do also cause energy losses in rivers: vegetation, channel resistance, spill resistance and sediment transport resistance (Ferguson, 2010). *Vegetation resistance* is caused by the drag of

riparian and in-channel vegetation on floodplains, river bars and banks. Section 2.3 further elaborates on this type of resistance. *Channel resistance* has to do with energy losses arising from the channel cross-section, planform geometry and variation in the slope of the river (Ferguson, 2010). For example, bars and meanders lead to complex turbulent flow fields leading to energy losses. *Spill resistance* is due to energy losses by turbulence during rapid accelerations and decelerations of flow around individual channel obstructions such as large boulders or fallen trees (Chow, 1959). *Sediment transport resistance* is caused by the extraction of flow energy by moving of sediments.

2.2.2 Modelling hydraulic resistance

Numerical model results need to be sufficiently accurate for decision making purposes (Williams et al., 2016a). Calibration is often used to increase the accuracy of numerical models. This involves the minimization of the error between predicted model outcomes and observations by altering model parameters. The hydraulic resistance is typically used as calibration parameter for hydrodynamic models because it is the most uncertain parameter (Domhof et al., 2018). Morvan et al. (2008) mention that this parameter is typically treated as a space and time independent dustbin to capture both the physical phenomena affecting roughness and model errors. Thus, this model parameter does not purely represent the actual physical characteristics of a river system such as grain size and the location of vegetation patches.

Various efforts have been made to quantify the hydraulic resistance for hydrodynamic and morphodynamic modelling, e.g. the formulations of Chézy, Manning and Darcy-Weisbach (Morvan et al., 2008). The depth-dependent roughness description of Chézy is widely accepted and used in numerical models such as Delft3D and TELEMAC to represent flow resistance (Ferguson, 2010). Typically, it is determined using the empirical Manning’s n value (Chow, 1959). The Chézy coefficient is used to calculate the bed shear stress (energy dissipation) induced by turbulent flow in the Shallow water equations of 2D (depth-averaged) hydrodynamical models. An higher bed roughness (lower Chézy coefficient) induces higher bed shear stresses due to an increase in turbulence and consequently it results into a reduction of the flow. Higher bed shear stresses do lead to larger sediment transport rates in modelled river systems as well. These relations can be seen in figure 2.4.

2.3 Alluvial vegetation

The first part of this section describes how vegetation affects hydro- and morphodynamics in rivers and vice versa. Afterwards, the second part elaborates on the modelling of vegetation resistance in morphodynamic models.

2.3.1 Vegetation dynamics

The presence of vegetation both modifies flow and sediment transport in alluvial river channels and consequently the morphological evolution of river systems. It affects hydrodynamics of rivers through effects on the hydraulic resistance by increasing drag and reducing flow velocity near the river bed and banks. Furthermore, vegetation initiates a reduction of turbulence inside vegetation patches. This causes a decrease of the bed shear stress up to 80 percent (Baptist, 2005). Consequently, vegetation

also affects the sediment transport and morphodynamics of rivers (Oorschot et al., 2016). In general, sediment transport rates inside vegetated areas are reduced, and sedimentation rates are increased (Bennett et al., 2008). The extent of the effect of vegetation is dependent on vegetation characteristics as well, such as density, diameter, height which can all vary in time and space (Huthoff, 2007). For example, emergent and submerged plants both influence the water flow in a different way (Baptist, 2005).

Conversely, hydrological and morphological processes do also influence vegetation development (Gurnell et al., 2016). These fluvial disturbances control the development and mortality of vegetation. For example, vegetation can only grow in regions which are only occasionally submerged. Fluvial disturbances are the depth and duration of inundation, shear stresses or drag imposed on plants by river flow, and sediment erosion (uprooting) and deposition (burial) (Gurnell et al., 2016). High flow velocities and shear stresses promote sediment mobilization and erosion during high-flow stages, and thus the highest potential for plants to be removed (damaged, uprooted or buried) (Gurnell et al., 2016).

2.3.2 Modelling vegetation

Vegetation processes are important factors determining the dynamics of river systems. Therefore, the effects of vegetation should be taken into account in morphodynamic river models. Two approaches are commonly used to include the hydraulic resistance induced by vegetation in 2D (depth-averaged) modelling. Traditionally, the hydraulic resistance of vegetation in rivers is estimated using an empirically determined Manning coefficient (Chow, 1959). This approach represents the flow resistance due to vegetation as an equivalent bed roughness. However, this approach has some shortcomings. It appears to be case- and flow-specific and is therefore hard to apply to new situations (Huthoff, 2007). More importantly, it does not represent the natural effects of vegetation on river hydro- and morphodynamics. It does not describe well the higher hydraulic resistance of vegetation (lower Chézy value) in combination with a lower bed shear stress, see the red lines in figure 2.4. It leads to high, potentially unrealistic, sediment transport rates (and erosion) in vegetated areas.

In the second approach, a vegetation model is used to incorporate the effects of vegetation resistance upon momentum and turbulence equations (e.g. Baptist (2005)). Turbulent flow induced by vegetation stems uses kinetic energy which effectively slows down the flow. Many different models (e.g. Baptist, Hoffmann and Klopstra) can be used to estimate the effects on the flow by vegetation resistance (Vargas-Luna et al., 2015). For example, Hoffmann (2004) proposed a model that uses a vegetative drag force, in analogy to rigid cylinder drag and Velzen et al. (2003) proposed a model that describes the hydraulic effects of vegetation based on an adjusted boundary layer velocity profile. These models do take into account the effects of vegetation on the reduction of the flow velocity and turbulence in vegetated areas. Hence, an increase of the hydraulic resistance (compared to no vegetation) goes together with a reduction of the flow velocity, bed shear stress and, consequently, a reduction of the sediment transport rate. For example, see the vegetation resistance predictor of Baptist (2005) (blue lines) in figure 2.4.

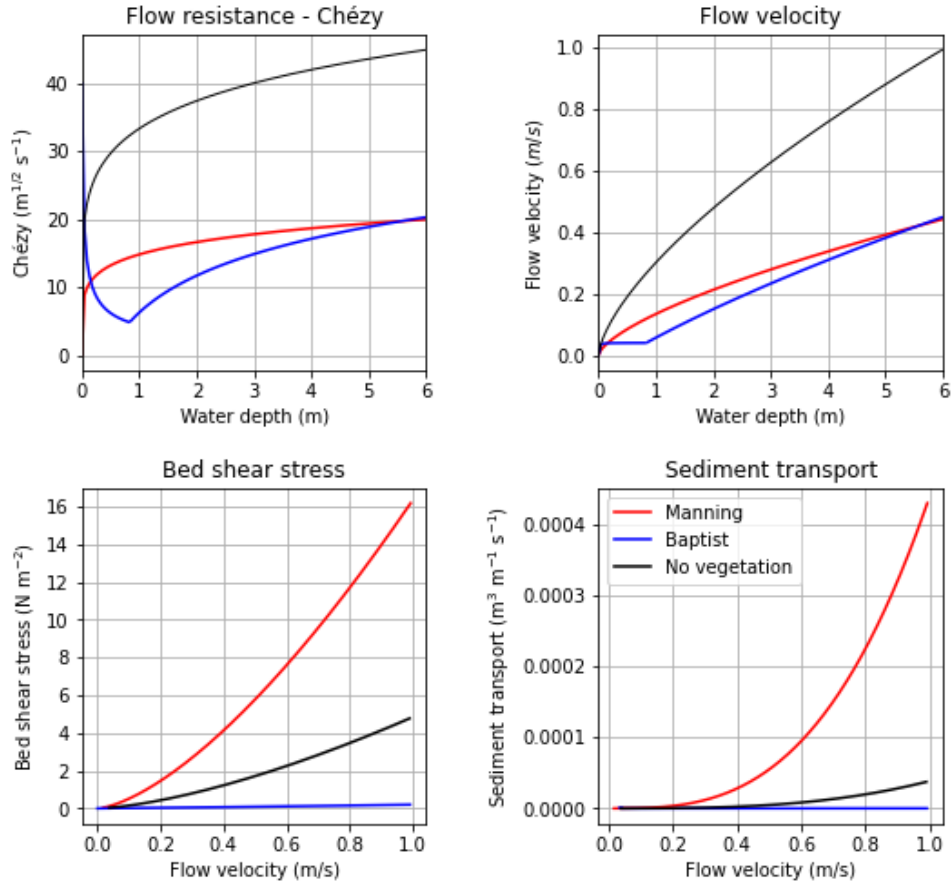


Figure 2.4 – Depth-dependent Chézy coefficient (upper left) and depth-averaged flow velocity (upper right) vs. water depth for different vegetation formulations. Bed shear stress (lower left) and sediment transport (lower right) vs. depth-averaged flow velocity for different vegetation formulations. *Manning* has a Manning’s n of $0.070 \text{ m}^{-1/3}\text{s}$ and *No vegetation* has a Manning’s n of $0.030 \text{ m}^{-1/3}\text{s}$. The figures are based on characteristics of the flow and vegetation on the mid-channel bar as simulated in the schematized model of this study.

The Delft3D-Flexible Mesh software is used to simulate (river) flow hydrodynamics, sediment transport and morphodynamics (see section 3.2 for an extensive description). This model incorporates two approaches to simulate additional vegetation resistance in a 2D (depth-averaged) state. The first approach is the use of the Manning coefficient of Chow (1959) (as described above). The second approach uses the analytical formulation of Baptist (2005) for the contribution of vegetation resistance to the total resistance in water flowing through vegetation. In figure 2.4, we can see that this resistance formulation leads to a higher flow resistance (lower Chézy value), a lower flow velocity, a lower bed shear stress and a lower sediment transport rate in vegetated areas. An extensive description of this vegetation resistance formulation is given in Appendix A.

Chapter 3

Methodology

Numerical simulations are used to gain insight in to what extent a present numerical morphodynamic model is capable of simulating the behaviour of vegetated migrating mid-channel bars in dynamic rivers. Therefore, a case study on the Ayeyarwady River in Myanmar is conducted. For the intent of analysis, a schematized morphodynamic river model based on the case is set up to perform numerical simulations in Delft3D Flexible Mesh. Four scenarios are created with different vegetation formulations, but having the same baseline model setup, see figure 3.1.

In the first scenario, a bare non-vegetated mid-channel bar is simulated to assess whether the baseline model results in a natural morphological development of the bar (*reference scenario*). The second and third scenario contain two frequently used static representations of vegetation in space and time in numerical models, respectively Manning’s roughness coefficient (*manning scenario*) and the roughness predictor by Baptist (2005) (*static vegetation scenario*). Scenario four includes a new procedure to dynamically update the location of vegetation such that the development of natural vegetation patterns is mimicked during a simulation (*dynamic vegetation scenario*).

In all scenarios, the vegetation is uniformly distributed over the entire mid-channel bar. This is in compliance with other studies (Tassi, 2007; Segura and Pitlick, 2015; Liu et al., 2019). These studies state that a single resistance value will not directly lead to poor model results if small-scale morphological development of bars is not of

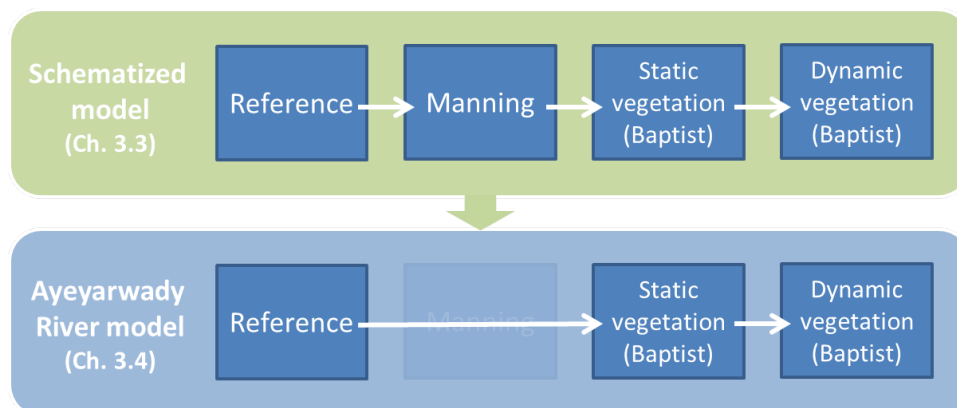


Figure 3.1 – Overview Methodology.

interest. Table 3.1 in section 3.3.1 gives an overview of the model parameters used in each scenario. All four scenarios are implemented in the schematized model. The schematized model has no prototype in nature against which the results could be evaluated. Therefore, internal model parameters and model output of all scenarios were compared with each other to attain a better understanding of the physical processes. Eventually, the schematized model set-up was expanded such that it captured the actual Ayeyarwady River dimensions to test the new *dynamic vegetation procedure* of the fourth scenario.

In the first section (3.1), a description of the Ayeyarwady River basin and study area is given. The second section (3.2) elaborates on the numerical model Delft3D-FM. In section three (3.3), a description of the schematized model is presented and the various scenarios are explained. The last section (3.4) gives a description of the Ayeyarwady River model and it elaborates on the conducted simulations.

3.1 Case: the Ayeyarwady River

3.1.1 Ayeyarwady River basin

The Ayeyarwady River is the main river of Myanmar running from north to south (Taft and Kühle, 2018). It is Myanmar’s most important waterway and central supply system with a total length of approximately 2000 kilometres. The Ayeyarwady River originates in the far north of Myanmar, the south-eastern Himalayas, from the confluence of the N’mai H’ka and Mali H’ka rivers (Taft and Kühle, 2018). The river continues its way through the centre of the country to the Ayeyarwady Delta where it eventually flows into the Andaman Sea in the Bay of Bengal.

Myanmar has a tropical and monsoonal climate which varies greatly among locations and from year to year (Hydro-Informatics Centre, 2017). In fact, the lower catchment area of the Ayeyarwady River has a humid tropical climate, while the upper catchment area has a more warm humid subtropical climate. The rainy season typically occurs from May to October as south-west winds blow across the Bay of Bengal (Anthony et al., 2019). However, extreme variation in precipitation are present within the country. The northern and southern parts of Myanmar are exposed to mean annual precipitation up to 6,000 mm, while the centre of the country experiences precipitation under 500 mm (Hydro-Informatics Centre, 2017). The monsoonal climate and rapid melting of snow and glaciers during summer causes large discharge fluctuations through the year between $2,300 \text{ m}^3/\text{s}$ and $32,600 \text{ m}^3/\text{s}$, the average being $13,000 \text{ m}^3/\text{s}$ (Simmance, 2013). This leads to a wide range in water levels in the river which can vary upto ten metres (Furuichi et al., 2009).

The fluctuating discharge regime in the Ayeyarwady River exerts a strong control on geomorphological processes (Hydro-Informatics Centre, 2017). The river is the fifth most heavily silted river in the world and the delta area extends towards the Adaman Sea with about 50 metres per year (Simmance, 2013). The characteristics of the Ayeyarwady River include steep slopes upstream of the confluence and an overall low slope downstream of it. Variability in the river slope and valley width controls the transport and deposition of sediment. It also accounts for areas of the river in which sediment reworking and channel migration occurs (Hydro-Informatics Centre, 2017). In general, the bulk of sediments in the river are very fine and efficiently transported through the river once in suspension. They are largely absent from the

banks, bars, and bed deposits in the river, which are formed during the peak flow season by rolling of sand and fine gravel (Hydro-Informatics Centre, 2017). The majority of the river can be classified as a laterally active braiding or meandering river form. Stable vegetated islands and unstable sandy bars are both common in the Ayeyarwady River (Hydro-Informatics Centre, 2017).

3.1.2 Study area: Nyaungdon

This study focusses on a river section close to the city of Nyaungdon. It is a port city of 216,000 people at the bifurcation point where the Pan Hlaing River bifurcates from the Ayeyarwady River (Hydro-Informatics Centre, 2017). The city of Nyaungdon is situated in the Ayeyarwady Delta and it tends to be hot and wet throughout the year. This delta is characterised by coastal processes, high population densities and cultivated land (Hydro-Informatics Centre, 2017). The average annual discharge flowing to Nyaungdon is slightly under $12,000 \text{ m}^3/\text{s}$. This discharge predominantly occurs in the six or so months of the wet season. Consequently, this leads to a distinct seasonal hydrograph having a dry (Dec.-Apr.) and a wet (May-Nov.) season, see Figure 3.2. It shows the clear water level difference between the dry and wet season. Furthermore, it shows that the water levels during the dry season are about stable and that a clear bell-shaped water level rise is present during the wet season.

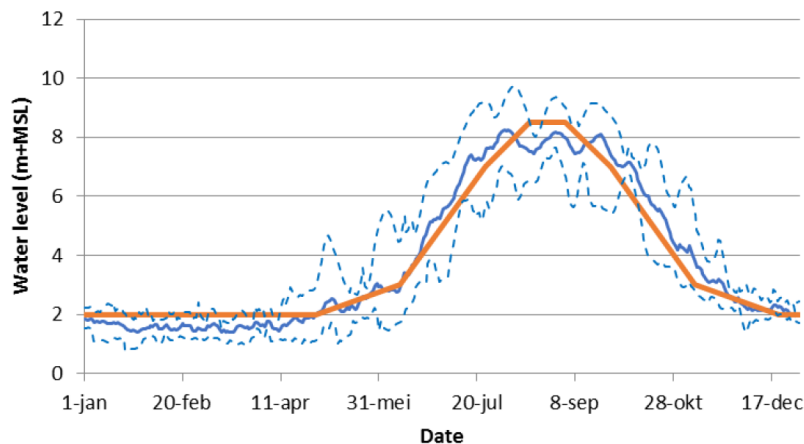


Figure 3.2 – Simplified yearly hydrograph for high flow conditions (orange line). Blue lines show minimum, maximum and average daily water levels at Danubyu (about 25 km upstream of Nyaungdon) during the period 2013-2017. Reprinted from Fig. 4 of Appendix I in Steijn et al. (2019).

The sediment transport is strongly skewed towards the wet season due to the low and continuous slope of the river (WWF, 2017). At the bifurcation of the Ayeyarwady River at Nyaungdon, the river shows intense migration of a large vegetated mid-channel bar, a so-called ‘walking island’, see figure 3.3. The bar has a length of ± 3 kilometres and a width of ± 1.3 kilometres. The intense migration causes a shift of the flow from the southernmost to the northernmost channel. Figure 3.4 shows the migration of mid-channel bar between the years 2017 and 2020. It shows that the bar was exposed to erosion at its upstream side (about 200 meters). Also, it shows that the bar significantly grew in downstream direction. The northern bar-tailed limb



Figure 3.3 – Present situation (in 2020) of the Ayeyarwady River at Nyaungdon Myanmar. Blue arrows show magnitude and direction of the flow. Orange arrows show migration of the mid-channel bar. Based on Steijn et al. (2019). Source background image: *GoogleEarth*.

increased in length with about 500 meters and the southern limb with more than one kilometre. The development of a clear bar-top hollow is also visible.

Vegetation development is visible in Figure 3.4 as well. Vegetation mortality occurred at the upstream side of the bar and vegetation returned to both bar-tailed limbs on the downstream side of the bar. In general, the riparian vegetation on the floodplains and river bars of the Ayeyarwady River is to a large extent disconnected from the river especially during the dry season. Therefore, it does not directly reflect any changes in the discharge regime. Periodically inundated woody vegetation grows at the highest elevations of river bars and scroll bars do comprise seasonally inundated vegetation and small back swamps (Moggridge and Higgitt, 2014).



Figure 3.4 – Location of the mid-channel bar at Nyaungdon in 2017 and 2020. Red line in the right panel shows the location of the bar in 2017. Source: *GoogleEarth*.

3.2 Hydrodynamic & morphodynamic model

Hydrodynamic and morphodynamic modelling is performed with the physical-based model Delft3D-Flexible Mesh (Delft3D-FM) (Deltares, 2019a). It numerically solves the Shallow water equations and computes sediment transport and bed level change on a flexible unstructured grid. This means that computations are performed on a grid consisting of quadrangles which are connected using triangles, pentagons and hexagons. This enables to use of local grid refinement (and coarsening) to increase the accuracy of the model around locations of interest and to reduce the accuracy elsewhere (Bomers et al., 2019). The numerical model has proven to be reliable and accurate in the demanding practice of river engineering (Schuurman et al., 2013). We use Delft3D-FM in a two-dimensional depth averaged (2DH) mode, because it has the advantage of computational efficiency.

3.2.1 Hydrodynamics

In Delft3D-FM, the hydrodynamics are modelled by applying conservation of momentum and mass (Shallow water equations), considering hydrostatic pressure and Boussinesq assumptions (Deltares, 2019a). The Shallow water equations only describe the behaviour of the mean flow field. All horizontal mixing patterns (2D-turbulence) are absorbed into a horizontal background viscosity coefficient of $1 \text{ m}^2/\text{s}$ (default). Vertical turbulence is excluded as we perform simulation in a 2DH-state. The vertical flow is parametrized in order to include the effect of secondary flow.

Boundary conditions are used to solve the system of Shallow water equations. An upstream (horizontal) boundary conditions is imposed in the form of a discharge time series. The downstream boundary condition has the form of a water level time series. Vertical boundary conditions close the system of equations at the bed and the free surface. Without precipitation, evaporation or ground water flow, no flow through the bottom or top of the water column is present. The boundary condition at the bed contains the bed shear stress. For 2D depth-averaged flow the shear stress at the bed is assumed to be given by (Deltares, 2019a):

$$\tau_b = \frac{\rho_0 g U |U|}{C^2} \quad (3.1)$$

where $|U|$ is the magnitude of the depth-averaged horizontal velocity and C the depth averaged Chézy roughness coefficient. Following e.g. Nicholas et al. (2013) and Schuurman (2015), a constant uniform bed roughness was applied, assuming bed forms were subgrid and thus captured by the bed roughness parameter. The Chézy coefficient is calculated using Manning's roughness formulation (Deltares, 2019a):

$$C = \frac{\sqrt[6]{R}}{n} \quad (3.2)$$

in which R is the hydraulic radius and n the Manning coefficient ($\text{m}^{-1/3}\text{s}$). Additional flow resistance by riparian vegetation can be included in Delft3D-FM by using an adapted Manning coefficient or by using the vegetation roughness predictor by Baptist (2005). The Baptist roughness predictor can be used to calculate the representative Chézy roughness coefficient for both submerged and non-submerged vegetation based on the vegetation density, diameter and height (Baptist et al., 2007). An extensive description of this roughness predictor is given in Appendix A.

3.2.2 Morphodynamics

The sediment transport and morphology module (D-Morphology) is closely integrated with the hydrodynamics module (D-Flow Flexible Mesh). Many different formulations can be chosen for the calculation of the transport of sediments. Most typical for rivers are the Engelund and Hansen formula, the Meyer-Peter & Müller formula and the van Rijn formula (Vargas-Luna et al., 2015). We used the transport formula: *General Formula*. It is based on the Meyer-Peter & Müller formula, using an adapted power exponent and it calculates the total sediment load, the sum of suspended and bed load ($kg\ m^{-1}s^{-1}$):

$$S = \alpha D_{50} \sqrt{\Delta g D_{50}} \theta^b (\mu \theta - \xi \theta_{cr})^c \quad (3.3)$$

where α is a calibration coefficient, D_{50} the mean sediment diameter (m), g is the gravity acceleration constant (m/s^2), μ the ripple factor, ξ is the hiding and exposure factor for the sediment fraction considered, θ_{cr} the critical mobility parameter, powers b and c and

$$\theta = \left(\frac{q}{C}\right)^2 \frac{1}{\Delta D_{50}} \quad (3.4)$$

in which θ is the mobility parameter, q is the magnitude of the flow velocity (m/s) and C the Chézy coefficient ($m^{0.5}/s$). The transport rate is imposed in the model as bedload transport due to currents. A Neumann boundary is used for the sediment transport at both the upstream and downstream boundary. This ensures that sediment transport through these boundaries will be near-perfectly adapted to the local flow conditions and very little accretion or erosion should be experienced near the model boundaries.

After each morphodynamic time step, the bed level is dynamically updated using the Exner equation for mass conservation of sediment. This ensures that the hydrodynamic flow calculations are always carried out using the correct bathymetry. At each time step, the change in the mass of bed material that has occurred as a result of the sediment sink and source terms and transport gradients is calculated. This change in mass is then translated into a bed level change. As morphological development takes place on a time-scale several times longer than flow changes, a morphological time-scale factor (MorFac) is typically used to speed up the changes in the morphology. For example, an hydrodynamic time step of 10 seconds results in a morphodynamic time step of 150 seconds when a MorFac of 15 is used.

A minimum water depth of 0.10 m is used for sediment transport (Steijn et al., 2019). Grid cells with smaller water depths were considered to be morphologically inactive. Reactivation can occur due to local water level rise or due to bank erosion. In Delft3D the process of bank erosion by mass failure is excluded (Deltares, 2019b). However, bank erosion processes can be represented by the process of fluvial erosion through extrapolated sediment transport from the primary flow. This is included by applying a simple algorithm: a dry grid cell erodes if erosion occurs in a neighbouring wet grid cell. A cell is dry when the water depth is smaller than 0.01 meter. Moreover, 60% of the erosion in a wet cell was shared with the dry cells, resulting in erosion of the dry cell. This is a quite high but also commonly used value for models where some degree of braiding is supposed to occur (Steijn et al., 2019).

3.3 Schematized model

The model setup, boundary conditions, and parameter values are first presented in this section. Afterwards, the scenarios touched upon in the introduction of this chapter are explained individually.

3.3.1 Model setup

Model parametrization, initial and boundary conditions are based on an existing Delft3D(4) model of the Ayeyarwady River at Nyaungdon in Myanmar. See figure 3.3 for the represented part of the Ayeyarwady River. The schematized model setup describes a 2DH-section of a straight river with oval-shaped mid-channel bar including floodplains. The baseline model includes a domain of eight kilometre long by two kilometre wide. In the model setup, this domain was composed of 320×80 cells, each measuring 25×25 meters. Simulations with finer grid resolutions were executed but the outcomes did not result in significantly more accurate results.

The bathymetry consists of a straight main channel with a length of eight kilometres and a width of one kilometre, see figure 3.5 and figure 3.6. The leftmost boundary of the main channels river bed is located at a height of -5 meters with respect to a reference level and the river contains a constant longitudinal slope of $8.3 \times 10^{-5} \text{ m/m}$. Floodplains with a width of 500 meters can be found on both sides of the main channel. They are located at a height of five meter above the reference level giving the rivers main channel a total depth of ten meters. The transition between the main channel and floodplains has a slope of $1/20 \text{ m/m}$. The top of the bar has a length of 600 meters and a width of 300 meters. The total length of the mid-channel bar is 1000 meters and the total width is 500 meters. Its height is seven meters above the river bed and it gradually diminishes towards the river bed with a slope of $1/15 \text{ m/m}$ in cross-channel direction and a slope of $1/30 \text{ m/m}$ in long-channel direction.

The baseline model contains an uniform hydraulic roughness (Manning's n) for both the active river channel, mid-channel bar and floodplains, $n = 0.030 \text{ s/m}^{1/3}$. This is a commonly used value for rivers. It represents the bed roughness of a clean and straight river without rifts or deep pools (Chow, 1959). Furthermore, the schematization contains an upstream discharge boundary condition and a downstream water level boundary condition. The discharge regime is based on the discharge regime of the Ayeyarwady River case study. We use the same simplified hydrograph as Steijn et al. (2019) did (shape of orange line in figure 3.2). The magnitudes of the discharge wave is idealized for our schematized bathymetry. The discharge is decreased to have a maximum of half a metre of water on the floodplains during the wet season. The applied discharge wave can be seen in figure 3.7A. We chose to have a dry period first, where the mid-channel bar is not submerged, to let the initial morphology develop to a slightly more natural state before the wet period arrives. The corresponding downstream water level boundary is derived using the Chézy formula in combination with Manning's n , see figure 3.7B.

As transport formula, the *General formula* in Delft3D-FM is used. The parameters required for this formula are based on a morphological study conducted by Deltares at the site of the case study (Steijn et al., 2019). The exponent b is set to 2, physically meaning that the sediment transport is related to the velocity to the

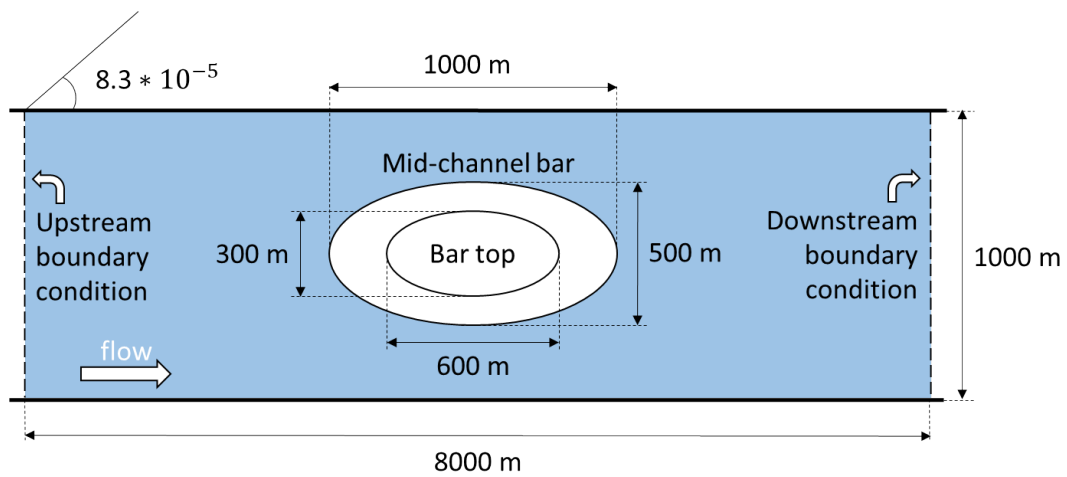


Figure 3.5 – Overview of schematized model (Not to scale). Floodplains are not shown.

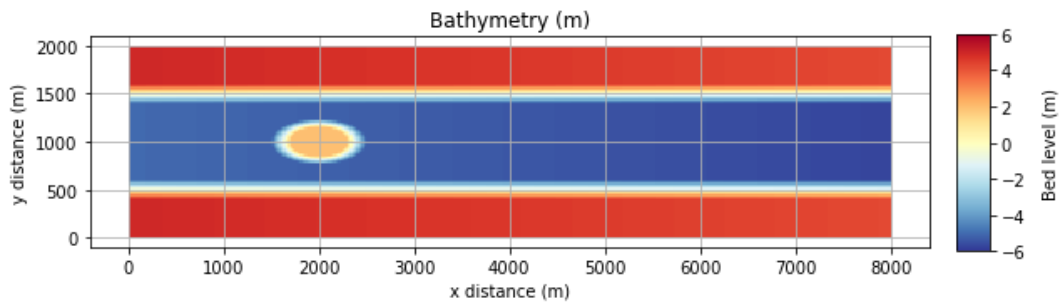


Figure 3.6 – Bathymetry of schematized model. Colorbar shows bed level in meters.

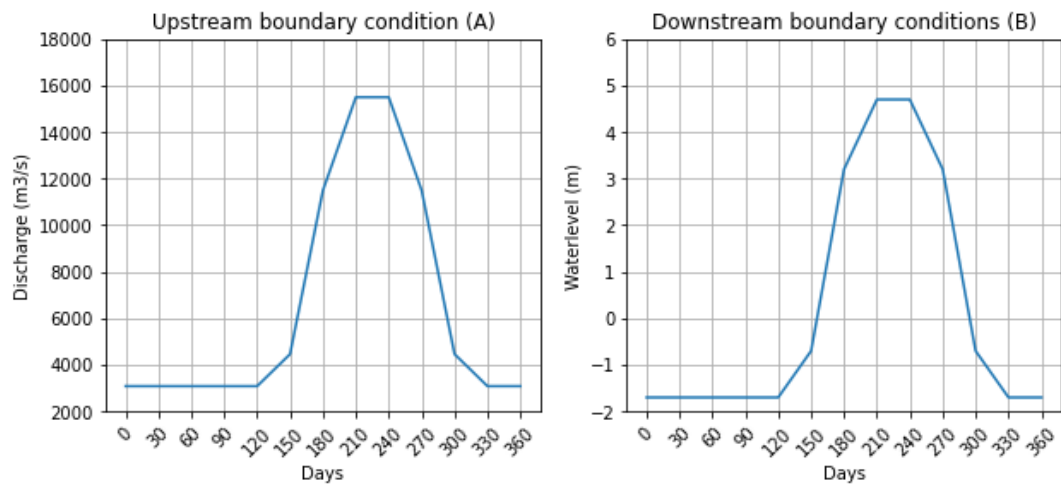


Figure 3.7 – Upstream (A) and downstream (B) boundary conditions of schematized model.

Table 3.1 – Overview of scenarios. SM: schematized model. ARM: Ayeyarwady River model.

Scenario	Channel roughness (Manning's n [$s/m^{1/3}$])		Vegetation formulation on mid-channel bar
	SM	ARM	
Reference	0.030	Variable: 0.027-0.030	-
Manning	0.030	-	Manning's $n = 0.070 s/m^{1/3}$
Static vegetation	0.030	Variable: 0.027-0.030	Static roughness predictor by Baptist (2005) with vegetation characteristics: $h_v = 0.75 m, m = 50 m^{-2}, D = 0.02 m, C_D = 1 (-)$
Dynamic vegetation	0.030	Variable: 0.027-0.030	Roughness predictor by Baptist (2005) with dynamic vegetation procedure and vegetation characteristics: $h_v = 0.75 m, m = 50 m^{-2}, D = 0.02 m, C_D = 1 (-)$

power 4. Exponent c was set to 0 to remove the influence of the ripple effect (μ) and the critical shear stress from the sediment transport model. No critical shear stress for sediment transport is used because (fine) sediment is transported during both low and high flow conditions in dynamic braided rivers (Hydro-Informatics Centre, 2017). The proposed calibration coefficient alpha is decreased from 8 to 2 to end up with a realistic yearly migration distance of the bar (maximum a couple of hundred meters) and to prevent excessive growth of the bar-tailed limbs. Hence, the resulting transport equation is: $S = 2D_{50}\sqrt{\Delta g D_{50}}\theta^2$. Furthermore, a morphological spin-up time of one hour is used. A constant median grain size of 0.35 mm is used throughout the whole domain and a MorFac-value of 15 is used to speed up the morphological calculations. This value is based on the study of Steijn et al. (2019) as well. They used a rather modest MorFac-value to avoid unrealistic sediment transport pulses.

The baseline model as described in this section is used as *reference scenario*. The modelled bar development and shape is compared with literature and individual examples found in nature. To be able to easily compare the several scenarios, the outer bar edges are determined. We assume that an area is defined as bar if it is submerged for a maximum period of 180 days (\pm half year). This corresponds to a water level of about -1 meter, see the hydrograph in figure 3.7B. Hence, a bed elevation threshold of -1 meter is used.

3.3.2 Manning scenario

In the *mannings scenario*, Manning's n is used to represent vegetation on the mid-channel bar in Delft3D-FM. We used a value of $n = 0.070 s/m^{1/3}$ for vegetation. Vegetation was placed on top of the mid-channel bar where the bed level is $+2$ meters. A Manning's n of $0.070 s/m^{1/3}$ has been chosen to represent the roughness of vegetation on the mid-channel bar. This value corresponds to the *normal* roughness of medium to dense brush on floodplains (Chow, 1959). Internal model parameters, the flow velocity, bed shear stress and sediment transport rate, and model output, bathymetry data, were compared to those of the reference scenario to identify the competence of Delft3D-Flexible Mesh to simulate the development of vegetated mi-

grating mid-channel bars in dynamic rivers using Manning’s roughness to represent vegetation.

The sensitivity of the *manning scenario*’s simulated channel morphology was assessed to changes in Manning’s n . This analysis is used to verify that the findings of the *manning’s scenario* are unbiased due to this model parameter choice and/or characteristics of the modelled system. Simulations were conducted with three different Manning’s n values, respectively 0.045, 0.070 and 0.110 $s/m^{1/3}$. These values correspond to the *minimum*, *normal*, and *maximum* roughness of medium to dense brush on floodplains according to Chow (1959). All other model settings are kept the same as in the reference scenario.

3.3.3 Static vegetation scenario

In the *static vegetation scenario*, the roughness predictor of Baptist (2005) is used to represent vegetation on the mid-channel bar in Delft3D-FM. The following parameters were used: vegetation height h_v is 0.75 m, vegetation density n is 1, number of stems is 50 and diameter is 0.02 m, and drag coefficient C_D is 1 (F. Huthoff, personal communication, 21 January 2020). These parameters do more or less describe the characteristics of young vegetation found on mid-channel bars in the Ayeyarwady River. Figure 2.4 shows how this translates to a Chézy coefficient (hydraulic roughness) and bed shear stress. Vegetation was placed on top of the mid-channel bar where the bed level is +2 meters. Again, model outcomes were compared to those of the reference scenario to identify the competence of Delft3D-Flexible Mesh to simulate the development of vegetated migrating mid-channel bars in dynamic rivers using the rigid vegetation model to represent vegetation.

The sensitivity of the *static vegetation scenario*’s simulated channel morphology was assessed to changes in the vegetation characteristics. The simulations are used to verify that the findings about the *static vegetation scenario* are unbiased due to these model parameter choices and/or characteristics of the modelled system. Three different vegetation densities and three different vegetation heights are used in this analysis. The vegetation characteristics as used in the base scenario are multiplied and divided with a factor two leading to respectively 0.5, 1.0 and 2.0 for the vegetation density ($1/m$) and 0.375, 0.75 and 1.5 for the vegetation height (m). All other model settings are kept the same as in the reference scenario.

3.3.4 Dynamic vegetation scenario

To ensure that a vegetated mid-channel bar can dynamically migrate through a river system, a procedure was developed to update the location of the vegetation during a morphodynamic simulation. We updated the location of the vegetation in Delft3D-FM using a Basic Model Interface (BMI) by retrieving internal model parameters from Delft3D-FM after each predefined vegetation update interval, calculating the new location of the vegetation based on simple conditions and restarting Delft3D-FM with updated information.

First, a description of the BMI is given which is used to couple the proposed *dynamic vegetation procedure* to Delft3D-FM. Afterwards, an explanation is given about the conditions to update the location of the vegetation during a simulation. The last section elaborates on how we analysed the robustness of the proposed procedure.

Model coupling

The *dynamic vegetation procedure* in Python will be coupled to Delft3D-FM using the Basic Model Interface (BMI) developed by the Community Surface Dynamics Modeling System (Peckham et al., 2013). The BMI can be seen as a standardized set of functions or methods. It facilitates the exchange of information between models. Besides, it allows complete control over model time steps and variables while conducting a simulation (Peckham et al., 2013). In short, a BMI ensures that conventional models can be interrogated and internal parameters can be changed while running. In general, a BMI-environment must be specifically created for each model-environment because each model has a different internal structure (e.g. the solver and data structure). However, it does negate the need to modify the source code of the model itself. The implementation of the BMI-environment for Delft3D-FM has been constructed by Deltares. The BMI will be used to pause Delft3D-FM at the beginning of each predefined vegetation update interval such that data can be retrieved from Delft3D's memory by the *dynamic vegetation procedure* in Python. After updating the location of the vegetation, the simulation in Delft3D-FM will be restarted with updated memory/information about vegetation. Figure 3.8 shows how the connection between Delft3D-FM and python is constructed.

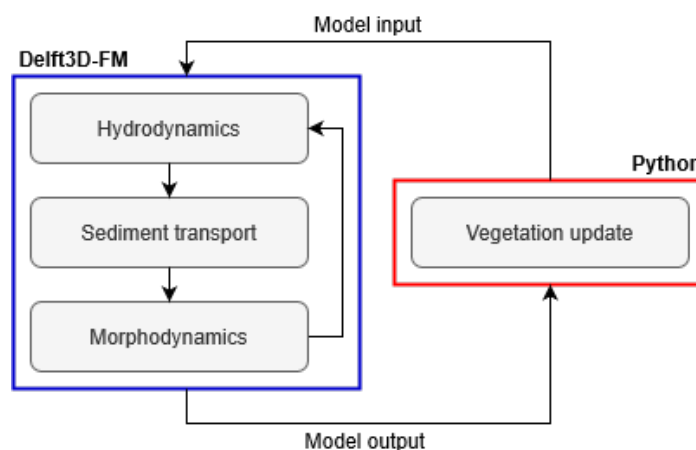


Figure 3.8 – Basic Model Interface.

Dynamic vegetation procedure

Initially, vegetation is placed on top of the bar where the bed level is +2 meters. The new location of the vegetation is determined at the beginning of each vegetation update interval. The following conditions are used:

1. The vegetation is removed from the modelling domain where the maximum flow velocity during the last vegetation update interval (T_{veg}) exceeds a certain user-defined critical flow velocity (u_{cr}).
2. The vegetation is returned to the modelling domain where the maximum depth of inundation does not exceed a certain threshold water depth at the end of each year in the dry period.

We use the flow velocity as critical threshold for vegetation removal because the link between vegetation and the flow regime is frequently described in literature (Moggridge and Higgitt, 2014; Vargas-Luna et al., 2015; Gurnell et al., 2016). The second condition of the procedure is valid for our case, because vegetation on the bars in the Ayeyarwady River is primarily disconnected from the flow during low-flow conditions. Hence, we do not have to return the vegetation gradually during the year as long as the vegetation is relocated when the high-flow season starts. A scenarios analysis is used to investigate the response of the river system to different critical flow velocities for vegetation removal. Therefore, the simulated flow velocities on the mid-channel bar during the peak of the discharge wave of the *static vegetation scenario* were analysed to come up with a range of realistic critical flow velocities. The threshold water depth for the second condition is set to 0.02 meter. This value should be larger than the thin layer of water commonly present on *dry* grid-cells in numerical morphodynamic models to prevent that vegetation is not returned to regions which are actually dry. Such a thin layer of water is often required for computational stability purposes (Deltares, 2019a). To be able to have several vegetation update intervals (T_{veg}) within the peak of the hydrograph (see figure 3.7) we chose to have an initial duration of the vegetation update interval of one week (F. Huthoff, personal communication, 12 March 2020).

Physical processes, the location of the vegetation and development of the bed are graphically displayed to determine whether they behave in a natural manner and to identify the differences between the simulations. Bar and vegetation dimensions were quantified to determine the differences between the model runs as well. Therefore, we defined three metrics: the migration distance of the bar and vegetation after one year and the total vegetated area on the bar over time. The migration distance is defined as the downstream migration distance of the leftmost corner of the bar or vegetation patch. The vegetated area on the bar was calculated after each vegetation update interval to be able to study the development of this metric over time. Although somewhat arbitrary, these metrics allows for an quantitative comparison between different simulations.

Sensitivity analysis

The sensitivity of the simulated model behaviour (morphology and location of vegetation) is analysed to changes in the duration of the vegetation update interval (T_{veg}) to identify the robustness of the proposed *dynamic vegetation procedure*. This analysis is also used to gain insight in the determination of the critical flow velocity for vegetation removal and the duration of the vegetation update interval.

The time-scale of the retreat and growth of vegetation is typically much longer than the time-scale of changes in hydrodynamic and morphodynamic conditions (Monegaglia, 2017). Therefore, we chose to have a minimum duration of the vegetation update interval of 2 days. Hence, in addition to the vegetation update interval of 7 days (of the previous section), we also tested intervals of 2 days, 4 days, 15 days and 30 days for all used critical flow velocities.

3.4 Ayeyarwady River model

The schematized model set-up was expanded such that it captured the actual Ayeyarwady River dimensions (see figure 3.3) to test the proposed *dynamic vegetation procedure*. Subsequently, this section elaborates on the model set-up and the conducted scenarios.

3.4.1 Model setup

An existing hydrodynamic (not morphodynamic) Delft3D-FM model of the Ayeyarwady River at Nyaungdon was used. The model was constructed by Stoeten (2019). It is an adapted version of the previously mentioned Delft3D(4) model constructed by Steijn et al. (2019). It contains the same model settings as mentioned in section 3.2 of this report. Stoeten (2019) updated the computational grid and bathymetry of the model to study the hydrodynamic impact of a sandbank in the Pan Hlaing river (tributary of the Ayeyarwady River). The morphological settings of the Delft3D(4) model of Steijn et al. (2019) were added to the Delft3D-FM model to calculate morphodynamics. No re-calibration of these model settings was performed. However, we compared the outcomes of the Delft3D-FM model with the outcomes of the Delft3D(4) model for a morphological run without vegetation. They showed similar behaviour on a large scale. However, on a small scale, they showed minor differences. Nevertheless, it was beyond the scope of this study to identify the causes for these differences.

The model setup describes a river section 30km up- and downstream of Nyaungdon (see figure B.1 of Appendix B). The model domain was composed of a combination of a curvilinear and triangular network of grid cells due to the complexity of the bifurcation point and the multi-channelling of the river in the modelled section (Stoeten, 2019). The network contains a refinement at the bifurcation point of the Pan Hlaing river. This refinement has not been removed for the modelling phase of this study. The composition of the grid can be seen in figure B.2. The bathymetry of the model was predominantly taken from the Delft3D(4) model. This bathymetry was constructed from input data from various sources: bathymetric data collected by DWIR from 2017, bathymetric data collected by Shore Monitoring in February 2018 and ESRI's World Terrain service data (Steijn et al., 2019). Stoeten (2019) added newly collected bathymetric data at the entrance of the Pan Hlaing river (January 2019) to the bathymetry of the model to study the influences of a newly formed sandbank. The model also includes recently constructed groynes (2016-2017) at the inner bend north of Nyaungdon, see figure B.1.

Stoeten (2019) recalibrated the bed roughness of the hydrodynamic model to achieve realistic water levels at the upstream boundary and at Nyaungdon city for high discharges. He ended up with a variable roughness map of *Manning's n* values between 0.027 and 0.030 for the channel bed and a value of 0.100 for the floodplains. The roughness map was again adapted for the morphodynamic modelling phase of this study by replacing all *Manning's n* values of the floodplains by the nearest *Manning's n* values of the channels, see figure B.4. Some roughness transitions were smoothed to avoid abrupt changes in the bed roughness. Abrupt transitions can potentially negatively influence sediment transport rates in the system.

The simplified yearly hydrograph of Steijn et al. (2019) was used as upstream discharge boundary condition at Danubyu, see figure B.3. Furthermore, a downstream water level at Pentanaw (main channel) and a downstream water level at Mezali (side channel) were used to close the system. All locations are mentioned in figure B.1.

The morphological settings of the model are copied from the Delft3D(4) model of Steijn et al. (2019). Hence, the *General formula* in Delft3D-FM was used to calculate the sediment transport. The corresponding settings were: calibration coefficient $\alpha = 8$, exponent $b = 2$ and exponent $c = 0$. The morphological spin-up time was set to 1 hour, a constant median grain size of 0.35 mm was used throughout the whole domain and a MorFac of 15 was used to speed up the morphological calculations.

3.4.2 Scenarios

The *dynamic vegetation procedure* of section 3.3.4 was implemented in the model setup as described in the previous section. We ran our *dynamic vegetation scenario* including removal and return of vegetation and two control runs: one without vegetation (*reference scenario*) and one with static vegetation in space and time (*static vegetation scenario*). The model settings of these scenarios in the Ayeyarwady River model are shown in table 3.1. An iterative process (*trial-and-error*) was used to find a suitable combination of the critical flow velocity for vegetation removal and the duration of the vegetation update interval (input parameters of the *dynamic vegetation procedure*). We examined the maximum flow velocities on the mid-channel bar during the peak of the discharge wave in the *static vegetation scenario* to come up with realistic critical flow velocity for vegetation removal (u_{cr}) as starting point. Furthermore, we initially used a vegetation update interval (T_{veg}) of 30 days for engineering purposes. The number of interruptions of the model should be minimized to prevent a significant increase of the calculation time. Afterwards, we used the patterns about the interconnectedness of the two input parameters of the procedure, identified in section 4.1.5, to guide the selection process of a suitable combination to simulate natural morphological behaviour.

The differences between the scenarios were analysed to determine to what extent the proposed *dynamic vegetation procedure* can be used to improve model results in a real-life case study. Therefore, we compared the physical processes (flow velocity, bed shear stress and sediment transport rate), the location of the vegetation and bar and the morphological development of the bed. An area is defined as bar if it is submerged for a maximum period of 180 days (\pm half year). Hence, a bed elevation threshold of 1.7 meter was used. This value corresponds to about the mean water level around the bar during low-flow conditions, see figure B.3.

Chapter 4

Results

Part one of this chapter presents the results of the schematized model and part two presents the results of the Ayeyarwady River model.

4.1 Schematized model

This section contains the results of the scenario analysis to gain more insight in our ability to simulate the development of vegetated migrating mid-channel bars. First, we shortly analyse the model results of the period till 120 days of all scenarios, see table 3.1 for a brief recap of the scenarios. These results are the same because the mid-channel bar is not flooded under low-flow conditions. As of section 4.1.1, we only focus on the differences between the model results starting from 120 days when the discharge increases. In section 4.1.1, the *reference scenario* is analysed. Thereafter, sections 4.1.2 and 4.1.3 elaborate on the numerical simulations of the *manning scenario* and *static vegetation scenario*. The results of the sensitivity analysis are presented afterwards in section 4.1.4. The last section elaborates on the results of the *dynamic vegetation scenario*.

Figure 4.1 shows that only minor morphological changes occurred during low flow conditions (upto 120 days) compared to the initial bathymetry (straight channel with oval-shaped mid-channel bar). A deepening of the surrounding channels and a steepening of the upstream bar flanks occurred. This is due to local flow divergence leading to higher bed shear stresses and associated transport rates. Deposition of sediments led to the development of bar-tailed limbs at the downstream side of the bar. Both bar-tailed limbs migrated faster, and with the same rate, than the higher bar center, resulting in expansion of the bar length. The equal migration rate of the bar-tailed limbs indicated that the discharge was evenly divided between both surrounding channels. Besides, a bar-top hollow developed at the centreline just downstream of the bar because this area was not exposed to sedimentation. Behind the bar (more downstream), the flow converged again resulting in the formation of a so-called scour hole or pool. Just after the scour hole, where an abundance of sediment was present, a bed level perturbations developed leading to the formation of a new mid-channel bar. This bar also propagated in downstream direction. This can be seen at the **X** in figure 4.1.

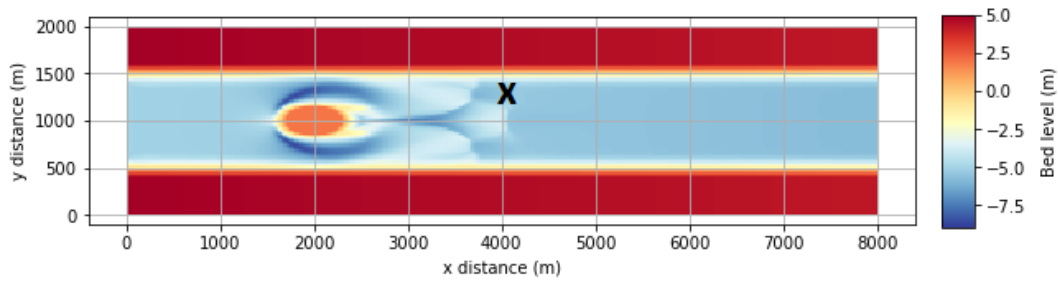


Figure 4.1 – Development of the bed after 120 days for low-flow conditions when the bar is not submerged. **X** shows the formation of a new mid-channel bar. Flow from left to right.

4.1.1 Reference scenario

Panel *A* of figure 4.2 shows the development of the channel morphology for the *reference scenario* after 360 days. In addition, the state of relevant physical processes (flow velocity, bed shear stress and sediment transport) after 240 and 360 days is attached in appendix C.

In general, the evolution and final shape of the mid-channel bar and river planform are in line with literature (Ashworth, 1996; Rice et al., 2009; Schuurman, 2015; Zhang et al., 2020). Under high flow conditions (as of 120 days), when the bar was totally submerged, the mid-channel bar started to migrate in downstream direction. The increase in flow (velocity) resulted in an increase of the bed shear stress on top of the bar. Consequently, this led to an increase of the sediment transport rate and erosion at the upstream side of the bar. The eroded sediments were again (partly) deposited at the downstream side resulting in downstream migration of the bar and the formation of bar-tailed limbs. As a result, the mid-channel bar started to obtain a more natural shape. It changed from a perfect oval-shaped bar to a more natural lozenge-shaped bar as defined by Hooke and Yorke (2011). They gave the following description of a mid-channel bar: ‘free bar in middle of channel, flow both sides; diamond- or lozenge-shaped; can be vegetated’ (p. 5). Some real-life examples of these lozenge-shaped bars were shown in figure 2.2 of chapter 2.

4.1.2 Manning scenario

Panel *B* of figure 4.2 shows the development of the channel morphology for the *manning scenario* after 360 days. Compared to the *reference scenario*, significantly different morphological behaviour occurred when the flow intensity started to increase and the bar became flooded. Heavy erosion occurred at locations where vegetation was specified on the mid-channel bar. An erosion hole with a depth of -8 meters developed. At this level, the user-defined maximum erodible sediment layer thickness of 10 meters was reached (bar is initially modelled at +2 meters). Heavy erosion of the bar occurred through high bed shear stresses. The maximum bed shear stresses were at least doubled compared to the reference scenario, see panel *B* of figure 4.3. Instead bed shear stresses should actually become lower through the presence of vegetation (Gurnell et al., 2016). The large bed shear stresses induced high sediment transport rates. This led to the rapid erosion of the mid-channel bar.

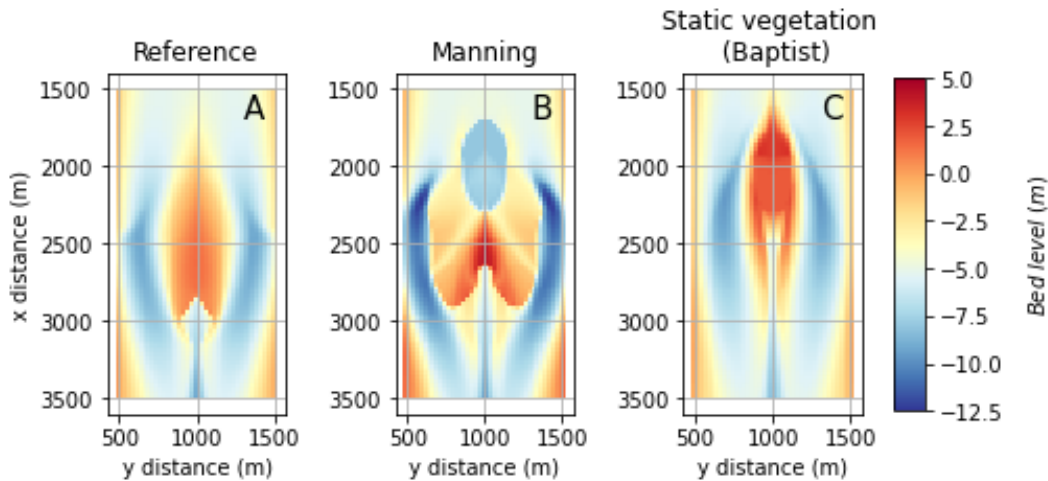


Figure 4.2 – Evolution of the river morphology after one year for the reference, manning and static vegetation scenario. Flow from top to bottom of figure.

The flow velocity and the hydraulic resistance are the main factors determining the bed shear stress and they are positively correlated (Deltares, 2019a). Since the flow velocity was not very large in the vegetated area, a non-realistic conversion of the hydraulic (vegetation) resistance to the bed shear stress is likely to be the main reason for high bed shear stresses in our model. In figure 2.4, we already saw that an increase of Manning’s n does lead to an higher flow resistance and lower flow velocity. But it did not result in a decrease of the bed shear stress and associated sediment transport rate (erosion) with respect to the *No vegetation* situation. This leads to an overestimation of the bed shear stress and sediment transport (erosion) inside vegetated areas.

Although figure 2.4 shows that the use of Manning’s roughness does not result in lower bed shear stresses and sediment transport rates in vegetated areas, the figure does not clearly show the cause for the very high stresses in our model (panel *B* of figure 4.3). This is due to the fact that figure 2.4 only shows a hypothetical equilibrium situation of the system. The sudden transition between a bare and a vegetated area (resp. Manning’s $n = 0.030 \text{ s/m}^{1/3}$ and $n = 0.070 \text{ s/m}^{1/3}$) is the main reason for the overly high bed shear stress and sediment transport rate in our model. At this transition, the flow needs to slow down suddenly according to the new equilibrium velocity. For example, see the difference in flow velocity between the red and black line at a water depth of 3 meters in figure 2.4. The flow velocity is not directly reduced to its new equilibrium state. Hence, relatively high flow velocities are present in the vegetated areas consequently resulting in very high bed shear stresses and sediment transport rates, see lower two panels of figure 2.4.

Also, figure 4.2 shows that the vegetation resistance did not migrate along with the development of the mid-channel bar. It was not removed from areas which experienced heavy erosion and it did not return to downstream areas where the abundance of eroded sediments from the erosion hole deposited again. However, it remained at the initial location of the bar.

An overview of the state of the other relevant physical processes (flow velocity and sediment transport rate) after 240 and 360 days is attached in appendix C.

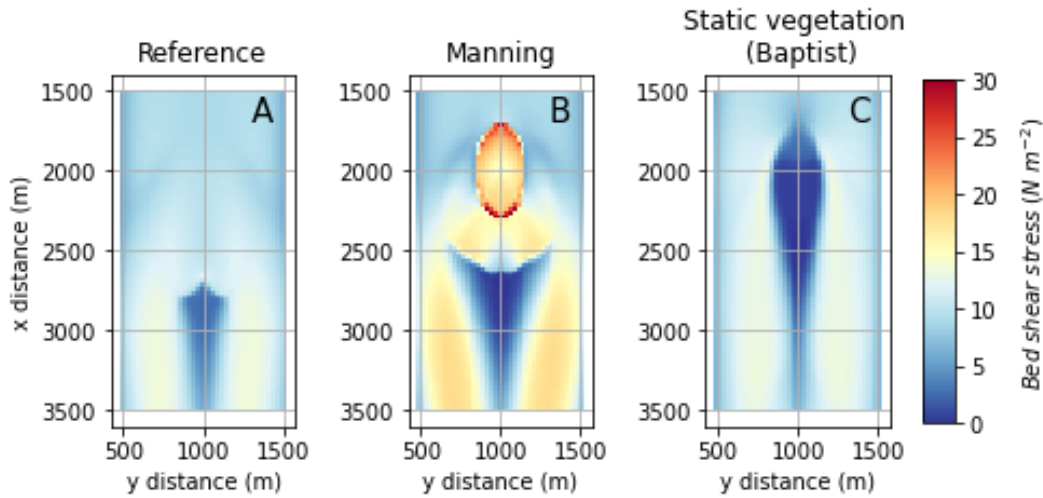


Figure 4.3 – State of the bed shear stress after 240 simulated days (during high flow conditions) for the reference, manning and static vegetation scenario. Flow from top to bottom of figure. The color bar is truncated to show a maximum stress of 30 Nm^{-2} .

4.1.3 Static vegetation scenario

Panel *C* of figure 4.2 shows the development of the channel morphology for the *static vegetation scenario* after 360 days. Under high flow conditions (as of 120 days), the mid-channel bar started to behave more dynamic compared to the first 120 days. However, during the year, the front of the bar still remained largely at its initial location. Only minor erosion of the upstream bar flanks occurred during high flow conditions, because the bed shear stresses remained relatively low due to vegetation (see figure 4.3). Sediments deposited at the downstream side of the bar where the flow velocities were relatively low leading to the formation of bar-tailed limbs at the lee of the bar. Hence, a bar-top hollows developed at the centreline just downstream of the vegetated mid-channel bar. This is in compliance with observations in the field as previously shown in figure 2.2.

Furthermore, a small height increase of the upstream section of the bar was present after one year, see figure 4.4. It is caused by a decrease of the sediment transport rate and associated deposition of sediments in vegetated areas. This height increase occurs in nature as well. Schuurman (2015) stated that the upstream part of fully developed bars are commonly the oldest and highest part with a steep erosive upstream edge bifurcating the river. Also, the bar width slightly decreased, see figure 4.4. This can be contributed to flow divergence in the channels around the bar due to the vegetation. Flow divergence led to higher bed shear stresses at the bar edges resulting in more erosion. An overview of the state of the flow velocity and sediment transport rate after 240 and 360 days is attached in appendix C.

Although the modelled mid-channel bar did show some migration (modelled vegetation is not totally blocking the flow), the bar did not migrate as a whole, e.g. the upstream most location of the bar in figure 4.4 was hardly changing. This had to do with the characteristics of the modelled vegetation. The present vegetation was modelled as a static and non-erodible component in space and time. In reality,

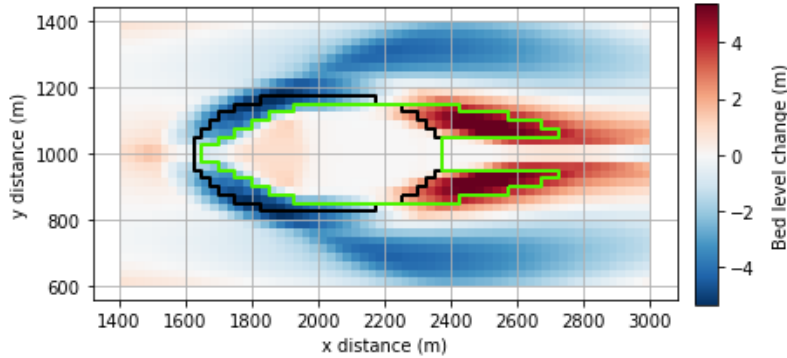


Figure 4.4 – Bed level change (m) after one year ($T = 360$) with respect to the start of the simulation ($T = 0$) of the *static vegetation scenario*. The black and green lines show respectively the initial and new location of the mid-channel bar.

vegetation and morphology are highly dynamic and strongly interconnected, meaning that they both actively affect each others development (Moggridge and Higgitt, 2014). Apparently, this connection should be considered when a dynamic braided river system is desired.

4.1.4 Sensitivity analysis

The sensitivity analysis is used to determine how sensitive the systems behaviour (morphological development) is to changes in the input parameters of the static vegetation formulations. This analysis is also used to verify that the findings from the previous sections (4.1.2 and 4.1.3) are unbiased due to our model parameter choices and/or characteristics of the modelled system.

In this section, we only show bed levels (differences) between the several simulations in this sensitivity analysis. For sake of clarity, we included the state of the physical processes of the simulations in figures C.3, C.4 and C.5 of appendix C.

Manning scenario

Figure 4.5 illustrates the bed level difference after one year for two Manning’s n values with respect to the *manning scenario*. For sake of clarity, the state of the physical processes is shown in figure C.3 of appendix C. It shows that a change in *Manning’s n* resulted in a significantly different morphological development of the mid-channel bar. An higher *Manning’s n* results in a lower Chézy coefficient. This caused a faster formation and larger depth of the scour hole at the location of the vegetation, because higher bed shear stresses were present leading to more sediment transport away from the bar. A lower *Manning’s n* resulted in an opposite response of the system. The eroded sediment deposited again somewhere downstream. Hence, a different development of the downstream side of the bar was present. Furthermore, in all simulations, the hole developed at the same location and it was present during the whole simulated period.

Hence, we can conclude that the unrealistic morphological behaviour had nothing to do with the chosen parameter value of *Manning’s n* . But, in general, it has to do

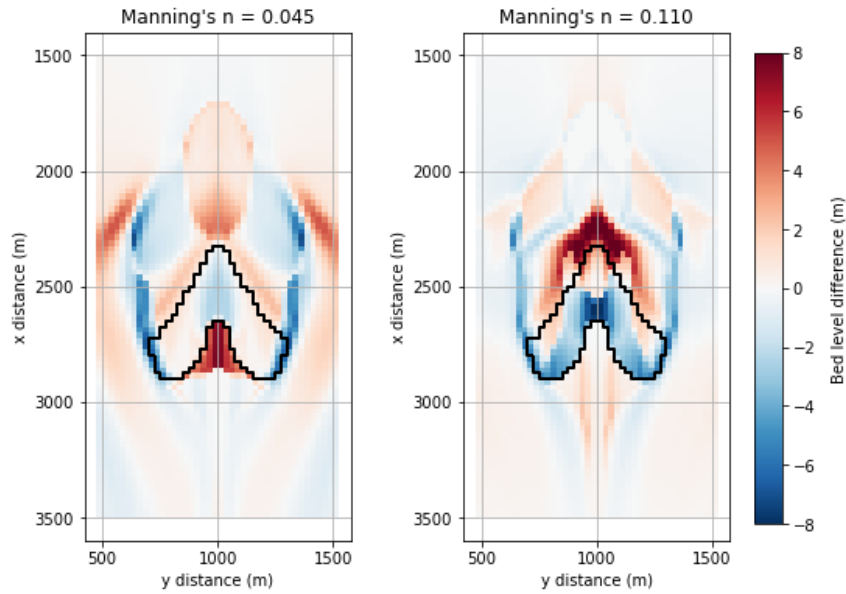


Figure 4.5 – Bed level difference after one year for two Manning’s n values (0.045 and 0.110) compared to the *manning scenario* with Manning’s $n = 0.070$. Black line shows the location of the mid-channel bar in the *manning scenario* as described in section 4.1.2.

with this kind of resistance formulation to represent vegetation in a morphodynamic model. Thus, we do no longer use this roughness formulation to represent vegetation resistance.

Static vegetation scenario

Figure 4.6 shows that a difference in vegetation density had a notable effect on the morphological development of the mid-channel bar. A lower vegetation density had a smaller ability to resist the movement of the water. Hence, high flow velocities could penetrate further onto the vegetation patch on the mid-channel bar. This led to higher bed shear stresses and associated sediment transport rates (erosion) at downstream sections of the bar. These sediments subsequently deposited on the middle section of the bar where low flow velocities were dominant leading to an increase of the bar height. Also, the eroded sediments deposited on the sides and bar-tailed limbs of the bar resulting in a wider bar, see left panel of figure 4.6. Opposite behaviour occurred in the situation with higher vegetation densities.

Figure 4.7 illustrates the bed level difference after one year for two values of the vegetation height (0.375 and 1.50) compared to *static vegetation scenario* ($h = 0.75$). It shows that the bar started to behave like a bare non-vegetated bar when the vegetation height was low and that the location of the bar was static over time (no migration) when the vegetation height was fairly high. For example, when the vegetation height was 0.375 meter, the bar showed significantly more migration than the bar in the *static vegetation scenario*. The front of the bar became up to 3-4 meters lower. This was caused by the ability of the flow to penetrate into the vegetation patch on the bar. Higher flow velocities induced higher bed shear stresses, leading to erosion of the bar front.

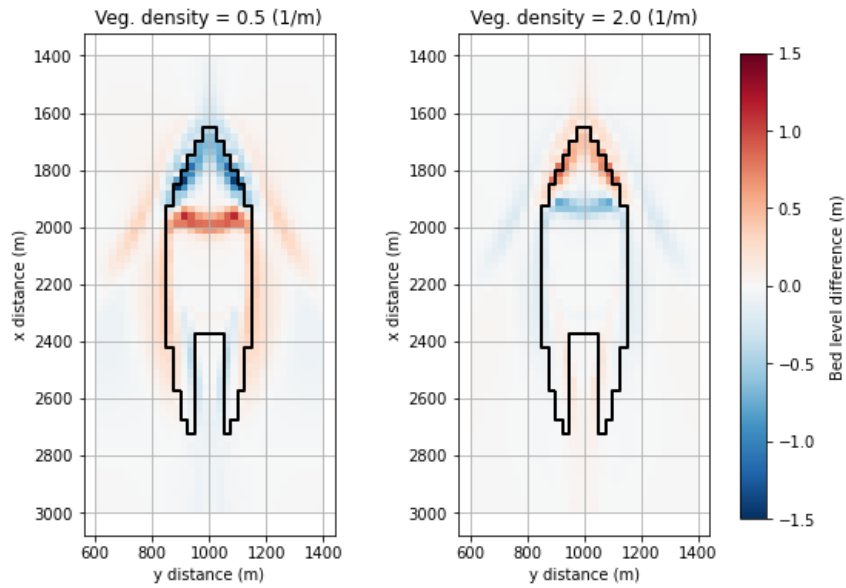


Figure 4.6 – Bed level difference after one year for two different vegetation densities (0.5 and 2.0) compared to the *static vegetation scenario* with a vegetation density of 1. Black lines show the location of the mid-channel bar in the *static vegetation scenario*.

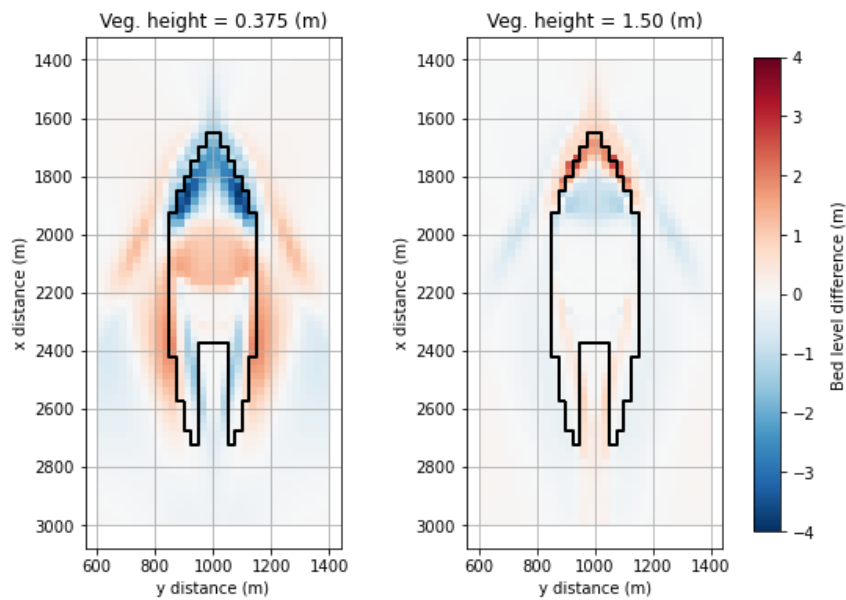


Figure 4.7 – Bed level difference after one year for two different vegetation heights (0.375 and 1.50) compared to the *static vegetation scenario* with a vegetation height of 0.75. Black lines show the location of the mid-channel bar in the *static vegetation scenario*.

We can conclude that the density and height of (static) vegetation are only minor indicators for the dynamic potential of mid-channel bars in morphodynamic models. For low densities or heights, bars did show some migration. Potentially, this can be used for modelling minor migration of a bar over a short time-scale. However, a bar with high or dens vegetation was hardly dynamic. In reality, these vegetated bars do migrate due to bank failure and vegetation erosion processes (Bywater-Reyes et al., 2018). Hence, vegetation dynamics (removal and return) should be considered when modelling the morphodynamics of a vegetated migrating mid-channel bar. Moreover, this indicates that there is no need to adapt our previously chosen vegetation characteristics for the remainder of this study, because the standstill of the bar had only to do with the static character of the modelled vegetation.

4.1.5 Dynamic vegetation scenario

This section presents the results of the *dynamic vegetation scenario*. The first subsection elaborates on the determination of the critical flow velocity for vegetation removal. The second subsection shows the results of the scenario analysis to investigate the response of the system for different critical flow velocities. Thereafter, the results of the sensitivity analysis for changes in the duration of the vegetation update interval are presented.

Critical flow velocity for vegetation removal

The flow velocities on the mid-channel bar during the peak of the discharge wave of the *static vegetation scenario* were analysed to come up with a range of realistic critical flow velocities for vegetation removal. Therefore we used panel *C* of figure C.1. As vegetation is predominantly removed at the front and upstream flanks of (mid-channel) bars in nature through failure of the bar edge (Li et al., 2014), we examined the maximum flow velocities in these areas. Accordingly, we tested critical flow velocities within the range of 0.7 to 1.1 m/s with increments of 0.1 m/s.

Rule-based vegetation dynamics

Figure 4.8 shows that the general morphological development of the mid-channel bar is in line with the development of the bar in the *static vegetation scenario* when vegetation can resist relatively high critical flow velocities. The mid-channel bar slightly migrated in downstream direction and the upstream section of the bar became higher due to the deposition of sediments in the vegetation patch. When the vegetation was easily removed (e.g. $u_{cr} = 0.7$ m/s), the bar started to behave like a bare (non vegetated) bar. The bed level differences after 360 days with respect to the *static vegetation scenario* are shown in the right column of figure 4.8. It shows that erosion at the upstream side of the bar was highly dependent on the chosen critical flow velocity for vegetation removal. The lower the critical flow velocity, the more removal of vegetation at the upstream side of the bar. Consequently, these areas were exposed to higher bed shear stresses and associated sediment transport (erosion). This led to migration of the bar, see also table 4.1. The amount of sediment deposition at the downstream side of the bar and bar-tailed limbs was directly related to the magnitude of the upstream erosion. Moreover, panel *D* of figure 4.8 shows the formation of gullies on the mid-channel bar during high-flow conditions.

The development of these gullies had to do with the vegetation removal on the bar. This will be thoroughly explained in the next section.

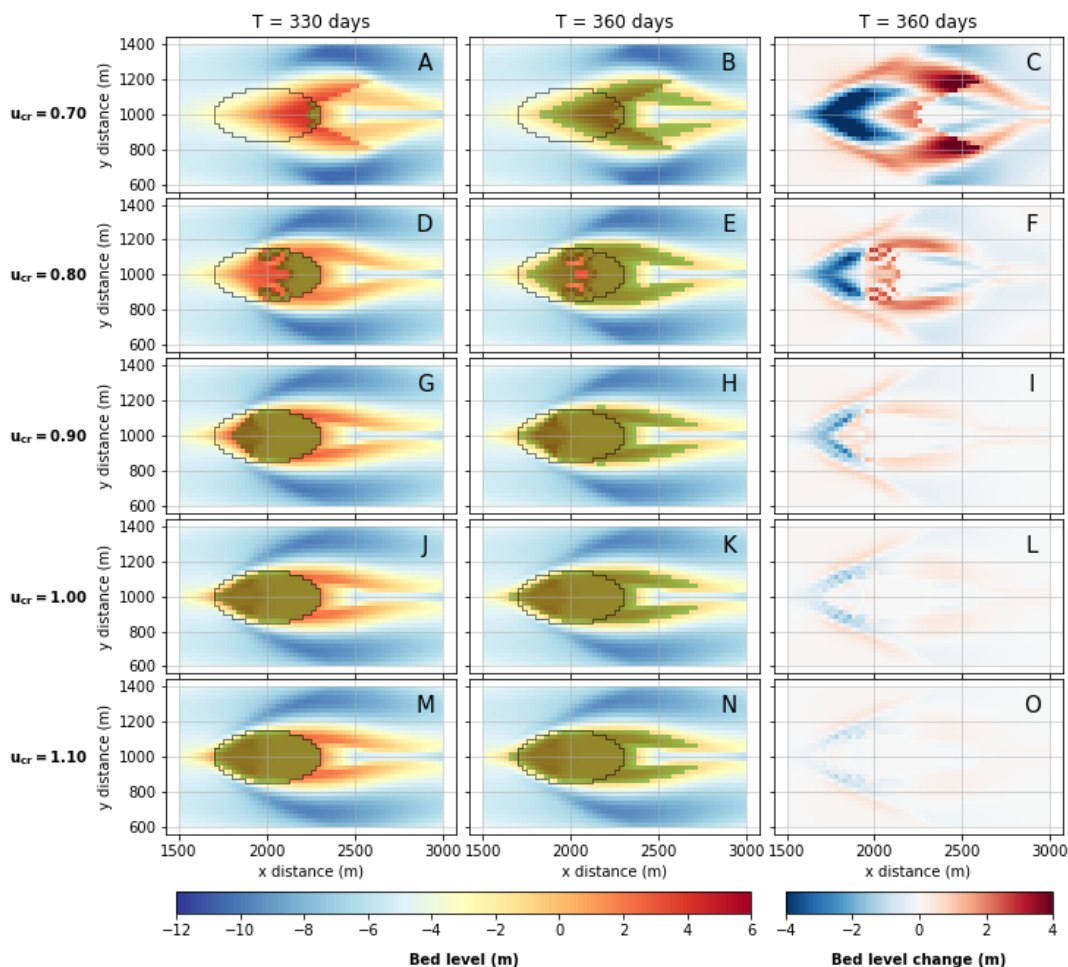


Figure 4.8 – Morphological development of river bed after 330 days (left column) and 360 days (middle column) and bed level differences w.r.t. static vegetation after 360 day (right column) for different values of the critical flow velocity for vegetation removal indicated on the left side ($T_{veg} = 7$ days). Green overlaid area shows the vegetation locations after 330 and 360 days and the black circle shows the initial location of vegetation. Flow from left to right.

Figure 4.8 and 4.9 show that the general pattern of the removal and return of vegetation on the mid-channel bar was the same for different critical flow velocities. Vegetation was stable during low-flow conditions, it was removed from the upstream side of the bar during high-flow conditions and it returned at the downstream side of the bar at the end of the year (under low-flow conditions) where bar-tailed limbs were formed. However, the precise development of the vegetation was highly dependent on the chosen critical flow velocity for vegetation removal. A relatively large critical flow velocity ($u_{cr} = 1.0$ m/s and $u_{cr} = 1.1$ m/s) led only to minor vegetation removal at the front and flanks of the bar, whereas low critical velocities ($u_{cr} = 0.7$ m/s and $u_{cr} = 0.8$ m/s) caused a halving or almost full removal of the vegetation on the bar.

Table 4.1 – Migration distance of mid-channel bar and vegetation for different critical flow velocity for vegetation removal after 360 days ($T_{veg} = 7$ days). Downstream migration (+). Negative migration is due to the initial location of the vegetation. Vegetation was initially only situated on the highest region of the mid-channel bar.

Critical flow velocity for vegetation removal (m/s)	Migration distance bar (m)	Migration distance vegetation (m)
0.70	175	125
0.80	100	50
0.90	50	0
1.00	25	-50
1.10	0	-50
static vegetation	0	0
no vegetation	375	N/A

Significant differences were present between the removal patterns of the vegetation on the bars. Relatively high critical flow velocities (e.g. $u_{cr} = 1.0$ m/s and $u_{cr} = 1.1$ m/s) caused the removal of vegetation at the front and upstream flanks of the bar, whereas low critical velocities caused the formation of unusual vegetation patterns which are not observed in the field (e.g. see panel *D* of figure 4.8). Unlike the simulated removal patterns, vegetation is in reality predominantly removed at the front and upstream flanks of the bar through failure of the bar edge (Li et al., 2014), see for example figure 3.4. The unusual removal patterns are caused by the formation of bumps of sediment on the upstream part of mid-channel bar. Corresponding flow velocities were lower on the bumps and higher in the surrounding regions on the bar due to flow divergence. This caused the formation of gullies. These gullies were exposed to higher flow velocities which caused more vegetation removal. Figure 4.8 shows that the precise shape of the vegetation return on the mid-channel bar was highly dependent on the morphological development of the bar and, therefore, indirectly also on the vegetation removal in the high-flow-season. Besides, the migration distance of the vegetation (after it returned at the end of the year) was larger for smaller critical flow velocities for vegetation removal (see table 4.1). This seems logical because we saw that the return of vegetation was highly connected to the morphological development of the bar during the high-flow season when vegetation was removed.

Sensitivity analysis

For the sensitivity analysis, the development of the bathymetry and vegetation was analysed after 330 days. After this period, we can conveniently analyse the removal of vegetation since vegetation had not yet returned to the mid-channel bar. We do not focus on the return of vegetation on the bar because we already concluded that the pattern of vegetation return does not significantly differ for various critical flow velocities for vegetation removal. For different vegetation update intervals, the vegetation only returned at a different moment during the simulated year, e.g. see

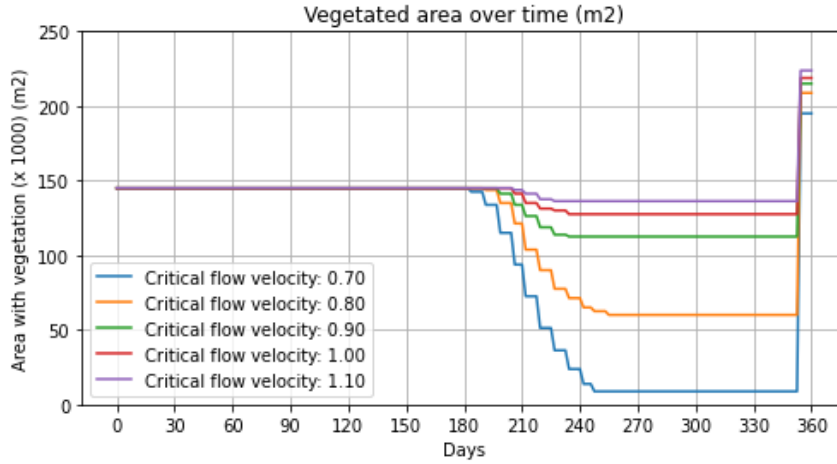


Figure 4.9 – Vegetation area over time for different values of the critical flow velocity for vegetation removal (m^2)

figure 4.10. We also do not elaborate on the differences between the size of the returned vegetation area since it had to do with the morphological development of the mid-channel bar during high-flow conditions. For sake of clarity, we included a figure having bed levels and vegetation development (including the return of vegetation) after 360 days in Appendix C.

First, we look at the vegetation shown in figure 4.11 in a row-wise manner. Except for the highest two critical flow velocities where almost no vegetation was removed ($u_{cr} = 1.0 m/s$ and $u_{cr} = 1.1 m/s$), we can identify a similar pattern for vegetation removal: the longer the duration of the vegetation update interval, the less the vegetation removal on the mid-channel bar. Also, the vegetation removal behaved in a more natural way as the duration of the vegetation update interval increased. In reality, vegetation is only caved in at the front and upstream sides of the mid-channel bar. Unnatural vegetation removal can for example be seen in panels *G*, *H*, *I* and *K* of figure 4.11 where vegetation was removed from more regions on the bar. The same unnatural vegetation patterns occurred during the simulations in panels *A*, *B*, *C*, *D* and *F*. However, these are invisible in figure 4.11 because (almost) all vegetation was removed during these simulations. Rapid vegetation removal at a certain location resulted into a cascade of vegetation removals at other locations. This occurred because sediment was easily eroded from areas where vegetation was not present anymore. In our case, the first areas experiencing vegetation removal are situated at the upstream flanks of the mid-channel bar. The eroded sediments deposited again on top of the bar further downstream leading to two elevated sections on both the left and right side. This induced flow divergence leading to higher flow velocities which could penetrate further onto the bar. Consequently, these higher flow velocities led to more removal of vegetation and more erosion of the bar leading to gullies. This process accelerated when the vegetation update intervals was smaller because we then more frequently checked whether vegetation should be removed.

Figure 4.12 shows that similar patterns hold for the development of the morphology: the smaller the vegetation update interval, the more the erosion at the front side of the mid-channel bar and the more deposition of sediments on the bar and the bar-tailed limbs. On the other hand, figure 4.12 shows that a too large vegetation

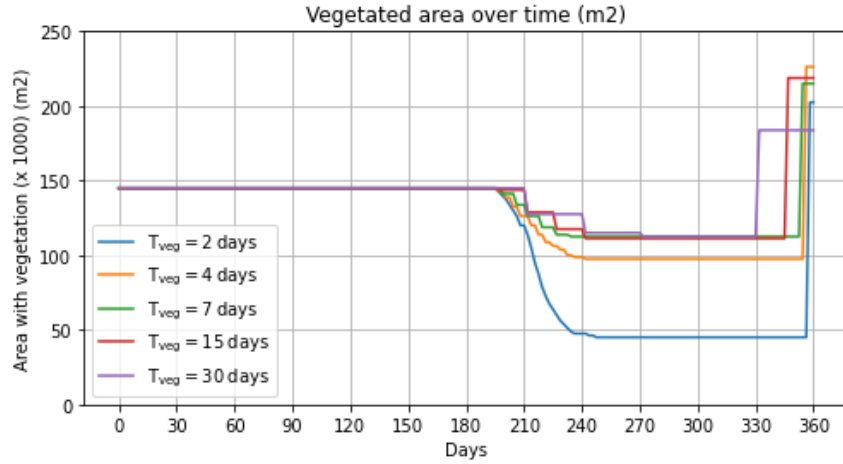


Figure 4.10 – Vegetation area over time for different vegetation update intervals ($u_{cr} = 0.90 \text{ m/s}$) (m^2)

update interval can result in the standstill of the bar. This is also not desired as we are modelling a vegetated migrating mid-channel bar. Therefore, the vegetation update interval should be chosen accordingly to obtain natural behaviour. Previously, it was already found that the critical flow velocity for vegetation removal significantly affects the development of the vegetation and the morphology of the mid-channel bar. A similar pattern was found: the higher the critical flow velocity, the less the vegetation removal on the mid-channel bar. Additionally, we also concluded that the vegetation removal behaved in a more natural way as the critical flow velocity increased.

Combining these two patterns indicates that the critical flow velocity for vegetation removal and the duration of the vegetation update interval are strongly interconnected. It suggests that low critical flow velocities should be implemented together with long durations of the vegetation update intervals and that high critical flow velocities should be used together with short durations of the vegetation update intervals to obtain natural morphodynamics and vegetation dynamics. Hence, a diagonal is present in figure 4.11 from the lower left corner to the upper right corner of suitable combinations of the two input parameters for the *dynamic vegetation procedure* resulting into natural behaviour of this river system.

For the Ayeyarwady River model (section 4.2), a *trial-and-error* procedure and satellite imagery will be used to find the suitable combination of the two input parameters. For engineering purposes, we will start the procedure with a relatively long duration of the vegetation update interval (and low critical flow velocity), because the number of interruptions of the model should be minimized to prevent a significant increase of the calculation time.

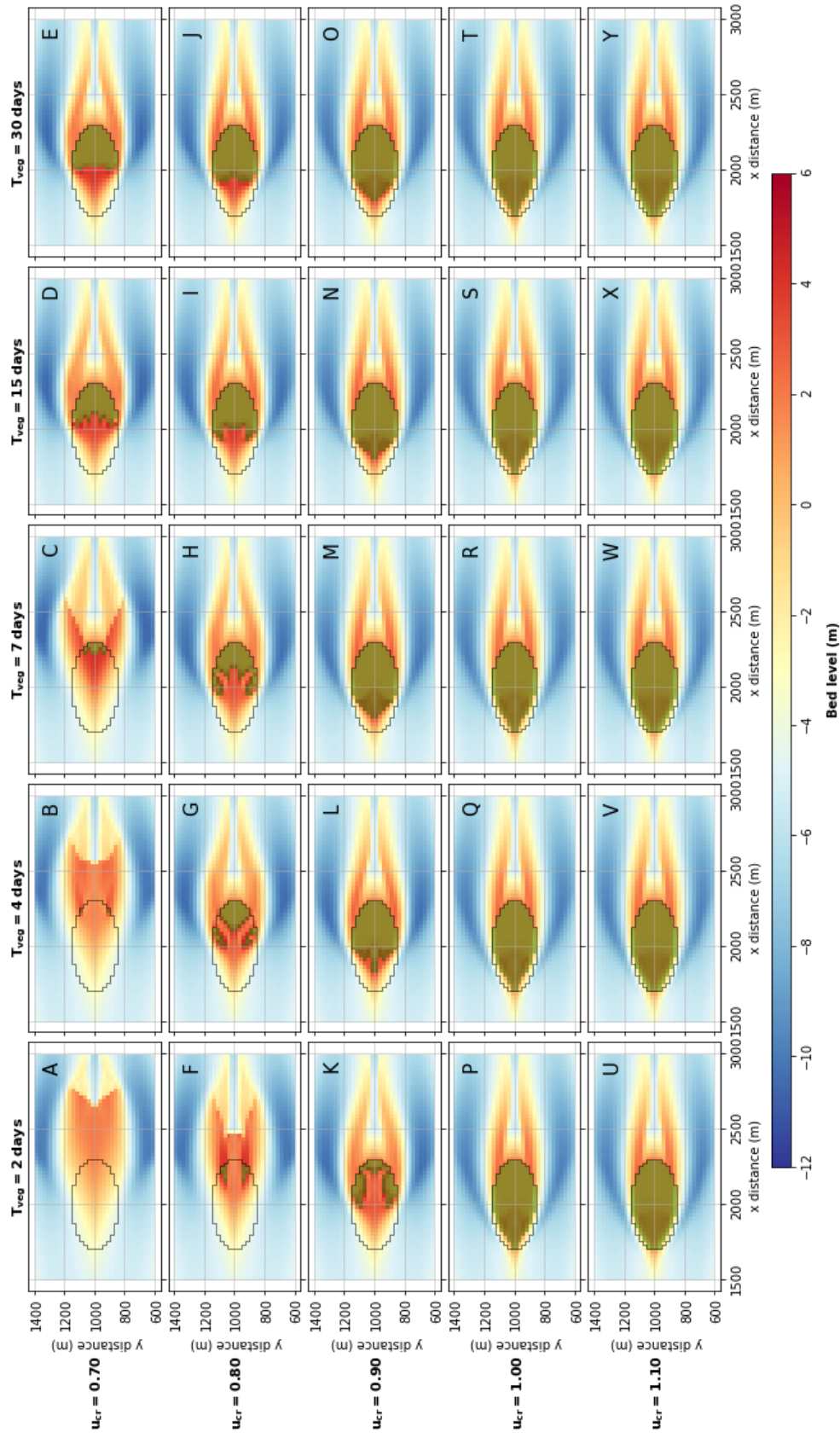


Figure 4.11 – Sensitivity analysis: bed levels (m) after 330 days for different vegetation update intervals (T_{veg}) and critical flow velocities for vegetation removal (u_{cr}). Green overlaid area shows the location of the vegetation after the peak of the discharge wave and black circle shows the initial location of vegetation. Flow from left to right.

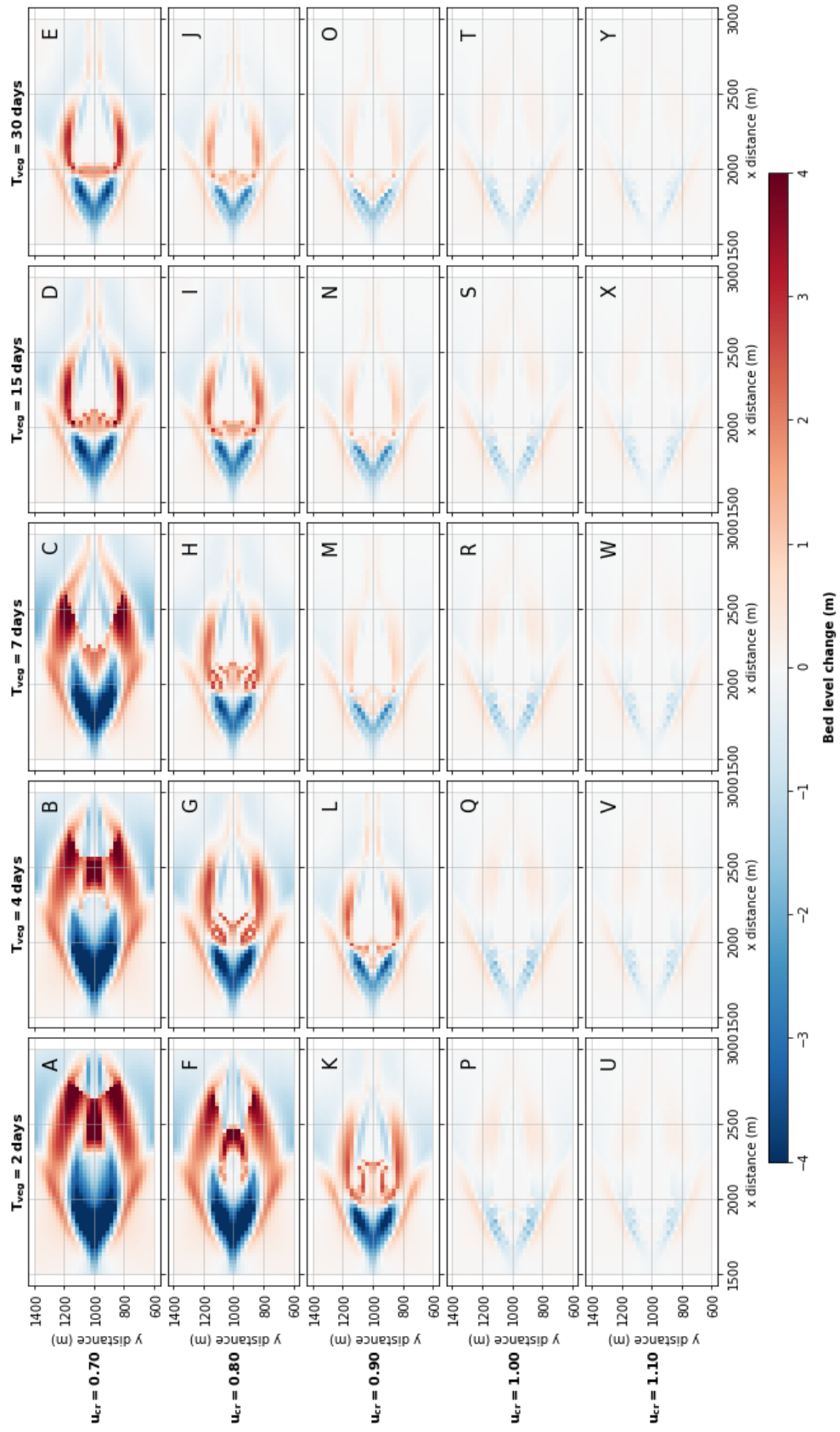


Figure 4.12 – Sensitivity analysis: bed levels differences (m) with respect to the *static vegetation scenario* after 360 days for different durations of the vegetation update intervals (T_{veg}) and critical flow velocities for vegetation removal (u_{cr}). Flow from left to right.

4.2 Ayeyarwady River model

The *reference scenario* and *static vegetation scenario* were used as control runs to compare the *dynamic vegetation scenario* with. Hence, we only give a brief explanation of the morphological development of the mid-channel bars in these scenarios.

Panels *A* and *C* of figure 4.13 show that significant changes of the river morphology were present after 360 days when the mid-channel bar was not vegetated. The upstream-side of the bar was exposed to erosion through relatively high flow velocities, bed shear stresses and associated sediment transport rates. This erosion led to the diffusion of the upstream bar morphology (bank lines were getting smoother). This diffusion is not desired, because vegetated mid-channel bars normally have distinct channel bank lines (Nicholas et al., 2013). This also holds for the mid-channel bar in the Ayeyarwady River close to Nyaungdon. In section 3.1 (figure 3.4), we saw that, in reality, the upstream slope did not get more gentle over time. Deposition of sediments occurred on the north-side and downstream side of the bar leading to bar widening and the migration of the mid-channel bar in downstream direction. Figure 3.4 shows that the widening of the bar does not occur in reality. Also, our model results do not show the formation of a bar-tailed limb at the south-side of the bar which actually does occur in reality.

Panels *B* and *D* of figure 4.13 show that the mid-channel bar in the *static vegetation scenario* did not experience notable morphological changes after 360 days. The mid-channel bar was retained at its initial location by the (static) vegetation on it. The vegetation significantly reduced the flow velocity, bed shear stress and sediment transport rate on the bar. Therefore, it was hardly exposed to upstream erosion and downstream sedimentation. However, compared to the natural behaviour of the Ayeyarwady River (figure 3.4), this scenario gets closer to the actual situation in which the bar migrates in south-west direction and in which large bar-tailed limbs develop. The formation of a minor bar-tailed limb on the south side of the bar could already be identified in our model, see the **X** in panel *D* of figure 4.13.

We found that the use of the *dynamic vegetation procedure* in a morphodynamic model positively contributed to the ability of the model to simulate a vegetated migrating mid-channel bar in the Ayeyarwady River. Compared to the natural behaviour of the mid-channel bar at Nyaungdon (section 3.1), the modelled behaviour showed many similarities. Figure 4.15 shows the development of the river morphology and the vegetation for two different combinations of the critical flow velocity for vegetation removal (u_{cr}) and the duration of the vegetation update interval (T_{veg}). A *trial-and-error* procedure was used to find combinations which resulted into natural behaviour of the vegetation and the bar during high-flow conditions. Furthermore, patterns about the interconnectedness of the two input parameters of the *dynamic vegetation procedure* (section 4.1.5) were used to guide this process. We indeed found that a low u_{cr} should be used with a longer T_{veg} and that an higher u_{cr} should be used with a shorter T_{veg} to end up with natural behaviour of the vegetation on migrating mid-channel bars. We defined unrealistic vegetation development as the total removal of vegetation, no removal of vegetation at all and as the formation of localized (small-scale) erosion patterns leading to the development of gullies.

Figure 4.15 shows that the vegetation removal pattern for various combinations of u_{cr} and T_{veg} significantly differs. A lower u_{cr} leads to more removal of vegetation, than an higher u_{cr} . The somewhat unusual removal pattern in panel *A* of figure

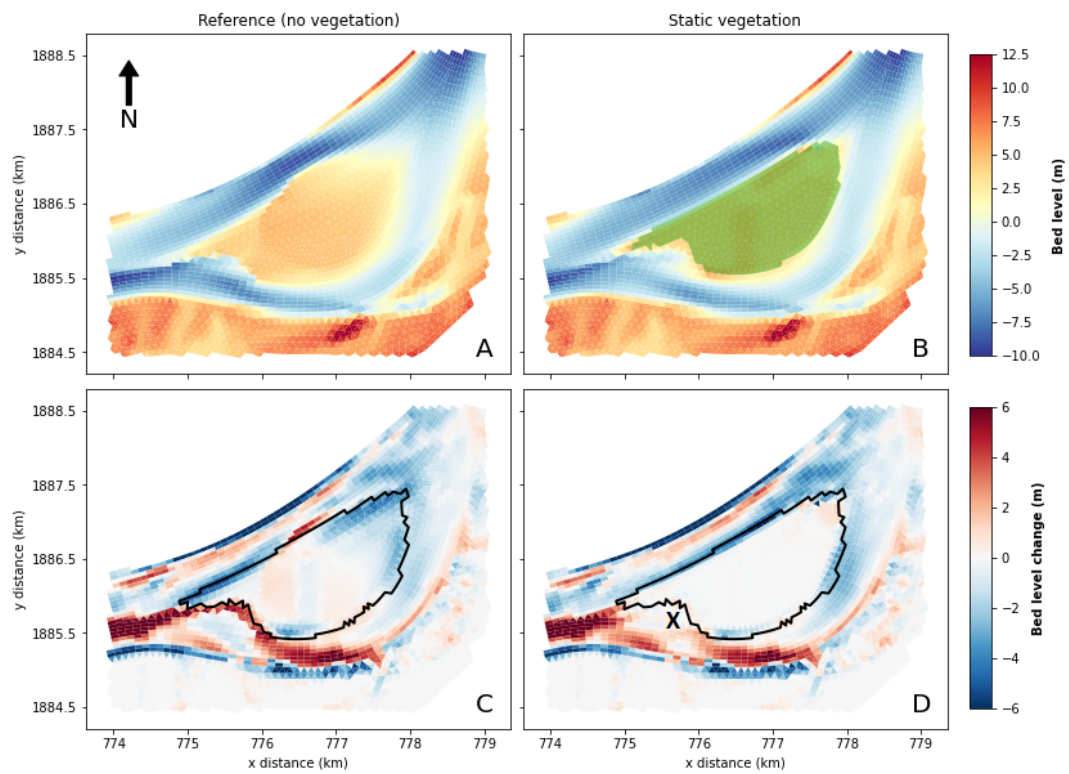


Figure 4.13 – Development of the river bed (upper row) and bed level change with respect to the initial bathymetry (lower row) after 360 days for the *reference scenario* and *static vegetation scenario*. Black line shows the initial location of the bar and the green overlaid area shows the location of the vegetation. Flow from right to left. **X** shows the formation of a minor bar-tailed limb.

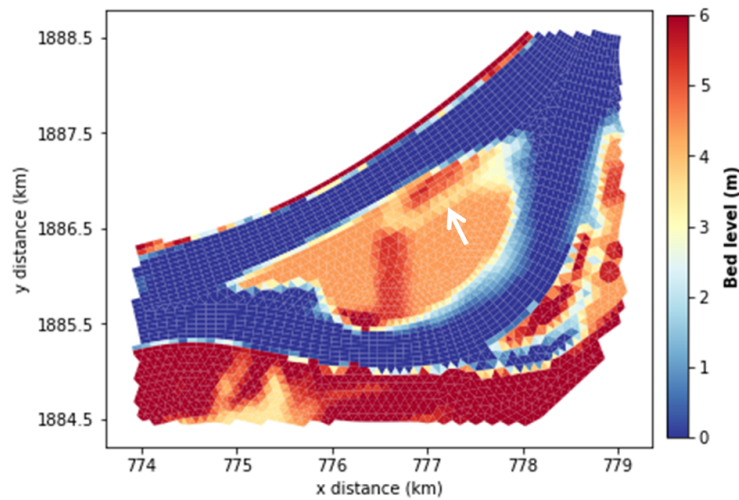


Figure 4.14 – Initial bathymetry (m). The color bar is truncated to show a range of 0 – 6 meters to highlight the elevation differences on the bar. White arrow indicates a low elevation region.

4.15 is due to elevation differences on the bar, see figure 4.14. They show that more vegetation removal is present at the low elevation region on the bar, see white arrow in figure 4.14. In reality, such a vegetation removal patterns is not observed, see figure 3.4. Vegetation should be predominantly removed at the front and upstream flanks of the bar through failure of the bar edge (Li et al., 2014).

The differences between the vegetation development patterns did not result in significant differences in the morphological development of the bars. Erosion of sediment occurred at the upstream side of the bar where vegetation was removed during high-flow conditions. This is in compliance with satellite observations as shown in figure 3.4. The absence (removal) of vegetation led to higher bed shear stresses and associated sediment transport rates (erosion) during high-flow conditions. Slight erosion also occurred at the downstream side of the bar where the northern bar-tailed limb decreased in width.

Deposition of sediments occurred at the downstream side of the bar. They led to the elongation of the northern bar-tailed limb and the formation of a new bar-tailed limb on the south-side of the bar. Growth of the bar-tailed limbs also occurred in reality, see figure 3.4. A major bar-tailed limb developed over the years at the south-side of the bar in the Ayeyarwady River. Figure 4.15 also shows the rapid return of vegetation on the developed bar-tailed limbs. This vegetation behaviour is in compliance with the actual development of the vegetation in the Ayeyarwady River. In reality, vegetation rapidly develops on the bar-tailed limbs of mid-channel bars which were formed during the high-flow season.

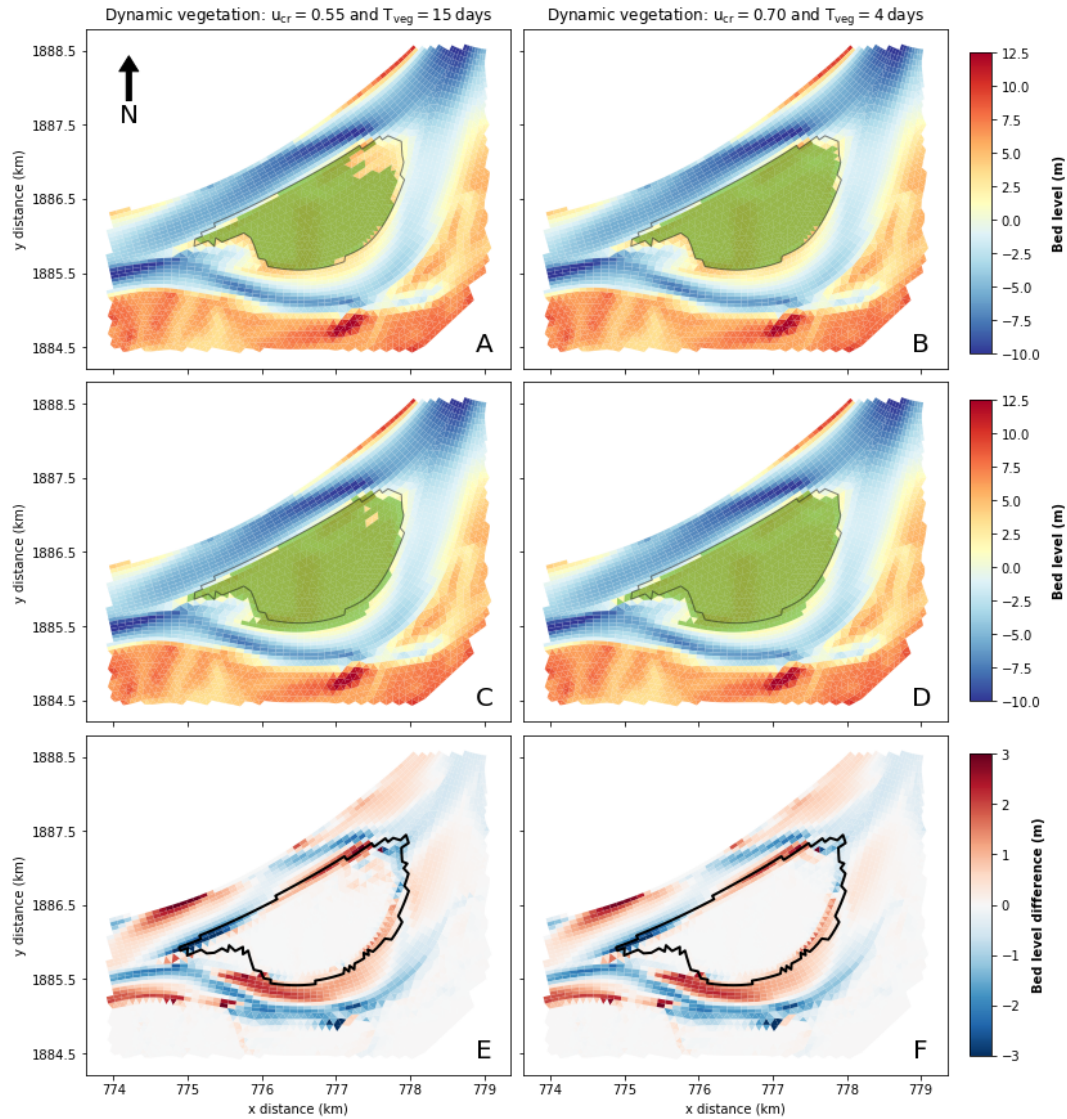


Figure 4.15 – Development of the river bed after 330 days (upper row), development of the river bed after 360 days (middle row) and the bed level difference with respect to the *static vegetation scenario* after 360 days (lower row) for two combination of the critical flow velocity for vegetation removal u_{cr} and the duration of the vegetation update interval T_{veg} . Black lines in upper and middle row show the initial location of the vegetation, black lines in lower row show the initial location of the bar and the green overlaid areas show the vegetation. The color bar of panels *E* and *F* is truncated to show a maximum difference of ± 3 meters.

Chapter 5

Discussion

Subsequently, we will discuss the following topics in this chapter: the scope of this research, morphodynamic modelling, vegetation modelling and the *dynamic vegetation procedure*. However, first, it is good to emphasize that the results discussed herein are for idealized rivers. Even the simulated river morphodynamics of the Ayeyarwady River model are inevitably less complex than in natural rivers. This is partly due to our assumptions about the river system, such as the simplified discharge hydrograph and equilibrium sediment supply, but also due to model shortcomings as discussed in this chapter. Yet, the idealized river in the schematized model could be used to analyse different vegetation formulations. The non-calibrated Ayeyarwady River model was used to test the *dynamic vegetation procedure*. Despite this model is not calibrated, it could be used to test the *dynamic vegetation procedure* in a more realistic model setup.

5.1 Scope

In this study, we focus on the large-scale morphodynamics of vegetated migrating mid-channel bars in the Ayeyarwady River. For example, we are interested in the morphological changes of the shape and location of mid-channel bars. We are not interested in small-scale bar and vegetation development. Therefore, we use constant vegetation characteristics as height, diameter and density over space and time. We neglect that these characteristics would normally differ on mid-channel bars and significantly influence small-scale bar development. We are also not interested in simulating small-scale vegetation processes as colonization, growth and mortality for the dynamic vegetation phase of this study. We only mimic the development of large-scale vegetation patterns by developing a *dynamic vegetation procedure* (see section 5.4) which contains simple conditions for vegetation removal and return.

Also, for sake of simplicity, we neglect that vegetation is normally present on the river banks and floodplains. We only focus on the development of vegetation on mid-channel bars. The inclusion of bank and floodplain vegetation can potentially result in different morphodynamic behaviour of the river. For example, vegetation on banks induces flow divergence leading to higher flow velocities, bed shear stresses and sediment transport rates in the channels. A detailed analysis of the effects of bank and floodplain vegetation is beyond the scope of this study. For future work, we recommend to study the effectiveness of the proposed methodologies on the

development of vegetation on bank and floodplains, see section 6.2.2 for more details.

5.2 Morphodynamic modelling

Present morphodynamic models, such as Delft3D-Flexible Mesh, are able to sufficiently produce many of the morphological characteristics and dynamics of braided river systems (Jagers, 2003; Williams et al., 2016b). However, they still have a limited predictive value due to many simplifications such as the modelled hydraulic resistance, the bank erosion procedure and the parametrisations of secondary flow and turbulence (Schuurman, 2015; Williams et al., 2016a,b). Yet, present morphodynamic models can still be useful for engineering purposes without giving precise predictions. They can give a rough estimate of the amount of sediment transport and the locations where erosion and deposition will occur at some moment in time. For example, these models can be used to assess locations of risk for sedimentation and erosion and they can be used to determine the impact of river training measures. The remainder of this section will shortly touch upon some model assumptions/simplifications and the effect of it on our results.

5.2.1 Bank erosion

In nature, bank erosion is one of the main mechanisms causing the migration of vegetated bars (Li et al., 2014). There are two main sets of bank-erosion processes and mechanisms, namely fluvial erosion and mass failure (Rinaldi and Darby, 2007). In Delft3D-FM, the process of bank erosion by mass failure is not included (Deltares, 2019b). Bank erosion is included by applying a simple algorithm: a dry grid cell erodes if erosion occurs in a neighbouring wet grid cell. This algorithm leads to the diffusion of the bar morphology during low-flow conditions; steep bank slopes become more gentle. This algorithm is not in use during high-flow conditions, because (mid-channel) bars are fully submerged. In fact, the algorithm is undesired for modelling vegetated migrating mid-channel bars which normally have distinct upstream channel bank lines (Nicholas et al., 2013). Relatively coarse grid cells do also contribute to the diffuse morphological behaviour of bank lines (Williams et al., 2016a). The finer the grid resolution, the better the bank topography can be simulated. Both affect the removal of vegetation by the proposed *dynamic vegetation procedure* as well. In reality, vegetation in the Ayeyarwady River is disconnected from the flow during low flow conditions due to a very steep (upstream) bar slope (Moggridge and Higgitt, 2014). However, in our procedure, vegetation removal might still occur during low-flow conditions if the bar slope has become gentler over time.

The bank erosion algorithm is also not able to produce bank erosion due to lateral channel migration in braided rivers (Schuurman, 2015). Therefore, the resulting channel morphology (e.g. see figure 4.1) did not show major lateral migration of the banks of the two channels around the mid-channel bar. Instead, the channels experienced a notable incision of the bed in response to the flow.

Yet, this simplistic bank erosion algorithm did not significantly affect our large-scale model results as the major morphological changes of interest (the development of the shape of the bar and the location of the bar) predominantly occur during high-discharge conditions when the mid-channel bar is submerged and the bank erosion algorithm is not in use.

5.2.2 Sediment transport formula

The applied sediment transport formula (*General Formula*) calculates the total sediment transport rate: the combination of bed load and suspended load. The transport rate is imposed in Delft3D-FM as bedload transport due to currents. Hence, we neglect the effect of suspension (advection-diffusion of sediments) on bar morphodynamics. According to Schuurman (2015), the inclusion of suspended-load transport results in longer bars and steeper transverse bed slopes in river bends due to secondary flow. The secondary flow steers flow near the river bed toward the inner bend, where the sediment concentration is high. So, potentially, we underestimated the simulated development of the bar length. Furthermore, our configuration of the *General Formula* does not include a threshold for sediment mobility. This threshold affects the sediment transport rate in locations of low sediment mobility, e.g. on top of bars. Hence, we might overestimate the sediment transport on top of bars leading to exaggerated bar erosion or bar lengths. A detailed analysis of the effects of suspended sediment and the use of a threshold for sediment mobility on the development of the bar morphology is beyond the scope of this study. However, a slight under- or overestimation of the bar length will not significantly affect our findings about the effectiveness of the *dynamic vegetation procedure* to simulate large-scale morphodynamics of vegetated migrating mid-channel bars.

5.2.3 Morphological acceleration factor

A morphological acceleration factor (MorFac) was used to speed up the morphological developments in our model to reduce computation time. The influence of the MorFac on the morphological development of the mid-channel bar is not thoroughly analysed. However, we used a rather modest MorFac of 15 to avoid unrealistic sediment transport pulses through the system based on the work of Steijn et al. (2019) at the site of the case study. This MorFac seems reasonable because it is a relatively low value compared to a default value of 25 commonly used in morphodynamic models of braided rivers (Schuurman, 2015).

5.3 Vegetation modelling

We found that a conventional roughness formulation as *Manning's n* cannot be used to simulate (static and dynamic) vegetation in numerical morphodynamic simulations, because it leads to very high bed shear stresses in vegetated areas. This finding is in compliance with the work of Baptist (2005) and Le Bouteiller and Venditti (2015). Baptist (2005) found that a high bed shear stress can be due to an enhanced hydraulic resistance. He stated that the bed shear stress should actually become lower due to the presence of vegetation, because near-bed flow velocities (turbulence) are reduced in vegetated patches on bars. This is not the case when using a conventional roughness formulation such as *Manning's n*. Figure 2.4 confirms this finding.

We use the Baptist roughness predictor to represent vegetation in our simulations. This predictor is based on the work of Baptist (2005) and it determines a Chézy roughness coefficient to represent vegetation (resistance). This Chézy coefficient is implemented in the hydrodynamic calculations in Delft3D Flexible Mesh. Therefore, it can be used to simulate flow resistance by vegetation reasonably well

(Vargas-Luna et al., 2015). The Baptist roughness predictor is not included in the morphodynamic part (sediment transport formula) of our model. Hence, we neglect that vegetation has a decreasing effect on the turbulence and associated bed shear stress in vegetated areas. Instead, the Chézy coefficient corresponding to a *Manning's n* of $0.030 \text{ s/m}^{1/3}$, the alluvial bed roughness, is used in the sediment transport formula. This results only in a partial reduction of the sediment transport rate in vegetated areas in our model. The partial reduction is caused by the flow velocity reduction from the hydrodynamic calculations which is implemented in the transport formula, see appendix A for more details.

All in all, an overestimation of the sediment transport rate in vegetated areas is present in our model, possibly affecting morphological behaviour, see figure A.1. However, we do not expect that significantly different morphological development (patterns) would have occurred. The effect of vegetation is only partly underestimated. A detailed analysis of the effects of the overestimated sediment transport rate through vegetated is beyond the scope of this study. However, we recommend, for future work, to use a more advanced method which also includes the effects of vegetation on the sediment transport rate in a more realistic way (see appendix A for more details).

5.4 Dynamic vegetation procedure

This study is a step forward in the morphodynamic modelling of vegetated migrating mid-channel bars in dynamic rivers for engineering purposes when the large-scale development of bed and land forms is mainly of interest. We found that the inclusion of dynamic vegetation removal and return can result in more natural morphodynamic model behaviour of migrating bars compared to including static vegetation in space and time. This is in compliance with the work of Nicholas et al. (2013), Bertoldi et al. (2014) and Oorschot et al. (2016). We removed vegetation using a Basic Model Interface which couples Delft3D-FM to a *dynamic vegetation procedure* in Python. This procedure contains basic conditions for the removal and return of vegetation dependent on two input parameters: a critical flow velocity for vegetation removal and a vegetation update interval.

5.4.1 Critical flow velocity

Oorschot et al. (2016) used a life-stage dependent critical flow velocity for alluvial vegetation mortality in a morphodynamic river model ranging from 0.55 m/s for seedlings to 12 m/s for tree-like vegetation. We use critical flow velocities in the range of 0.55 to 1.10 m/s to mimic the development of natural vegetation patterns. This suggests that our used critical flow velocities are on the low end of the actual critical flow velocities for vegetation removal (mortality) which are present in the field. However, we are not only modelling vegetation removal through high flow velocities. By using a relatively low critical flow velocity, we try to include more vegetation removal processes (e.g. burial and uprooting) at once to mimic the development of natural vegetation patterns. Hence, our critical flow velocity is allowed to be lower than the critical flow velocities as observed in the field.

5.4.2 Interconnectedness of input parameters

In section 4.1.5, we identify a strong interconnection between the critical flow velocity for vegetation removal and the duration of the vegetation update interval. The combination of both parameters strongly affects the development of the vegetation and the morphology of a modelled system. A small change in one of these parameters could induce a significantly different, potentially unrealistic, development. This suggests that selecting a suitable combination of the vegetation update interval and critical flow velocity for vegetation removal is very important. As no rules to select the right combination are present (yet), calibration data of the morphological and vegetation development and knowledge about vegetation development in the river system are always required.

In section 4.2, we state that a suitable combination of the two input parameters for a modelled system cannot simply be implemented in a model of another river system. This suggests that the combination is highly dependent on the physical characteristics of the system one attempts to model, such as the vegetation characteristics, discharge regime and initial bathymetry. This seems logical because flow characteristics, vegetation and morphology do strongly affect each others development (Moggridge and Higgitt, 2014). For example, we found that vegetation removal patterns are dependent on the bathymetry of the bar. The bathymetry of the bar significantly affects the flow velocities on top of it leading to vegetation removal patterns which follow elevation patterns of the bar. Figure D.1 of Appendix D shows the vegetation removal on the bar in the Ayeyarwady River model for an unsuitable combination of the critical flow velocity and the duration of the vegetation update interval. It shows that vegetation is removed from the low elevation region on the centre of the bar. Vegetation removal at this region is not realistic because vegetation is in reality predominantly removed from the front and upstream flanks of mid-channel bars through failure of the bar edge (Li et al., 2014). So, when using the proposed *dynamic vegetation procedure*, we recommend to always verify that the flow velocity is the main driver of vegetation removal in the river system. If not, another condition with a different driver (process) for vegetation removal can potentially be used, e.g. a critical erosion depth or bed shear stress.

Furthermore, we found that the morphological development of mid-channel bars is highly sensitive to changes in the vegetation height and density (section 4.1.4). Therefore, the critical flow velocity for vegetation removal and the duration of the vegetation update interval are also dependent on these vegetation characteristics. If these characteristics are adapted in the model setup or significantly change over time in reality, the critical flow velocity for vegetation removal and the vegetation update interval probably need to be adapted as well to obtain natural vegetation behaviour.

5.4.3 Applicability to other rivers

The characteristics of the Ayeyarwady River are used for the development of the conditions for vegetation removal and return in the proposed *dynamic vegetation procedure*. Hence, the present procedure is only valid for monsoonal regions with a clear water level difference between the low- and high-flow season (such as the simplified discharge hydrograph in figure 3.7) and in regions where rapid vegetation return on bars during the low-flow season normally occurs. We assume that (fully grown)

vegetation returns to the mid-channel bar at the end of the year during the low-flow season. In fact, this condition does not represent the natural behaviour of vegetation return on bars. Normally, vegetation would gradually return to dry areas on bars. However, this easy condition can be used in our case because vegetation on bars in the Ayeyarwady River is disconnected from the flow during low-flow conditions. So, there is no need to simulate the gradual return of vegetation during the low-flow season as long as the vegetation at the start of the high-flow season is relocated. All in all, this limits the applicability of the present procedure to simulate vegetation dynamics in other rivers. However, the proposed procedure can easily be applied to other river systems as well. Similar rule-based conditions for vegetation removal and return can be set up for rivers having different physical characteristics. Section 6.2.2 further elaborates on this topic.

5.4.4 Long-term applicability

The applicability of the *dynamic vegetation procedure* is potentially limited over long time-scales. Modelling vegetation removal and return over long time-scales gives new challenges, compared to the short time-scale, because we only mimic the development of natural vegetation patterns of the past. We are not modelling actual vegetation processes (e.g. seed dispersal, growth, etc.) which can change over time due to for example environment changes. Hence, the *dynamic vegetation procedure* may be unsuitable for systems where vegetation development patterns can significantly change over time. We recommend to study the effectiveness of the proposed procedure over long simulation periods to gain a better insight in the predictive value of the procedure. See section 6.2.1 for more details.

Chapter 6

Conclusions and recommendations

6.1 Conclusions

The objective of this thesis is to model and explore the effect of incorporating vegetation dynamics on the large-scale morphodynamics of vegetated migrating mid-channel bars in dynamic rivers. To reach this objective, we have set up a schematized model based on the Ayeyarwady River in Myanmar to study the effect of static (in space and time) vegetation formulations on the morphological development of mid-channel bars. Then, a procedure was developed to include the removal and return of vegetation in space and time, based on basic conditions, on migrating mid-channel bars in the schematized model. The *dynamic vegetation procedure* was coupled to Delft3D-Flexible Mesh using a Basic Model Interface which has a direct control over model time steps and variables during a simulation. Finally, we tested the procedure in more realistic model setup of the Ayeyarwady River. In this section, we answer the research questions formulated in section 1.3.

Q1 To what extent are present numerical morphodynamic models capable of simulating the development of vegetated migrating mid-channel bars in dynamic rivers using different static (in space and time) approaches to include vegetation?

A present morphodynamic model is capable of simulating the large-scale morphologic development of bare (non-vegetated) migrating mid-channel bars in braided rivers, whereas it has difficulties with simulating the development of vegetated mid-channel bars in dynamic rivers. Unrealistic morphological behaviour occurs around migrating mid-channel bars when a conventional roughness formulation as *Manning's n* is used to represent vegetation. This formulation wrongly simulates the behaviour of the flow within vegetated areas resulting in high bed shear stresses, consequently leading to massive erosion. The use of the Baptist roughness predictor to represent vegetation gives more realistic results. However, this representation of vegetation (resistance) does not enable the migration of the mid-channel as a whole, because the location of the modelled vegetation is static over time. This implies that morphodynamics are strongly interconnected with vegetation dynamics. Thus, the connection between vegetation and morphology

cannot be neglected when someone wants to model a highly dynamic river system in which vegetated migrating mid-channel bars occur.

Q2 How can we include the removal and return of vegetation in space and time on migrating mid-channel bars in numerical morphodynamic models in a simplistic and dynamic way?

A procedure was developed to include the dynamic removal and return of vegetation in space and time on migrating mid-channel bars in numerical morphodynamic models. The procedure is specifically developed to mimic the development of natural vegetation patterns on mid-channel bars in the monsoonal Ayeyarwady River. It reads as follows: vegetation is removed from the mid-channel bar during high-flow conditions where the flow velocity during the last vegetation update interval exceeds an user-defined critical value and vegetation returns to the bar where the maximum inundation depth does not exceed an user-defined water depth at the end of each year during low-flow conditions.

We found that the use of the *dynamic vegetation procedure* enabled vegetated migrating mid-channel bars to more dynamically behave in a modelled river. Instead of being static over time, mid-channel bars were now exposed to upstream erosion and downstream deposition of sediments resulting in the formation of bar-tailed limbs and the migration of the bars as a whole. Vegetation removal induced higher flow velocities at the upstream side of the bar. This resulted in higher bed shear stresses and associated erosion of the upstream bar edge. The sensitivity analysis showed that the critical flow velocity for vegetation removal and the duration of the vegetation update interval are strongly interconnected and the combination of both parameters highly influences vegetation development and morphology. It also showed that unnatural model behaviour can occur when these parameters are not carefully chosen. Patterns were identified to guide the selection process of suitable parameter-combinations for engineering purposes. We recommended to use low critical flow velocities together with long durations of the vegetation update interval and to use high critical flow velocities together with short durations of the vegetation update interval to obtain natural morphodynamics and vegetation dynamics. It is important to devote much attention to the selection process of a suitable parameter-combination for the *dynamic vegetation procedure* for the river system one wants to model.

Q3 To what extent can the proposed modelling procedure for dynamic vegetation be used to improve morphodynamic model results of a vegetated migrating mid-channel bar in a real-life case study?

The proposed *dynamic vegetation procedure* was implemented in a morphodynamic model of the Ayeyarwady River in Myanmar. The case study showed that it is difficult to select a suitable combination of the critical flow velocity for vegetation removal and the duration of the *vegetation update interval*, because these parameters are highly interconnected and they strongly influence vegetation and morphological development. We recommend to use calibration data of the vegetation patterns and morphology, such as satellite imagery and in-situ meas-

urements, to find a suitable combination of the two parameters. We found that the *dynamic vegetation procedure*, with suitable input parameters, significantly increased the ability of the morphodynamic model to simulate natural large-scale morphodynamics of a vegetated migrating mid-channel bar. Instead of having a static location over time, the mid-channel bar showed substantial migration when vegetation was dynamically removed and returned throughout the year. Many similarities were found in the development of the vegetation on the bar compared to the actual behaviour of vegetation in the Ayeyarwady River. Vegetation was removed from the upstream side of the bar during high-flow conditions and it returned to the downstream bar-tailed limbs during low-flow conditions.

The case study showed that the *dynamic vegetation procedure* can only contribute to more natural bar and vegetation dynamics when the flow velocity is the main driver of vegetation removal in the modelled river system. If not, another condition with a different driver (process) for vegetation removal, for example a critical erosion depth or bed shear stress, can potentially be used to end up with more natural results. Therefore, we recommend to always verify this by identifying physical characteristics of the river system such as the discharge regime, the vegetation characteristics and behaviour in nature and the topography of the bed.

The use of the *dynamic vegetation procedure* in combination with a morphodynamic model gives new challenges over long time-scales (multiple years to decades), because we are not modelling the precise behaviour of vegetation. Instead we are only mimicking the development of natural vegetation patterns. This implies that the *dynamic vegetation procedure* can be used for predicting vegetation patterns and the morphology of mid-channel bars over a couple of years if the general development of the vegetation patterns in the future is expected to be similar to development in the past. For example, this holds if the flow velocity remains the dominant factor affecting vegetation removal (mortality) in the river system one wants to model.

6.2 Recommendations

This chapter concludes with some recommendations for future research with respect to the proposed *dynamic vegetation procedure*. We also discuss some recommendations for the practical usage of the proposed procedure.

6.2.1 Future research

First of all, we only examined the effectiveness of the *dynamic vegetation procedure* on the morphological development of migrating mid-channel bars over a short time-scale (1 year). We concluded that the use of the procedure can lead to more natural large-scale morphodynamic behaviour of vegetated mid-channel bars over this time-scale. For the calibration of the procedure, we recommend to use satellite imagery and in-situ measurements of the past vegetation development. Hence, modelling the vegetation removal and return over long time-scales gives new challenges because we only mimic the natural development of vegetation patterns and we are not modelling actual vegetation processes (e.g. seed dispersal, growth, etc.). Thus, we assume that the development of the vegetation patterns in the future is similar to the development

of these patterns in the past. This assumption is valid when no notable changes occur in the discharge regime, vegetation characteristics and topography of the bed all affecting the behaviour of vegetation patterns. Consequently, the procedure can be used to predict vegetation patterns and (mid-channel) bar morphodynamics over a couple of years, whereas new challenges arise when you want to predict over long time-scales as decades. Hence, we recommend to study the effectiveness of the proposed procedure over long simulation periods to gain a better insight in the predictive value of the procedure. Possibly, long time series of satellite imagery can be used to calibrate the procedure to investigate to what extent vegetation and morphodynamic river behaviour of the past can be reconstructed.

Secondly, mimicking the behaviour of bank and floodplain vegetation was beyond the scope of this study. We only updated the location of vegetation on migrating mid-channel bars. However, the proposed *dynamic vegetation procedure* can potentially also contribute to a more dynamic simulation of braiding or meandering river system as a whole. We recommend to study the effectiveness of the proposed *dynamic vegetation procedure* to model dynamic floodplains vegetation on a simple model setup first. Consequently, unimportant river processes are excluded and the model results can be interpreted more easily. Afterwards, the model setup can be extended such that it captures actual characteristics of a case study just as we did.

Lastly, we used a *trial-and-error* procedure to find a suitable combination of the critical flow velocity for vegetation removal and the duration of the vegetation update interval for the *dynamic vegetation procedure*. In section 4.2, we showed that it is fairly difficult to end up with a suitable combination of the two, because vegetation development and morphological development are highly sensitive to the chosen combination. Therefore, for future work, we recommend to reduce the number of calibration parameters from two to one. The critical flow velocity for vegetation removal should be given a more physical character. For example, the critical flow velocity for vegetation removal might be determined using a joint analysis of aerial imagery of vegetation patterns on river banks and the flow regime. The duration of the vegetation update interval should be treated as a dustbin to capture both all other physical phenomena affecting the location of vegetation but also model uncertainties/errors. It is recommended to perform the calibration of the duration of the vegetation update interval using satellite imagery or in-situ measurements to be able to realistically mimic the behaviour of vegetation on migrating mid-channel bars.

6.2.2 Practical usage

A possible field of application for the proposed methodology is river management. For example the large-scale bar, channel and vegetation response to measures in monsoonal dynamic braided rivers can be evaluated in a more realistic way on the short-term. The approach could be used to compare the short term morphological effects on (vegetated) bar dynamics of different river management strategies in dynamic braided rivers. Furthermore, the large-scale bar, channel and vegetation response to different future vegetation characteristics and vegetation removal mechanisms (scenario analysis) can effectively be evaluated, because the *dynamic vegetation procedure* only needs one/two so-called ‘calibration-parameters’ which is ideal for engineering purposes. Besides, the inclusion of vegetation dynamics in Delft3D Flexible Mesh us-

ing a Basic Model Interface did not result in significantly different calculation times which is ideal for e.g. a scenario analysis.

Note that the proposed procedure can easily be applied to any hydrodynamic or morphodynamic model because the *dynamic vegetation procedure* (in Python) can be coupled to any model with a Basic Model Interface without making changes to the source code of it. Only a properly working Basic Model Interface needs to be constructed to gain control over model time steps and variables during a simulation. Moreover, the proposed procedure can be applied to any river system of which sufficient information about vegetation dynamics and calibration data is available. Presently, the conditions are set up for a monsoonal and highly dynamic river system with the assumption of immediate vegetation return in the low-discharge period. Similar rule-based conditions for vegetation removal and return can be set up for regions having other hydrologic and vegetation removal/return conditions. For example, the vegetation return condition can be adapted to gradually return vegetation to regions on bars which are dry for a certain period. This condition might be useful for regions experiencing only minor water level differences and vegetation return during the whole year. Again, satellite imagery can for example be used to study the goodness-of-fit of the developed conditions.

Bibliography

- Anthony, E.J., Besset, M., Dussouillez, P., Goichot, M., Loisel, H., 2019. Overview of the Monsoon-influenced Ayeyarwady River delta, and delta shoreline mobility in response to changing fluvial sediment supply. *Marine Geology* 417, 106038. doi:10.1016/j.margeo.2019.106038.
- Ashmore, P.E., 2013. *Morphology and Dynamics of Braided Rivers*. volume 9. Elsevier Ltd. doi:10.1016/B978-0-12-374739-6.00242-6.
- Ashworth, P.J., 1996. Mid-channel bar growth and its relationship to local flow strength and direction. *Earth Surface Processes and Landforms* 21, 103–123. doi:10.1002/(SICI)1096-9837(199602)21:2<103::AID-ESP569>3.0.CO;2-0.
- Ashworth, P.J., Best, J.L., Roden, J., Bristow, C., Klaassen, G.J., 2000. Morphological evolution and dynamics of a large, sand braid-bar, Jamuna River, Bangladesh. *Sedimentology* 47, 533–555. doi:10.1046/j.1365-3091.2000.00305.x.
- Baptist, M., Babovic, V., Rodríguez Uthurburu, J., Keijzer, M., Uittenbogaard, R., Mynett, A., Verwey, A., 2007. On inducing equations for vegetation resistance. *Journal of Hydraulic Research* 45, 435–450. doi:10.1080/00221686.2007.9521778.
- Baptist, M.J., 2005. *Modelling floodplain biogeomorphology*. Ph.D. thesis. TU Delft. URL: <http://resolver.tudelft.nl/uuid:b2739720-e2f6-40e2-b55f-1560f434cbee>.
- Bennett, S.J., Wu, W., Alonso, C.V., Wang, S.S.Y., 2008. Modeling fluvial response to in-stream woody vegetation: implications for stream corridor restoration. *Earth Surface Processes and Landforms* 33, 890–909. URL: <http://doi.wiley.com/10.1002/esp.1581>, doi:10.1002/esp.1581.
- Bertoldi, W., Siviglia, A., Tettamanti, S., Toffolon, M., Vetsch, D., Francalanci, S., 2014. Modeling vegetation controls on fluvial morphological trajectories. *Geophysical Research Letters* 41, 7167–7175. doi:10.1002/2014GL061666.
- Best, J., Woodward, J., Ashworth, P., Sambrook Smith, G., Simpson, C., 2006. Bar-top hollows: A new element in the architecture of sandy braided rivers. *Sedimentary Geology* 190, 241–255. doi:10.1016/j.sedgeo.2006.05.022.
- Bomers, A., Schielen, R.M.J., Hulscher, S., 2019. The influence of grid shape and grid size on hydraulic river modelling performance. *Environmental Fluid Mechanics* 19, 1273–1294. doi:10.1007/s10652-019-09670-4.

- Bywater-Reyes, S., Diehl, R.M., Wilcox, A.C., 2018. The influence of a vegetated bar on channel-bend flow dynamics. *Earth Surface Dynamics* 6, 487–503. doi:10.5194/esurf-6-487-2018.
- Chang, H.H., 2008. River morphology and river channel changes. *Transactions of Tianjin University* 14, 254–262. doi:10.1007/s12209-008-0045-3.
- Chow, V.T., 1959. *Open Channel Hydraulics*. McGraw-Hill Book Company, Inc.
- Church, M., Ferguson, R.I., 2015. Morphodynamics: Rivers beyond steady state. *Water Resources Research* 51, 1883–1897. doi:10.1002/2014WR016862.
- Coleman, S.E., Smart, G.M., 2011. Fluvial sediment-transport processes and morphology. *Journal of Hydrology New Zealand* 50, 37–58. URL: <https://www.jstor.org/stable/43945013>.
- Deltares, 2019a. D-Flow Flexible Mesh: User Manual. Version 1.5. URL: https://content.oss.deltares.nl/delft3d/manuals/D-Flow_FM_User_Manual.pdf.
- Deltares, 2019b. D-Morphology: User Manual. Version 1.5. URL: https://content.oss.deltares.nl/delft3d/manuals/D-Morphology_User_Manual.pdf.
- Domhof, B.C., Berends, K.D., Spruyt, A., Warmink, J.J., Hulscher, S., 2018. Discharge and location dependency of calibrated main channel roughness: Case study on the River Waal. *E3S Web of Conferences* 40, 06038. doi:10.1051/e3sconf/20184006038.
- Duivendijk, H., Schultz, B., van Westen, C.J. (Eds.), 2002. *Dams and Dikes in Development*. CRC Press. doi:10.1201/b12889.
- Ferguson, R.I., 2010. Time to abandon the Manning equation? *Earth Surface Processes and Landforms* 35, 1873–1876. doi:10.1002/esp.2091.
- Furuichi, T., Win, Z., Wasson, R.J., 2009. Discharge and suspended sediment transport in the Ayeyarwady River, Myanmar: centennial and decadal changes. *Hydrological Processes* 23, 1631–1641. doi:10.1002/hyp.7295.
- Gurnell, A.M., Corenblit, D., García de Jalón, D., González del Tánago, M., Grabowski, R.C., O'Hare, M.T., Szewczyk, M., 2016. A Conceptual Model of Vegetation-hydrogeomorphology Interactions Within River Corridors. *River Research and Applications* 32, 142–163. doi:10.1002/rra.2928.
- Hoffmann, M.R., 2004. Application of a Simple Space-Time Averaged Porous Media Model to Flow in Densely Vegetated Channels. *Journal of Porous Media* 7, 183–192. doi:10.1615/JPorMedia.v7.i3.30.
- Hooke, J.M., Yorke, L., 2011. Channel bar dynamics on multi-decadal timescales in an active meandering river. *Earth Surface Processes and Landforms* 36, 1910–1928. doi:10.1002/esp.2214.
- Huthoff, F., 2007. Modeling hydraulic resistance of floodplain vegetation. Ph.D. thesis. University of Twente. URL: <https://research.utwente.nl/en/publications/modeling-hydraulic-resistance-of-floodplain-vegetation>.

- Hydro-Informatics Centre, 2017. Ayeyarwady SOBA 2017: Synthesis Report Ayeyarwady SOBA Synthesis Report. Technical Report Volume 1. URL: https://themimu.info/sites/themimu.info/files/documents/Report_Ayeyarwady_SOBA_Synthesis_Report_V1_AIRBM.pdf.
- Jagers, B., 2003. Modelling planform changes of braided rivers. Ph.D. thesis. University of Twente. URL: <https://research.utwente.nl/en/publications/modelling-planform-changes-of-braided-rivers>.
- Jourdain, C., Claude, N., Antoine, G., Tassi, P., Cordier, F., 2018. Influence of flood regime on riparian vegetation dynamics in rivers with alternate bars. *E3S Web of Conferences* 40, 02025. doi:10.1051/e3sconf/20184002025.
- Kleinhans, M.G., 2010. Sorting out river channel patterns. *Progress in Physical Geography: Earth and Environment* 34, 287–326. doi:10.1177/0309133310365300.
- Le Bouteiller, C., Venditti, J.G., 2015. Sediment transport and shear stress partitioning in a vegetated flow. *Water Resources Research* 51, 2901–2922. URL: <https://onlinelibrary.wiley.com/doi/abs/10.1002/2014WR015825>, doi:10.1002/2014WR015825.
- Li, Z., Wang, Z., Pan, B., Zhu, H., Li, W., 2014. The development mechanism of gravel bars in rivers. *Quaternary International* 336, 73–79. doi:10.1016/j.quaint.2013.12.039.
- Liu, Z., Merwade, V., Jafarzaghan, K., 2019. Investigating the role of model structure and surface roughness in generating flood inundation extents using one- and two-dimensional hydraulic models. *Journal of Flood Risk Management* 12, e12347. doi:10.1111/jfr3.12347.
- Moggridge, H.L., Higgitt, D.L., 2014. Interactions between riparian vegetation and fluvial processes within tropical Southeast Asia. *Progress in Physical Geography: Earth and Environment* 38, 716–733. doi:10.1177/0309133314548745.
- Monegaglia, F., 2017. Meandering rivers morphodynamics – integrating nonlinear modeling and remote sensing. Ph.D. thesis. Queen Mary University of London. URL: <http://qmro.qmul.ac.uk/xmlui/handle/123456789/33927>.
- Morvan, H., Knight, D., Wright, N., Tang, X., Crossley, A., 2008. The concept of roughness in fluvial hydraulics and its formulation in 1D, 2D and 3D numerical simulation models. *Journal of Hydraulic Research* 46, 191–208. doi:10.1080/00221686.2008.9521855.
- Mukherjee, J., 2011. No voice, no choice: Riverine changes and human vulnerability in the ‘chars’ of Malda and Murshidabad. Occasional Paper No. 28, Institute of Development Studies, Kolkata, India 28.
- Nanson, G., Knighton, D., 1996. Anabranching rivers: Their cause, character and classification. *Earth Surface Processes and Landforms* 21, 217–239. doi:10.1002/(SICI)1096-9837(199603)21:3<217::AID-ESP611>3.0.CO;2-U.

- Nicholas, A.P., Ashworth, P.J., Sambrook Smith, G.H., Sandbach, S.D., 2013. Numerical simulation of bar and island morphodynamics in anabranching megarivers. *Journal of Geophysical Research: Earth Surface* 118, 2019–2044. doi:10.1002/jgrf.20132.
- Oorschot, M., Kleinhans, M.G., Geerling, G., Middelkoop, H., 2016. Distinct patterns of interaction between vegetation and morphodynamics. *Earth Surface Processes and Landforms* 41, 791–808. doi:10.1002/esp.3864.
- Peckham, S.D., Hutton, E.W., Norris, B., 2013. A component-based approach to integrated modeling in the geosciences: The design of CSDMS. *Computers & Geosciences* 53, 3–12. doi:10.1016/j.cageo.2012.04.002.
- Powell, D., 2014. Flow resistance in gravel-bed rivers: Progress in research. *Earth-Science Reviews* 136, 301–338. doi:10.1016/j.earscirev.2014.06.001.
- Rice, S.P., Church, M., Wooldridge, C.L., Hickin, E.J., 2009. Morphology and evolution of bars in a wandering gravel-bed river; lower Fraser river, British Columbia, Canada. *Sedimentology* 56, 709–736. doi:10.1111/j.1365-3091.2008.00994.x.
- Rinaldi, M., Darby, S.E., 2007. Modelling river-bank-erosion processes and mass failure mechanisms: progress towards fully coupled simulations, in: *Gravel-Bed Rivers VI: From Process Understanding to River Restoration*. chapter 9, pp. 213–239. doi:10.1016/S0928-2025(07)11126-3.
- Schuurman, F., 2015. Bar and channel evolution in meandering and braiding rivers using physics-based modeling. Ph.D. thesis. doi:10.13140/RG.2.1.3582.3529.
- Schuurman, F., Kleinhans, M.G., Middelkoop, H., 2016. Network response to disturbances in large sand-bed braided rivers. *Earth Surface Dynamics* 4, 25–45. URL: <https://www.earth-surf-dynam.net/4/25/2016/>, doi:10.5194/esurf-4-25-2016.
- Schuurman, F., Marra, W.A., Kleinhans, M.G., 2013. Physics-based modeling of large braided sand-bed rivers: Bar pattern formation, dynamics, and sensitivity. *Journal of Geophysical Research: Earth Surface* 118, 2509–2527. doi:10.1002/2013JF002896.
- Segura, C., Pitlick, J., 2015. Coupling fluvial-hydraulic models to predict gravel transport in spatially variable flows. *Journal of Geophysical Research: Earth Surface* 120, 834–855. doi:10.1002/2014JF003302.
- Simmanee, A., 2013. Environmental Flows for the Ayeyarwady (Irrawaddy) River Basin, Myanmar. Technical Report. URL: http://burmariversnetwork.org/images/stories/publications/english/A_Simmanee2013-AyeyarwadyRiverBasin-public.pdf.
- Steijn, R., Huthoff, F., Stoeten, K., Huizer, T., Agerbeek, B., Sloff, K., 2019. River bank and bed protection Ayeyarwady River - Nyaungdon. Technical Report April. Netherland Enterprise Agency (RVO). Zwolle.

- Stoeten, V., 2019. Internship report: A hydrodynamic analysis in Delft3D Flexible Mesh. Technical Report. Arcadis. Delft.
- Taft, L., Kühle, L., 2018. Glacier Changes between 1976 and 2015 in the Source Area of the Ayeyarwady (Irrawaddy) River, Myanmar. *Water* 10, 1850. doi:10.3390/w10121850.
- Tassi, P., 2007. Numerical modelling of river processes: flow and river bed deformation. Ph.D. thesis. University of Twente. Netherlands. URL: <https://research.utwente.nl/en/publications/numerical-modelling-of-river-processes-flow-and-river-bed-deforma>.
- Vargas-Luna, A., Crosato, A., Uijttewaal, W.S., 2015. Effects of vegetation on flow and sediment transport: comparative analyses and validation of predicting models. *Earth Surface Processes and Landforms* 40, 157–176. doi:10.1002/esp.3633.
- Velzen, E.H., Jesse, P., Cornelissen, P., 2003. Stromingsweerstand vegetatie in uiterwaarden: Deel 1 Handboek. Versie 1-2003. Technical Report. Ministerie van Verkeer en Waterstaat, Directoraat-Generaal Rijkswaterstaat, RIZA Rijksinstituut voor Integraal Zoetwaterbeheer en Afvalwaterbehandeling. URL: <https://books.google.nl/books?id=1i1hmwEACAAJ>.
- Williams, R., D., Brasington, J., Hicks, D.M., 2016a. Numerical Modelling of Braided River Morphodynamics: Review and Future Challenges. *Geography Compass* 10, 102–127. doi:10.1111/gec3.12260.
- Williams, R., Measures, R., Hicks, D.M., Brasington, J., 2016b. Assessment of a numerical model to reproduce event-scale erosion and deposition distributions in a braided river. *Water Resources Research* 52, 6621–6642. doi:10.1002/2015WR018491.
- WWF, 2017. SOBA 3 : Sediments and Geomorphology Ayeyarwady State of the Art. Technical Report. World Wide Fund for Nature (WWF) Greater Mekong. URL: http://airbm.org/downloads/SOBA/SOBA_3_Sediments_geomorphology_2017_FINAL.pdf.
- Zhang, K., Wu, S., Feng, W., Zhang, J., Wen, S., 2020. Bar dynamics in a sandy braided river: Insights from sediment numerical simulations. *Sedimentary Geology* 396, 105557. doi:10.1016/j.sedgeo.2019.105557.

Appendix

Appendix A

Baptist roughness predictor

The Baptist roughness predictor (*vegetationmodelnr* = 1 in Delft3D-FM) can be used to calculate the Chézy coefficient to represent vegetation resistance (Baptist et al., 2007). It is commonly used for floodplains of rivers and in the intertidal areas of estuaries to determine the flow resistance of vegetation in a channel. This roughness predictor is based on the work of Baptist (2005). He obtained a simplified but accurate version of his analytical formula for the representative Chézy roughness coefficient for both submerged and non-submerged vegetation (Deltares, 2019a):

$$C_{veg} = \sqrt{\frac{1}{\frac{1}{C_b^2} + \frac{C_D n h_v}{2g}} + \frac{\sqrt{g}}{\kappa} \ln\left(\frac{h}{h_v}\right)} \quad \text{if } h > h_v \quad (\text{A.1})$$

$$C_{veg} = \sqrt{\frac{1}{\frac{1}{C_b^2} + \frac{C_D n h}{2g}}} \quad \text{if } h < h_v \quad (\text{A.2})$$

with h the water depth (m), g the gravitational acceleration (m/s^2), κ the Von Kármán constant ($-$), h_v the vegetation height (m), n the vegetation density ($1/m$), C_D the drag coefficient ($-$) and C_b the alluvial bed roughness ($m^{1/2}/s$). The vegetation density can be determined by multiplying the number of stems per squared meter with the diameter of the stems. The alluvial bed roughness is calculated using *Manning's n*:

$$C_b = \frac{\sqrt[6]{R}}{n} \quad (\text{A.3})$$

in which R is the hydraulic radius (m). We used a Manning n of $0.030 \text{ m}^{-1/3} \text{ s}$ for the river bed. C_{veg} is implemented in the bottom friction term of the momentum part of the Shallow-water equations. The bottom friction term reads:

$$\tau_b = \frac{\rho g u |u|}{C_{veg}^2} \quad (\text{A.4})$$

where $|u|$ is the magnitude of the depth-averaged horizontal velocity. C_{veg} is always lower (rougher) than C_b . Hence, vegetation causes an increase of the bottom friction term resulting in additional flow resistance and a reduction of the flow velocity.

The effect of vegetation is not included in the morphodynamic calculations in Delft3D-FM in a direct manner. C_{veg} was not included in the computation of the

mobility parameter of the sediment transport formula, because this would have led to a significant overestimation of the transport in vegetated areas. Including C_{veg} in the morphodynamic calculations would have led to behaviour similar to the red lines (Manning's roughness) in figure 2.4. Instead, the alluvial bed roughness C_b is used in the sediment transport formula. This bed roughness is calculated using equation A.3 and a Manning's n of $0.030 \text{ m}^{-1/3}\text{s}$. Hence, the transport formula is (for $c = 0$):

$$S = \alpha D_{50} \sqrt{\Delta g D_{50}} \theta^b \quad (\text{A.5})$$

$$\text{Mobility parameter : } \theta = \left(\frac{u}{C_b} \right)^2 \frac{1}{\Delta D_{50}} \quad (\text{A.6})$$

The use of C_b in the morphodynamic calculations also resulted in an overestimation of the sediment transport rate in vegetated areas, because the mobility parameter was still too large, see black line in figure A.1. However, the reduction of the flow velocity (u in equation A.6) from the hydrodynamic part of Delft3D-FM did cause a minor reduction of the mobility parameter in an indirect manner, see green line in figure A.1. These lines show that there is indeed a minor decrease of the bed shear stress and sediment transport rate compared to the *No vegetation* (black line) situation.

In reality, a significant decrease of the bed shear stress and sediment transport rate should occur due to vegetation (Baptist, 2005). To obtain this behaviour, the mobility parameter should have decreased significantly. Therefore, the C_b should have been increased. Delft3D-FM contains a methodology (*Trachytope 154*) which specifically determines the Chézy coefficient of vegetation for the morphodynamic computations. It increases the Chézy coefficient of vegetation leading to less flow resistance ($C_{veg} > C_b$). The formulation of this Chézy coefficient reads (Deltares, 2019a):

$$C_{veg} = C_b + \frac{\sqrt{g}}{\kappa} \ln\left(\frac{h}{h_v}\right) \sqrt{1 + \frac{C_D n h_v C_b^2}{2g}} \quad (\text{A.7})$$

Additionally, an extra flow resistance term is implemented in the Shallow water equations to obtain the correct hydrodynamic behaviour. All in all, this would have resulted in the behaviour as shown in the blue line in figure A.1. These lines shows a significant decrease of the bed shear stress and sediment transport rate when *Trachytope 154* is used. However, we could not use this methodology because it could not be used in combination with the present implementation of the Basic Model Interface in Delft3D-FM.

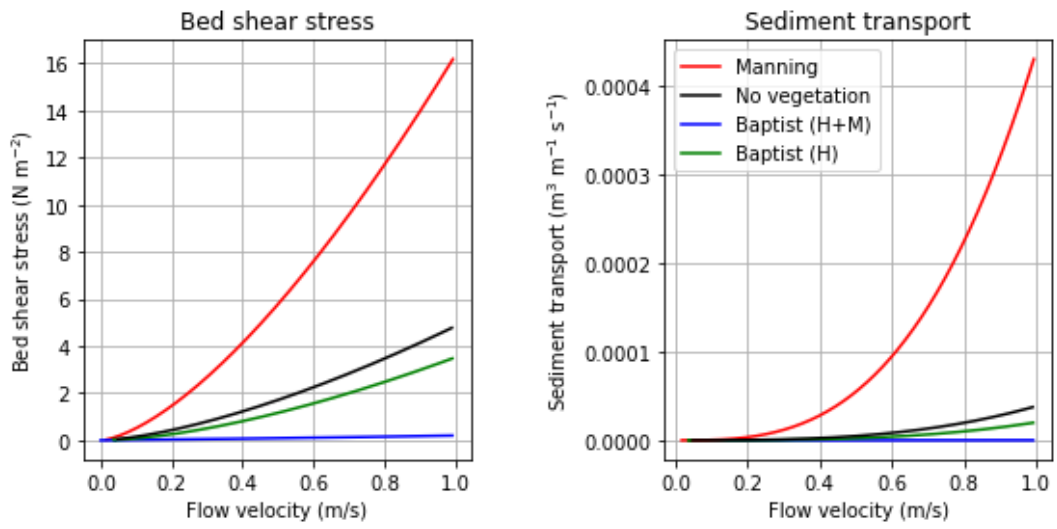


Figure A.1 – Bed shear stress (left) and sediment transport (right) vs. depth-averaged flow velocity for different vegetation formulations. *Manning* has a Manning’s n of $0.070 \text{ m}^{-1/3}\text{s}$ and *No vegetation* has a Manning’s n of $0.030 \text{ m}^{-1/3}\text{s}$. The figures are based on characteristics of the flow and vegetation on the mid-channel bars of the case study.

Appendix B

Model set-up: Ayeyarwady River model

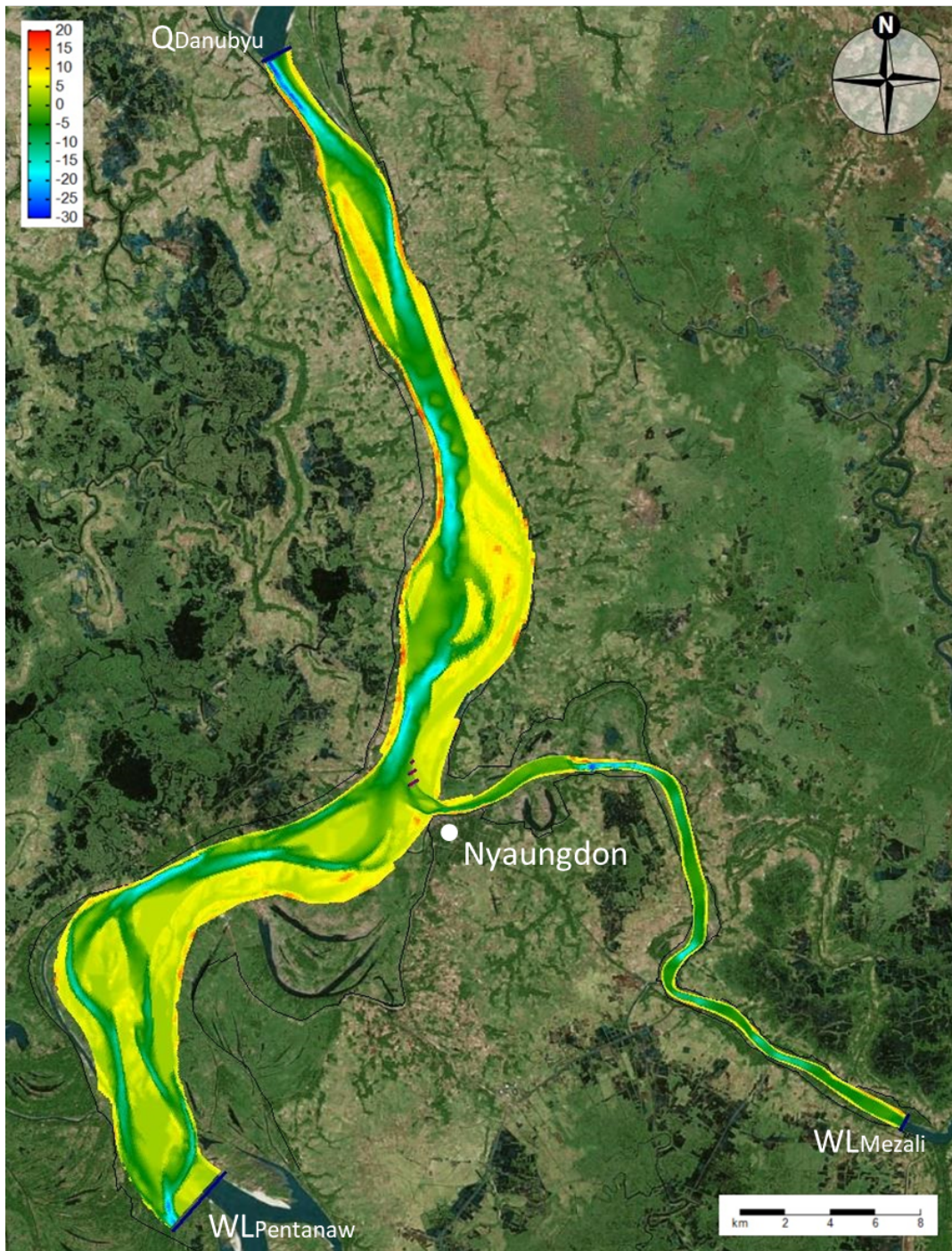


Figure B.1 – Ayeyarwady River model: Bathymetry of the entire modelling domain (m+MSL). Colorbar shows the magnitude of the bed level and the three groyne north of the bifurcation area are indicated in red.

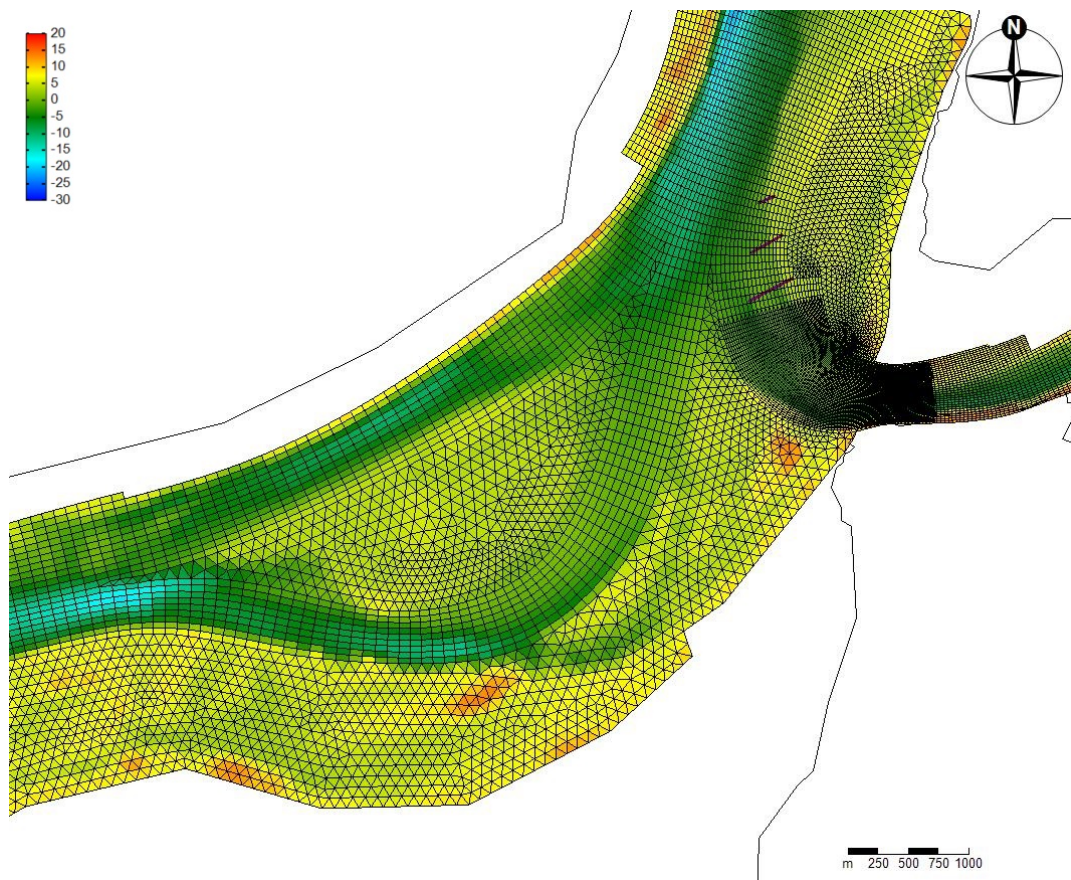


Figure B.2 – Ayeyarwady River model: A section of the curvilinear and triangular network of grid cells around Nyaungdon plotted on the bathymetry. The grid refinement at the bifurcation point of the Pan Hlaing river can clearly be seen. Thin black lines indicate the dikes.

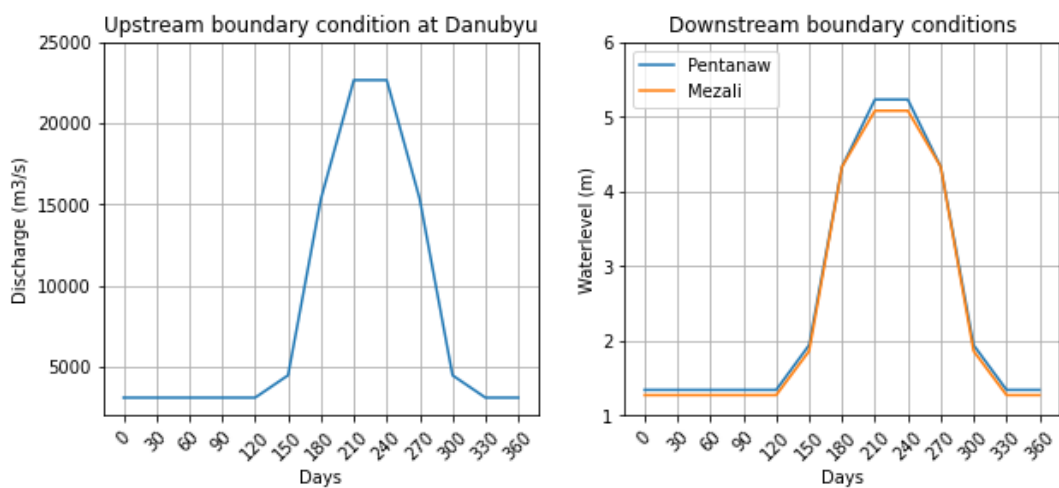


Figure B.3 – Upstream and downstream boundary conditions of the Ayeyarwady River model.

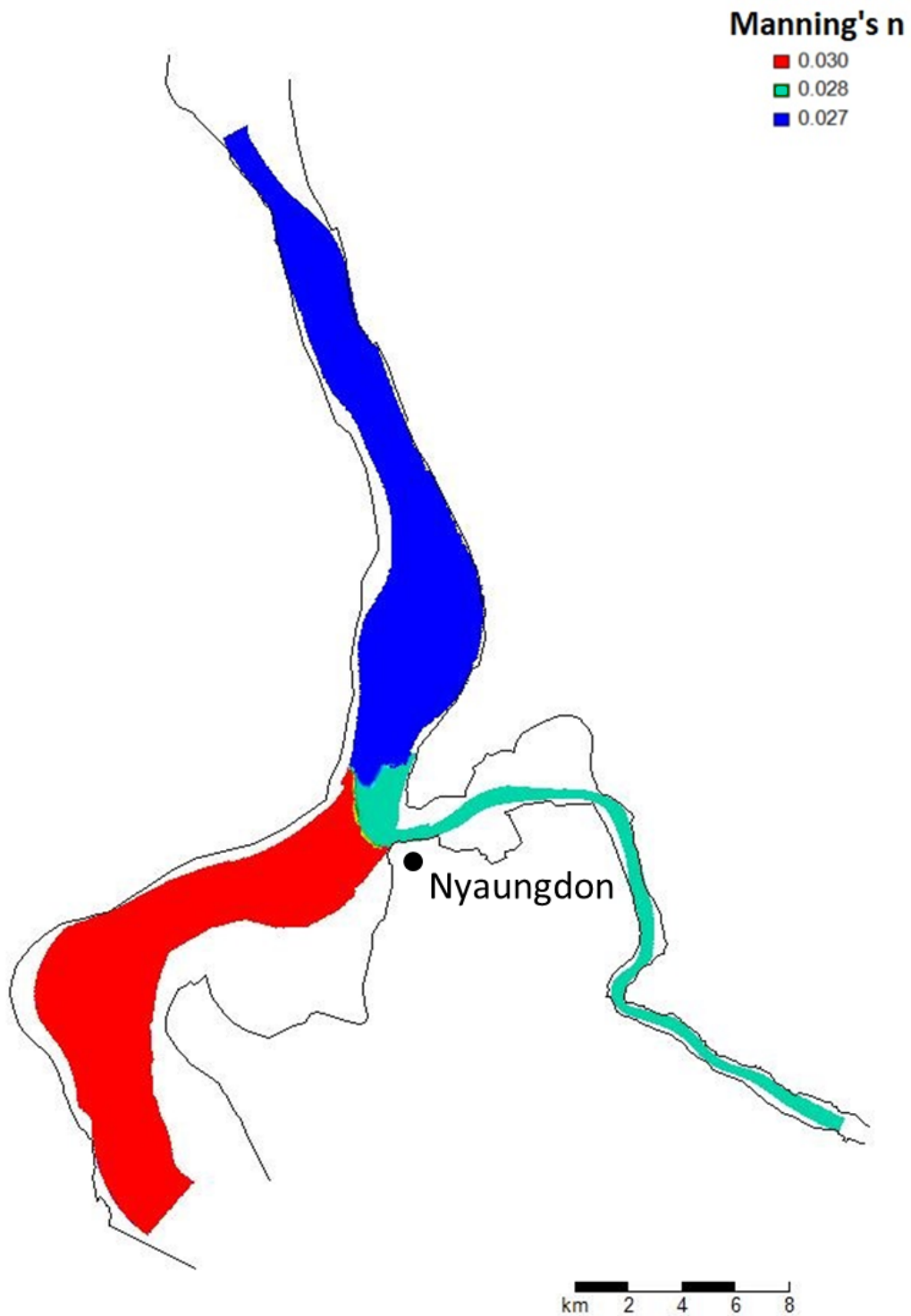


Figure B.4 – Ayeyarwady River model: Roughness map (*Manning's n*) of the entire modelling domain ($s/m^{1/3}$). Smooth transitions between the sections are visible in the figure. Thin black lines indicate the dikes.

Appendix C

Results: Schematized model

Extended results: Scenario analysis

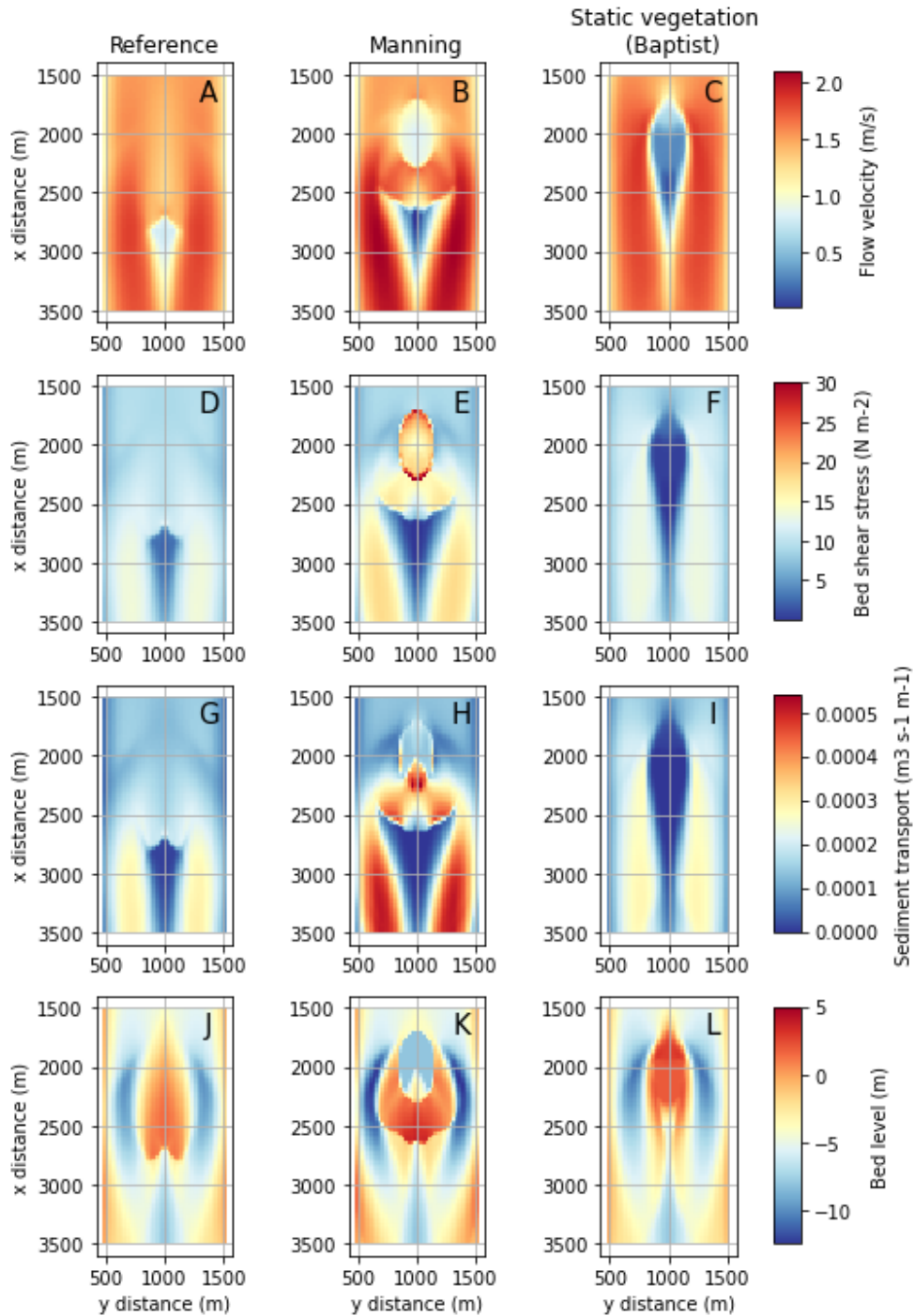


Figure C.1 – State of the flow velocity, bed shear stress and sediment transport and evolution of the bed level after 240 days during high flow conditions for the reference, manning and static vegetation scenario. Flow from top to bottom of figure. The color bar for bed shear stress is truncated to show a maximum stress of $30\ N\ m^{-2}$.

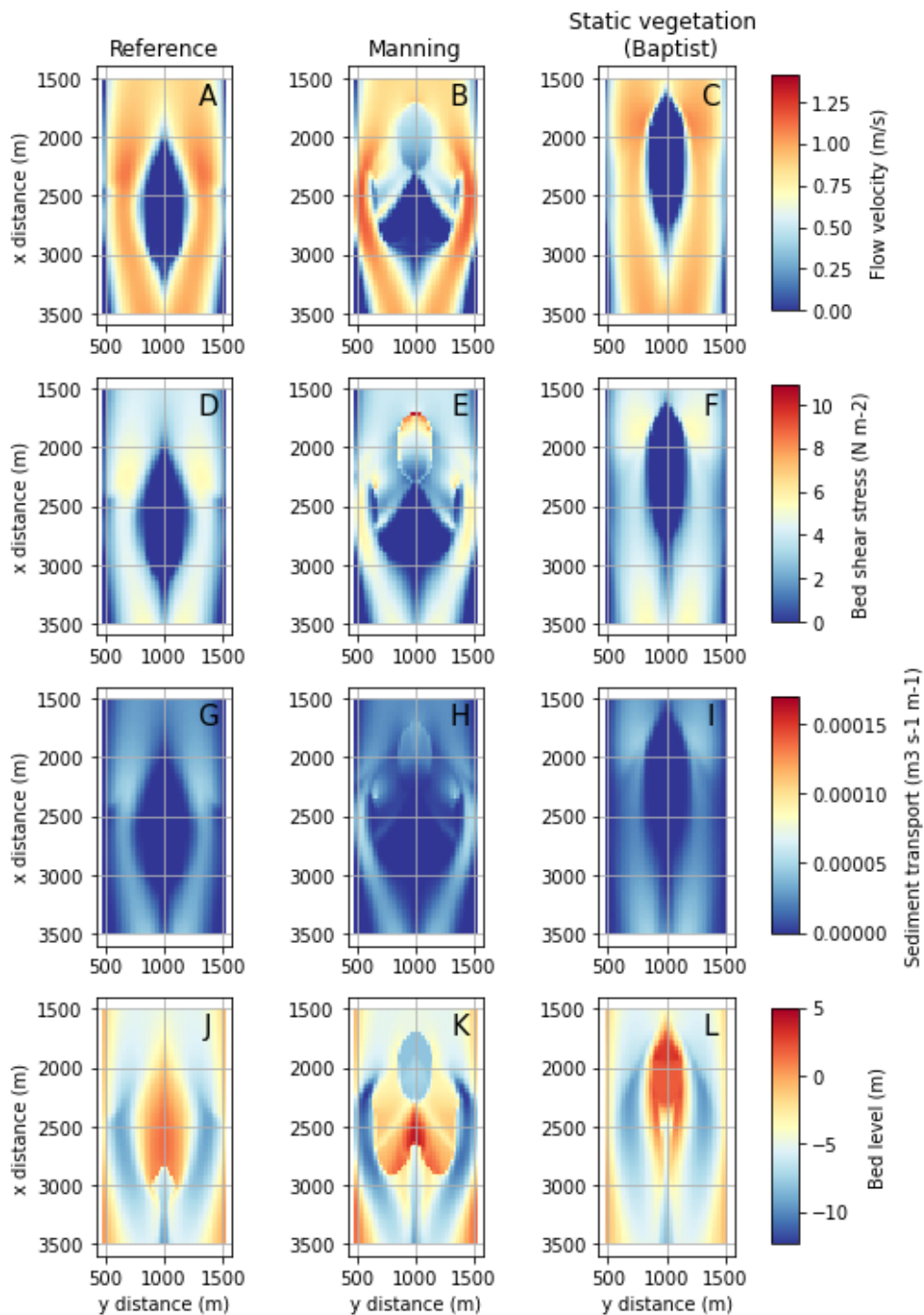


Figure C.2 – State of the flow velocity, bed shear stress and sediment transport and evolution of bed level after 360 days during low flow conditions for the reference, manning and static vegetation scenario. Flow from top to bottom of figure.

Sensitivity analysis: Static vegetation

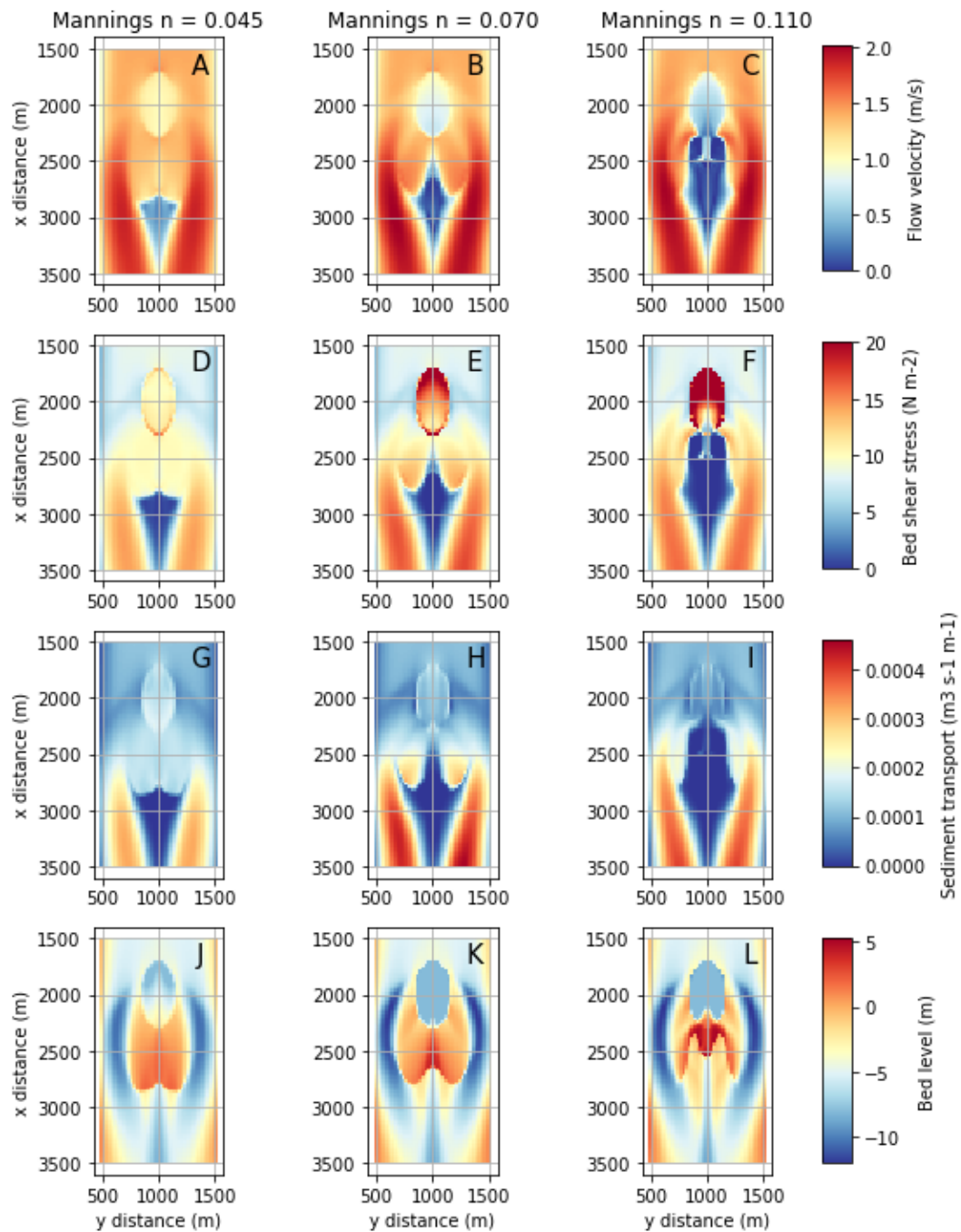


Figure C.3 – Sensitivity of physical processes and channel evolution for the *Manning scenario* after about 260 simulated days. The parameter differences are indicated above the panels. Unit of Manning's n is $s/m^{1/3}$

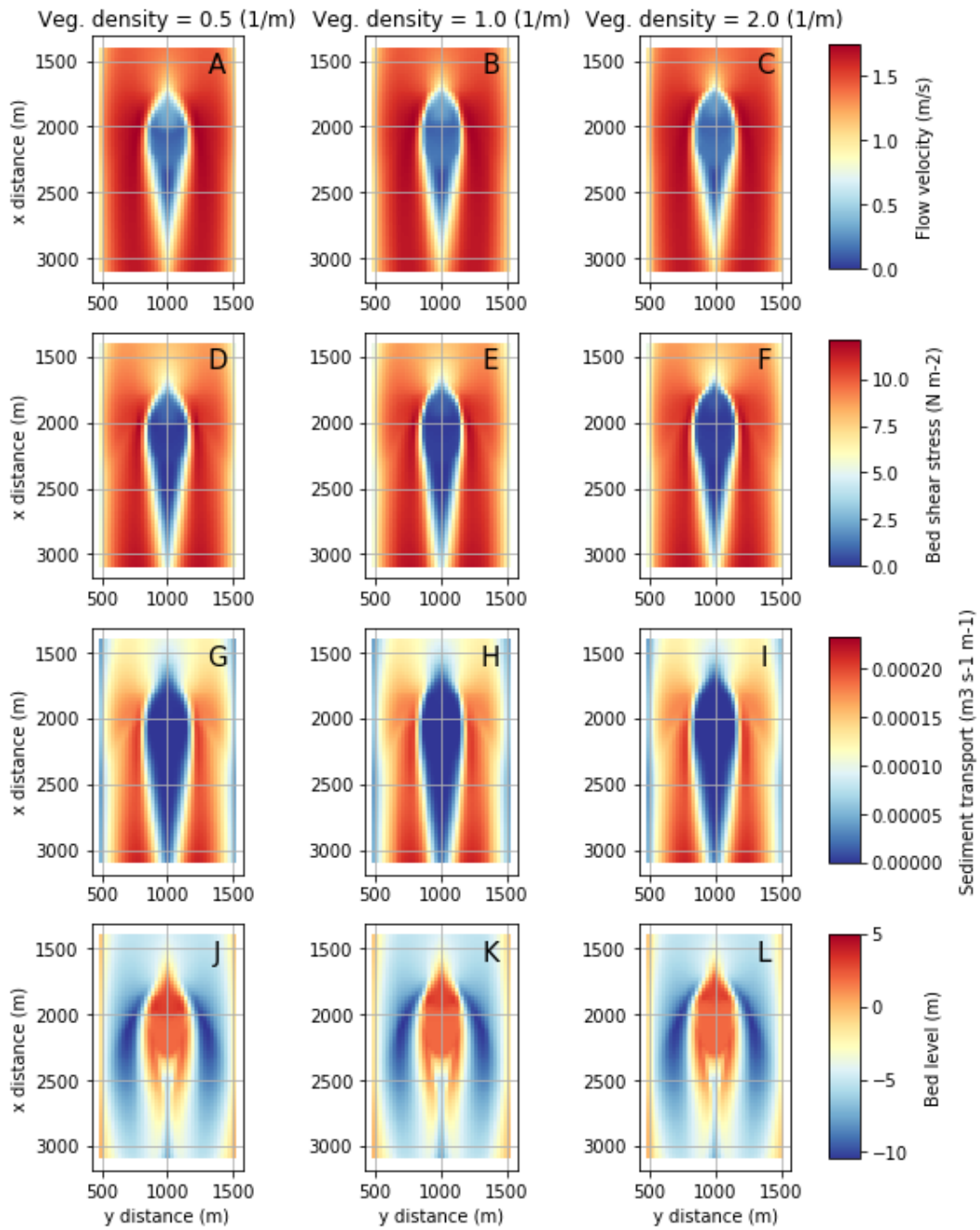


Figure C.4 – Sensitivity of physical processes and channel evolution for the *static vegetation scenario* to changes in the vegetation density after about 260 simulated days during high flow season. The parameter differences are indicated above the panels.

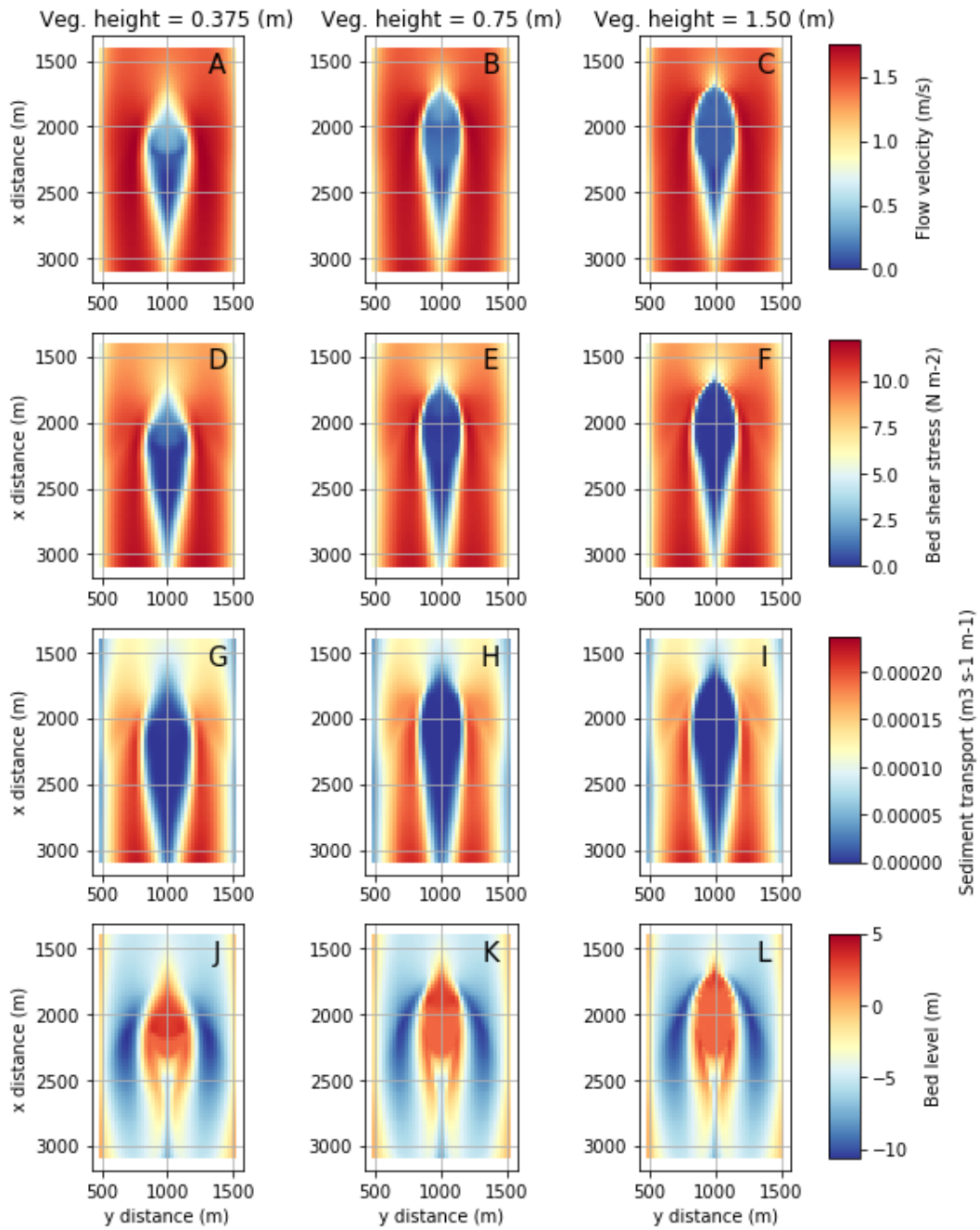


Figure C.5 – Sensitivity of physical processes and channel evolution for the *static vegetation scenario* to changes in the vegetation height after about 260 simulated days during high flow season. The parameter differences are indicated above the panels.

Sensitivity analysis: Dynamic vegetation

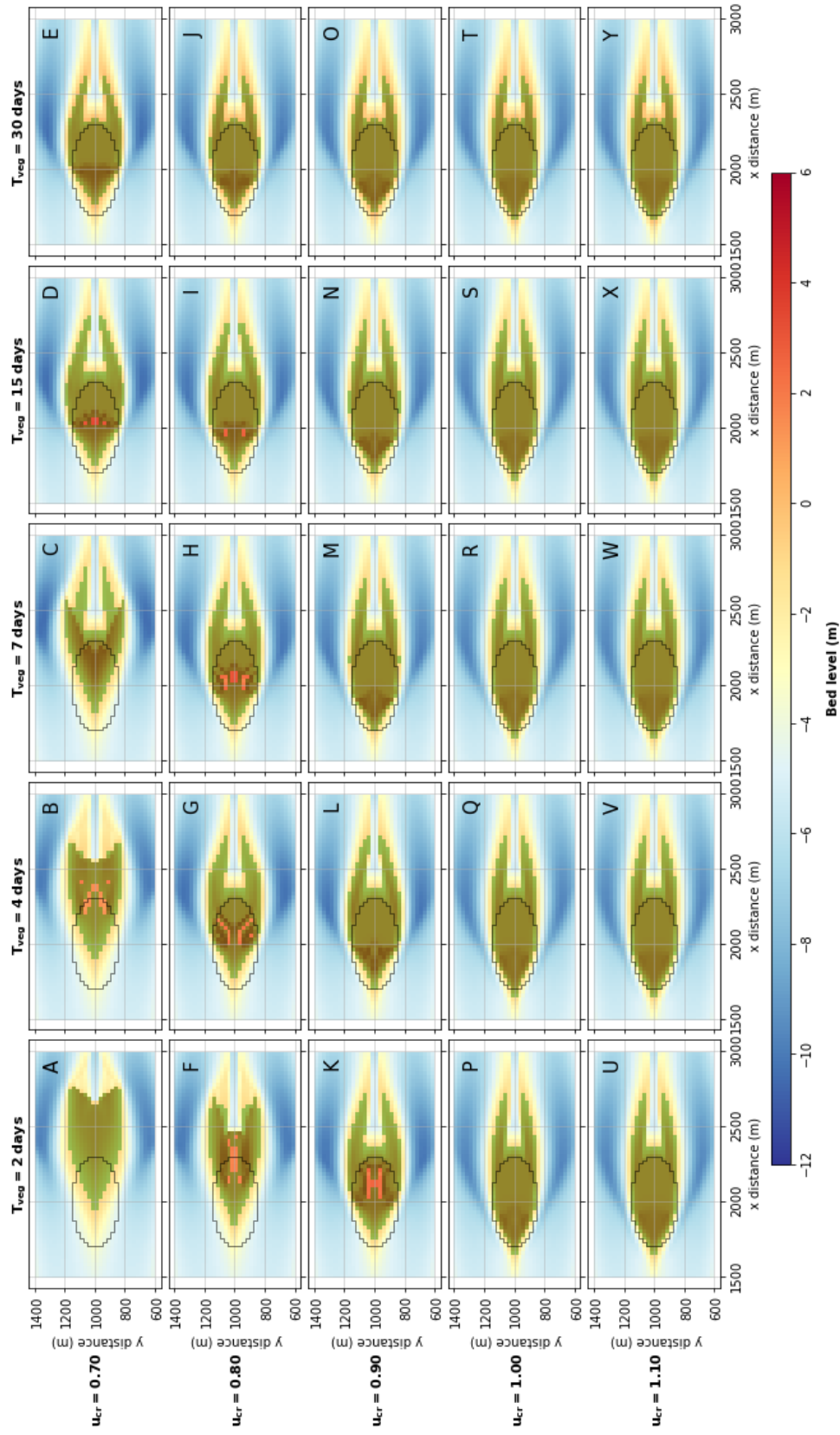


Figure C.6 – Sensitivity analysis: bed levels (m) after 360 days for different durations of the vegetation update interval (T_{veg}) and critical flow velocities for vegetation removal (u_{cr}). Green overlaid area shows the location of the vegetation after the peak of the discharge wave and black circle shows the initial location of vegetation.

Appendix D

Results: Ayeyarwady River model

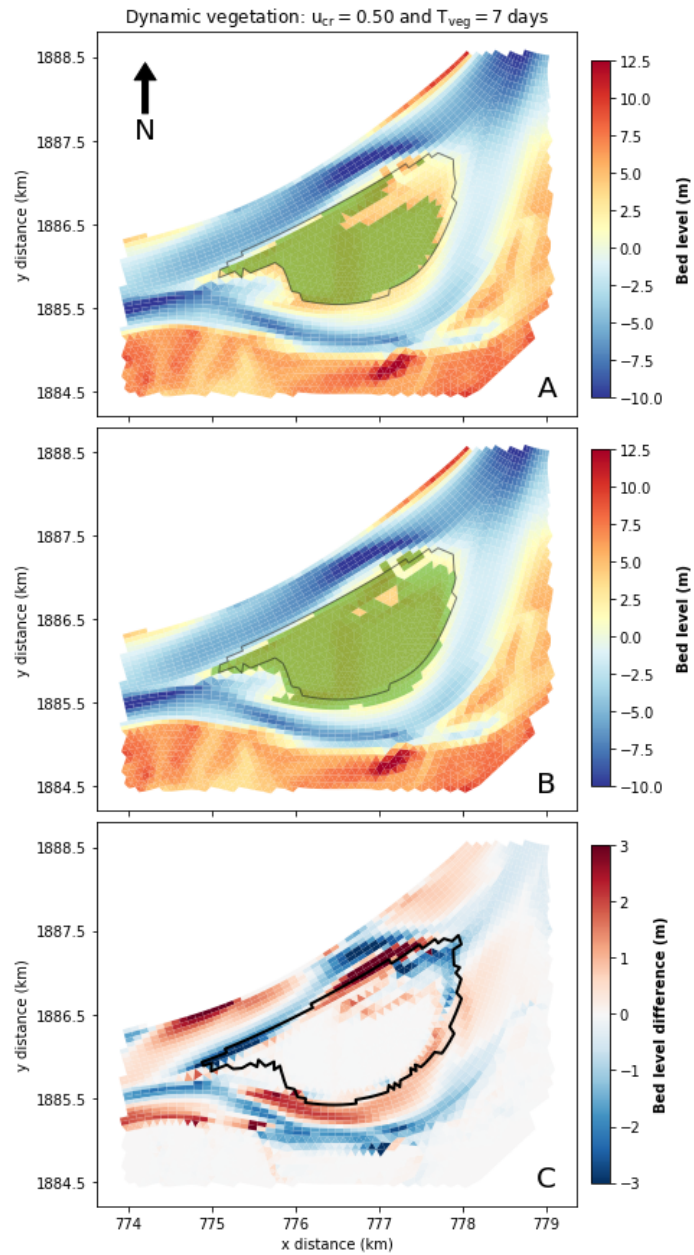


Figure D.1 – Development of the bed after 330 days (*A*), development of the bed after 360 days (*B*) and the bed level difference with respect to the *static vegetation scenario* after 360 days (*C*) for a unsuitable combination of the critical flow velocity for vegetation removal u_{cr} and the duration of the vegetation update interval T_{veg} . Black lines in upper and middle panels show the initial location of the vegetation, black line in lower panel show the initial location of the bar and the green overlaid areas show the vegetation. The color bar of panel *C* is truncated to show a maximum difference of ± 3 meters.